Anti-tumor effect of the mitochondrial respiratory chain complex inhibitors

on canine mammary gland tumor cells

（犬悪性乳腺腫瘍に対するミトコンドリア呼吸鎖複合体阻害薬の抗腫瘍効果）

佐伯　亘平

Contents

Chapter 1

General introduction

Preface: cancer and metastasis

World Health Organization reported that cancer is the leading cause of mortality in human worldwide, with approximately 14 million new cases and 8.2 million cancer-related deaths in 2012[a]. In the United States, approximately 40% of all people are expected to be diagnosed as a certain kind of cancer in their lifetime based on the data collected during 2009-2011, and five year survival rate of all cancer patients was 66.1% (2004-2010) according to Surveillance, Epidemiology and End Results Program, National Cancer Institute[b].

Cancer is also a leading cause of disease-related death in dogs, with nearly half of dogs aged older than ten years old dying from cancer (Withrow et al., 2012). In surveillance performed in Italy, 143 dogs in 100,000 dogs were estimated to develop malignant tumors in a year, which was comparable to that in human statistics (460.4 cases / 100,000 men and women per year; 2007-2011[b]) (Vascellari et al., 2009).

In both human and dog, there would be no doubt that systemic dissemination of cancer cells, or metastasis, is the end stage of cancer progression, turning the localized neoplasm into multiple organ-affecting and life-threatening disease (Clemente et al.,

---

[a] http://www.who.int/mediacentre/factsheets/fs297/en/

[b] http://seer.cancer.gov/

2010; Fidler, 1978; Hanahan and Weinberg, 2011; Withrow et al., 2012). Cancer usually progresses as follows; the cells start to invade surrounding extracellular matrix (ECM) and intravasate into systemic circulation. Then, the cells are trapped in capillary vessels, extravasate at the particular organs and finally colonize the secondary site with angiogenesis. Proliferated metastasis destructs normal function of the colonized organ. Since this formation of metastasis directly threatens survival of the cancer-bearing patients, priority of cancer treatment should be set on a control of the disseminating cancer cells.

Cancer heterogeneity

Cancer does not consist of uniform cells but heterogeneous cells with spectrum of phenotypical diversity (Marte, 2013), and some specific group of cells in the heterogeneous population are thought to have metastatic potential (Dieter et al., 2011; Fidler, 1978; Fidler and Kripke, 1977; Marte, 2013). It was reported that only one percent of malignant B16F1 melanoma cells formed liver macrometastasis after injectiom into the portal vein (Luzzi et al., 1998). Another report demonstrated that the success rate for brain macrometastasis formation of melanoma and lung carcinoma cells injected into the carotid artery was 1.0-7.0% (Kienast et al., 2010). This cancer

heterogeneity is explained by coexisting theories; cancer stem cell model, clonal evolution and heterogeneous microenvironment (Meacham and Morrison, 2013).

Cancer stem cell model

Cancer stem cell (CSC) model explains horizontal heterogeneity of cancer cell phenotype. In CSC model, cancers are organized into a hierarchy of tumorigenic CSC and non-tumorigenic progenies (Fig. 1.1) (Kreso and Dick, 2014; Meacham and Morrison, 2013). This hierarchy is considered to be a reflection of normal tissue homeostasis because the same surface markers frequently could be utilized to characterize the stem cells of the normal tissue and CSCs in the cancer from the same tissue (Al-Hajj et al., 2003; Kreso and Dick, 2014). The demonstration that the LGR5 molecule could be used for isolating the stem cells from the normal large intestine as well as the CSCs from the colorectal cancer tissues was one such example (Barker, 2014). The CSC model has been suggested initially in a human hematological malignancy, followed by some types of solid cancers as well as malignancies in small animals (Al-Hajj et al., 2003; Bhatia et al., 1997; Michishita et al., 2012). In CSC hierarchy theory, CSCs are recognized as the only cells that can self-replicate, disseminate, repopulate and therefore finally form metastasis. Other progenies which compose of the bulk of the

cancer mass are non-tumorigenic and non-metastatic.

Clonal evolution

Clonal evolution is the other model which explains cancer heterogeneity. Carcinogenesis is accomplished through serial genetic lesions comprised of mutations in oncogenes and tumor suppressor genes (Vogelstein et al., 2013; Vogelstein and Kinzler, 1993). A fully developed cancer has genomic instability due to abnormal cell division and mutational inactivation of several DNA repair pathways, which might be acquired during carcinogenesis (Burrell and Swanton, 2014). This genomic instability may in turn further accelerate the carcinogenesis process with accumulating genetic insults (Burrell et al., 2013). As a consequence, one cancer could contain a catalogue of up to thousands of genetic mutations (Vogelstein et al., 2013). However, some of these somatic mutations are not shared homogenously throughout cancer cells. Recent massive analyses using the advanced sequencing techniques have revealed that there are multiple tumor cell clones with different genetic lesions and distinct phenotypes in one cancer tissue. (Burrell and Swanton, 2014; Ding et al., 2012; Gerlinger et al., 2012; Walter et al., 2012). This kind of clonal heterogeneity may develop during the cancer cell division where the impaired DNA repair or check systems allow to survive the cells

with the novel genetic wounds. This notion of clonal diversity, or heterogeneity

coincides with the previous observation in which not all the established clones from one

melanoma cell line had same metastatic potential as the parental cell line did (Fig. 1.2A)

(Fidler, 1978). This result indicates that CSC theory does not explain cancer

heterogeneity fully. In that article published more than three decades ago, the author

questioned, "Does the process of metastasis represent the random survival of tumor cells,

or does it result from the survival and growth of a specialized subpopulation of cells?"

The recent technical advances could answer that the latter is true. The same discussion

would be applied to the cancer relapse after failure of the chemotherapy. The pressure

by the cytotoxic agents seem to allow the proliferation of the selected clones which are

resistant to the therapy (Fig. 1.2B). These heterogeneities are called as a clonal evolution

after Darwinian selection or adaptive evolution. In this model, metastatic potential is

considered to be restricted to the special clones that acquired metastatic potential by

chance via some unique genetic and epigenetic changes after carcinogenesis.

Microenvironment

Microenvironment surrounding the cancer cells could affect phenotype of

cancer cells as well (Hanahan and Weinberg, 2011; Junttila and de Sauvage, 2013).

Cancer formation involves co-evolution of surrounding ECM, vasculature, stroma and immune cells. Direct and indirect interaction between the cancer cells and the microenvironment could enable the cancer cells to proliferate, invade the surrounding tissue and evade immune surveillance, which give them the chance to survive and metastasize. The previous study which indicated the possibility of tumor infiltrating T lymphocyte to render the tumor cell malignant phenotype in canine mammary gland tumor tissues may be one example of interaction between tumor and surrounding components in veterinary malignancies (Saeki et al., 2012).

These mechanisms which make the cancer cells diverse and heterogeneous are not mutually exclusive but can coexist in one context (Meacham and Morrison, 2013) (Fig. 1.3). Dieter et al. exhibited that different kind of CSCs are exist in colorectal cancer specimen and only fraction of CSCs could survive serial passage in the immune-deficient animals (Dieter et al., 2011). Metastatic formation was also accomplished by the fraction of CSCs. They concentrated the CSC population by the suspension stem cell culture method and labeled each single cell by lentiviral transfection. After injection of these CSCs into immune-deficient mouse and formation of systemic disease, clonal tracking was performed utilizing unique lentiviral insertion site in each clone. Their

results showed that some CSCs can self-renew, repopulate progeny and form cancer mass, but do not metastasize. This observation is now understood as co-existence of clonal evolution and CSC hierarchy in the cancer. Phenotypically different clones could be maintained by each stem cell populations (Kreso and Dick, 2014; Meacham and Morrison, 2013).

Bridging remarks to the thesis

Canine mammary gland tumors (CMGTs)

As mentioned above, cancer is a leading cause of death in elderly client-own dogs and metastatic spread of cancer often results in cancer-related death. Especially, CMGTs are the most common neoplasm in sexually intact female dogs and account for approximately half of all tumors that develop naturally in these animals (Dorn et al., 1968; Rostami et al., 1994; Withrow et al., 2012). In addition, metastasis is a critical prognostic factor for CMGT (Chang et al., 2005). Overall survival after regional mastectomy of CMGT patients with macrometastasis in regional lymph nodes is significantly shorter (8.3 ± 6.8 months) than that in non-metastatic patients (19.0 ± 6.4 months) (Szczubiał and Łopuszynski, 2011). A series of 72 necropsies on CMGT patients showed that death was associated with systemic spread of metastatic lesions

rather than local recurrence or invasion (Clemente et al., 2010). Therefore, prevention

and control of metastasis is important for improving the prognosis of CMGT patients.
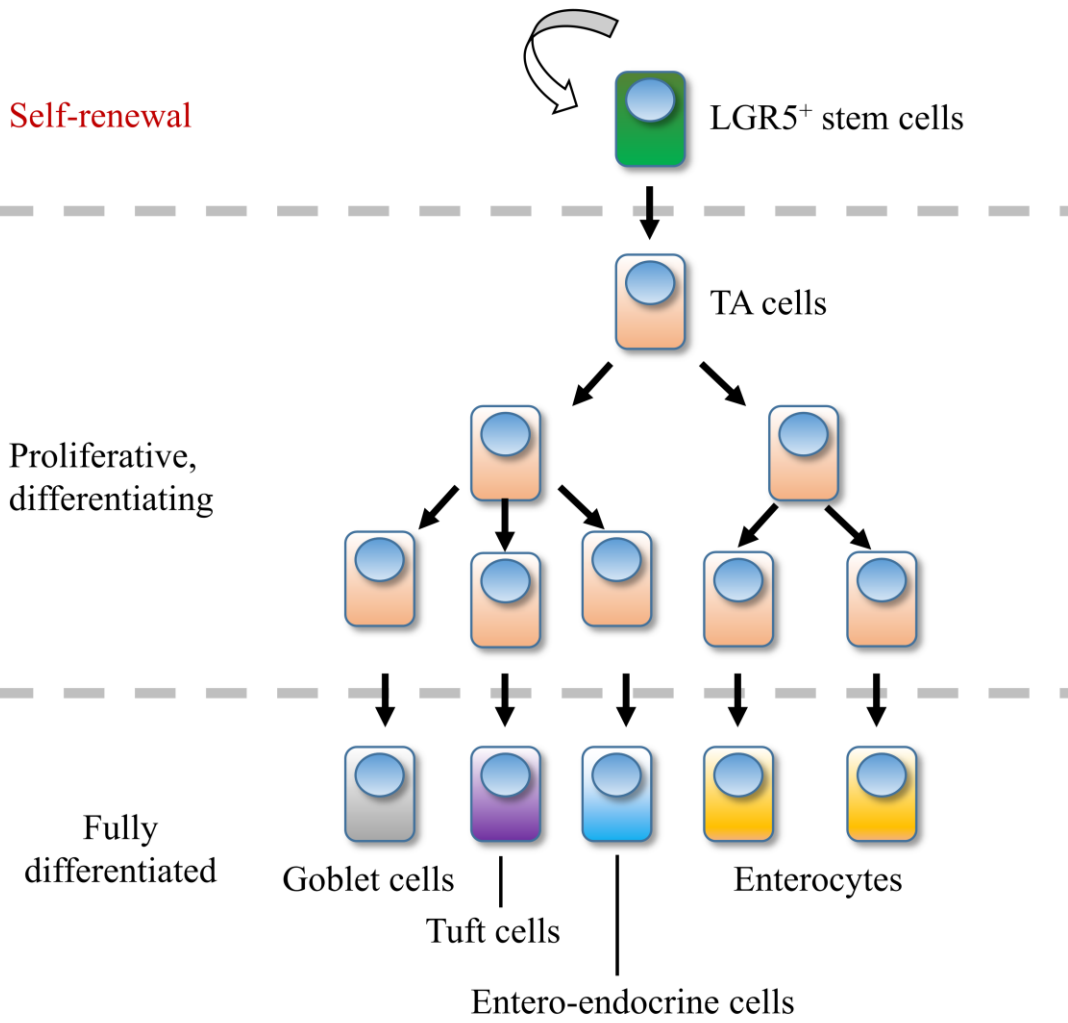

Purpose of this study

Accumulated evidences have suggested importance of control of metastatic

cells in CMGT patients. However, the phenotypical and genetic differences between

metastatic cells and non-metastatic cells were still unclear in CMGT. Therefore, the way

that we could specifically target metastatic cells had been not determined.

The purpose of this thesis was to find metastatic CMGT cell specific inhibitory

agents and clarify its mechanism for improvement of cancer treatment. For this purpose,

in the chapter 2, I adopted an unbiased drug screening using the CMGT clones with

contrasting metastatic potential established in the previous study (Murai et al., 2012),

and searched for metastatic clone selective inhibitors. In the chapter 3, clinical

applicability of the identified metastatic clone-specific inhibitor was investigated.

Furthermore, mainly in the chapters 3 and 4, *in vitro* mechanism of the action

of the selected inhibitor was pursued. Further presentation, interpretation and discussion

of the experiments will be found in the following chapters.

A

Self-renewal — LGR5$^+$ stem cells

TA cells

Proliferative, differentiating

Fully differentiated

Goblet cells

Tuft cells

Entero-endocrine cells

Enterocytes

B

Self-renewal, tumorigenic, metastatic — LGR5$^+$ cancer stem cells

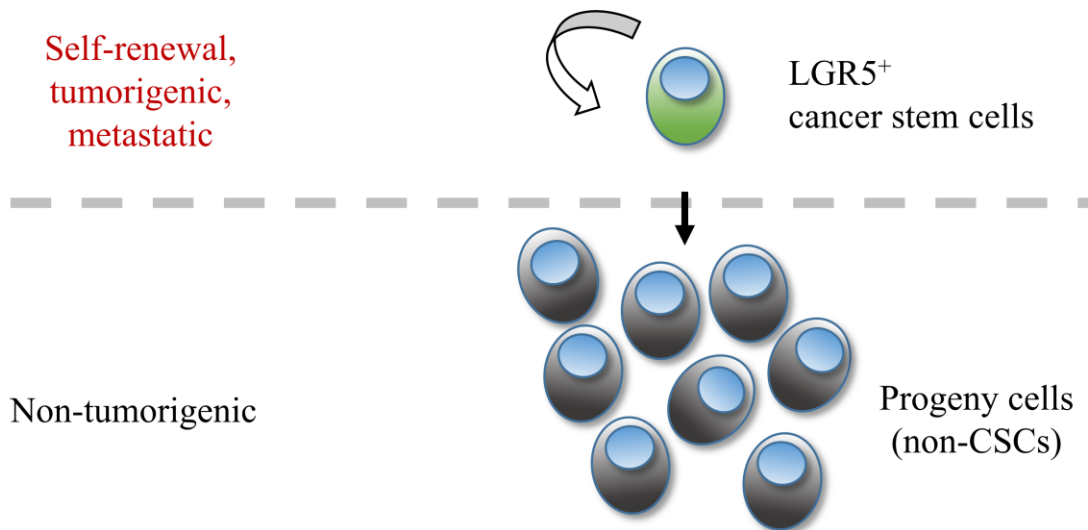Non-tumorigenic

Progeny cells (non-CSCs)

Fig. 1.1. Hierarchical organization of the normal tissue and the tumor tissue

(A) Hierarchical organization of the epithelia of the large intestine is illustrated as a
representative of the normal tissue. Leucine-rich repeat-containing G-protein coupled
receptor 5 (LGR5)-positive intestinal stem cells reside at the bottom of the crypt. LGR5$^+$
stem cells give rise to transit amplifying (TA) cells which actively proliferate and move
along intestinal villi. TA cells finally differentiate into the several specialized cells. These
fully differentiated cells operate intestinal functions. In this hierarchy, only LGR5$^+$ stem cells
have self-renewal potential, with depletion of the stem cell population resulting in
destruction of the entire epithelia. TA cells and differentiated cells have only limited capacity
of proliferation. New cells are supplied from the bottom of the crypt, climbing up the villi
with proliferation and differentiation, and finally got rid of at the top of the villi into the
intestinal lumen.

(B) Hierarchical organization of the tumor tissues. In the cancer stem cell (CSC) model, CSCs
locate at the top of the hierarchy and only CSCs have potential to self-renew, repopulate, and
form metastasis. Expression of LGR5 is considered as the marker for CSC in the several
types of cancer developed in the digestive tract, including colorectal adenocarcinoma. Since
proportion of CSCs in the tumor tissue is estimated to be small (sometimes <1%), bulk of
tumor mass is comprised of non-tumorigenic progenies (non-CSCs).

A

Parental B16 mouse melanoma

Cloning of 17 different subclones
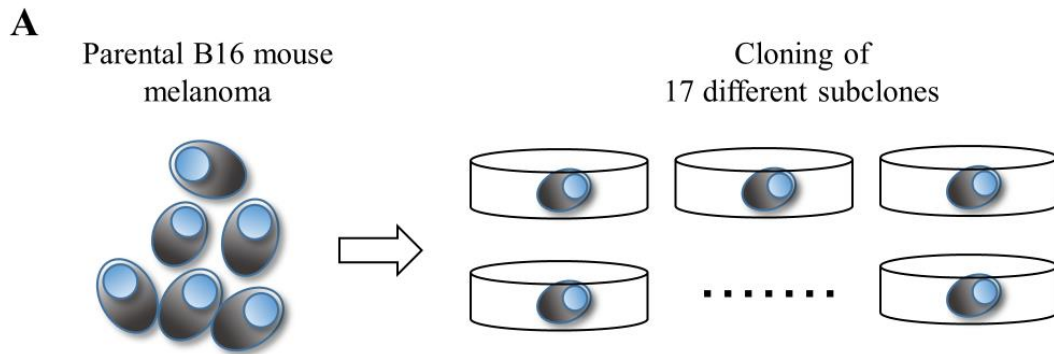
IV injection of each clone into mice

Clone name	Median # of pulmonary metastatic foci (range)
Clone 16	3.5 (2-15)
Clone 15	5 (2-20)
…	
Parent B16	40.5 (8-131)
…	
Clone 13	250 (50-350)
Clone 14	>500

B

Normal cells

Genetic insult

Pre-cancerous lesion

Cancer composed of multiple clones with different metastatic potential

Primary lesion

Chemotherapy accelerates further clonal evolution
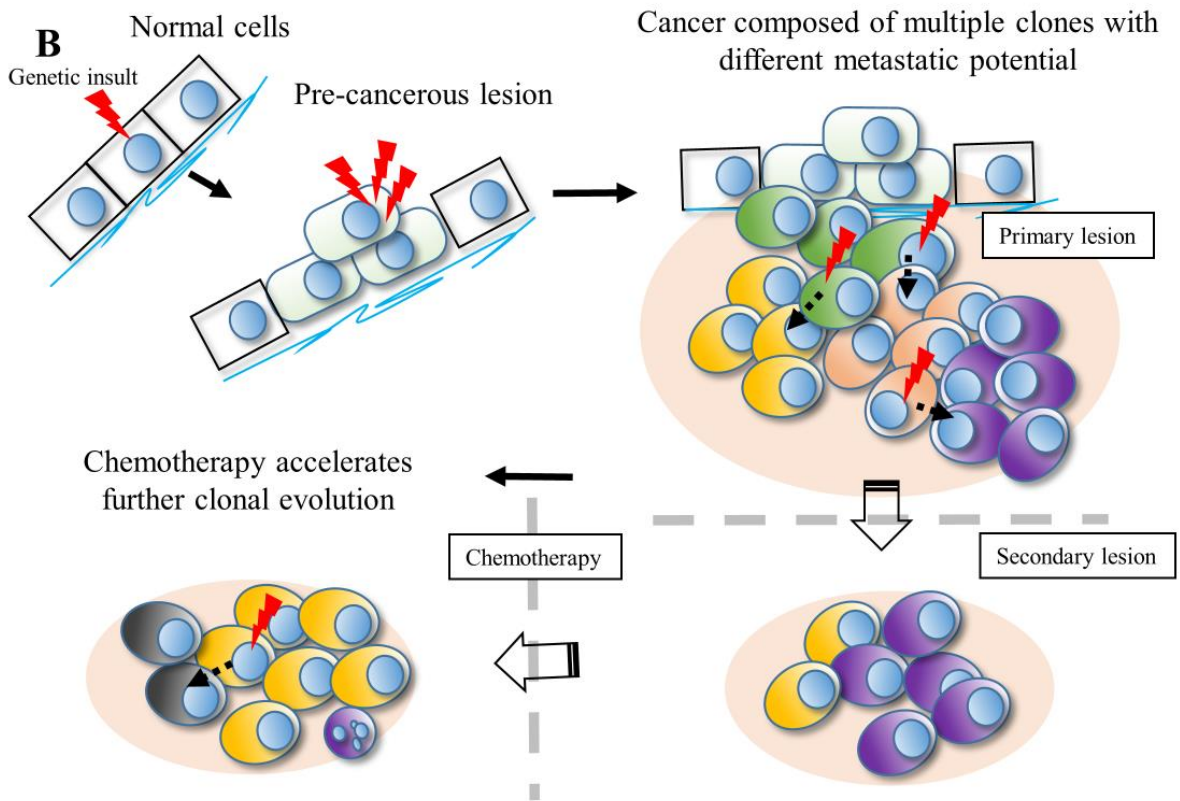
Chemotherapy

Secondary lesion

Fig. 1.2. Clonal diversity and evolution of the cancer

(A) In the 1977 paper, Fidler et al. showed clonal diversity and heterogeneous metastatic potential of each clone using mouse melanoma B16 cells. They isolated 17 different clones from one parental B16 cell line and investigated their colonization potential in the lung after intravenous injection. The metastatic potential of clones differed greatly ranging from less than ten to > 500 metastatic foci, indicating that there might exist the specific clones responsible for metastasis formation in the seemingly uniform cancer cells.

(B) Carcinogenesis is accomplished through serial genetic mutations which render the cells the hallmark of cancer. Fully developed tumors would be equipped with genomic instability and likely to diversify in the tumor tissue with multiple novel mutations after carcinogenesis. When this diversification results in generation of the phenotypically malignant clones by chance (yellow and purple), metastasis in the secondary site may be developed by them. Chemotherapy could be one evolutionary pressure in the cancer tissue. In this scheme, chemotherapy successfully eradicated purple cells, but the yellow clone survived, leading to expansion of the clone and birth of the novel clone from them (black).
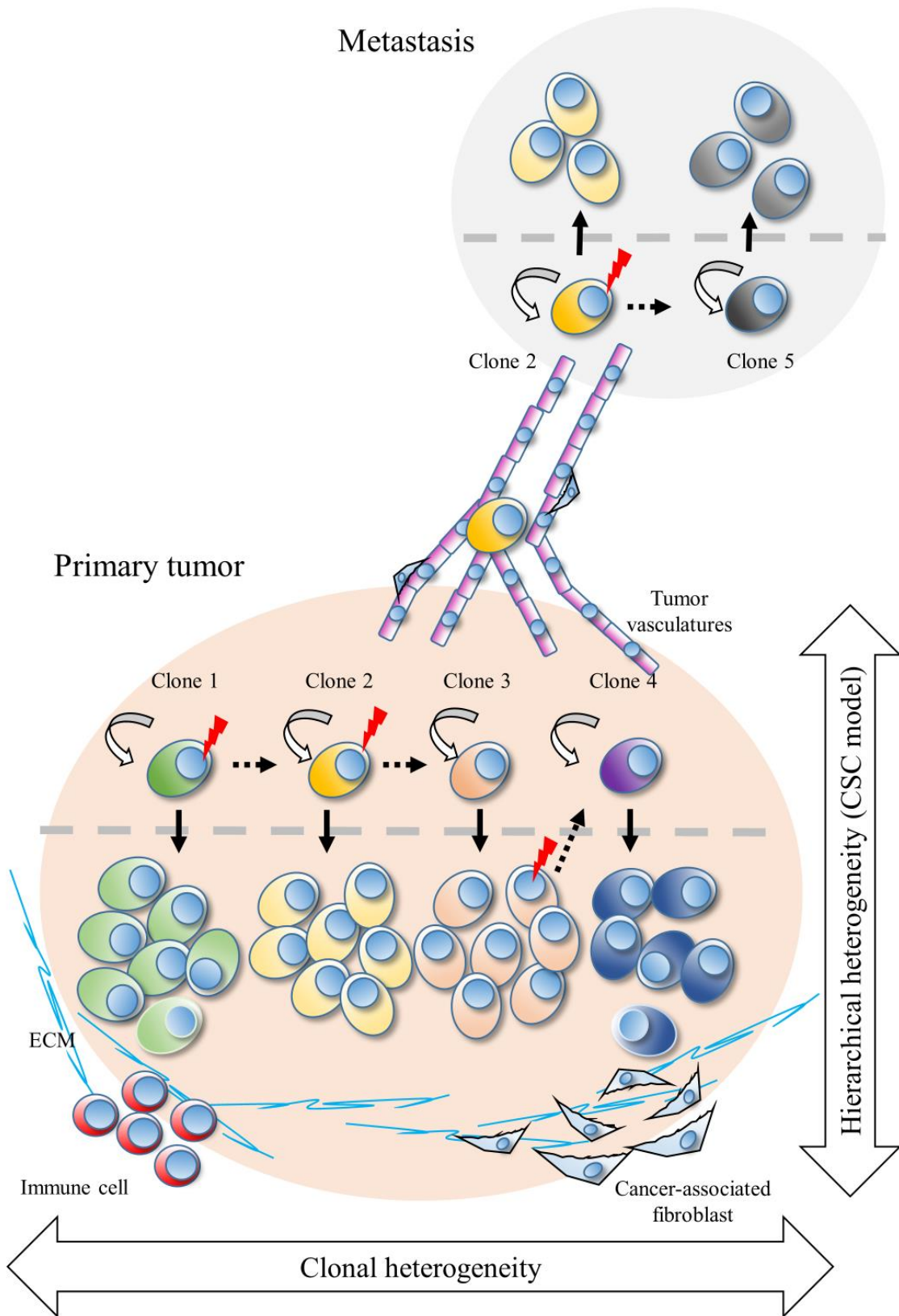
Fig. 1.3. Integrated model for understanding of the cancer heterogeneity.

Heterogeneities by the cancer stem cell model, the clonal evolution and the tumor microenvironment are not mutually exclusive and can be integrated in one context. The tumor tissue is composed of several distinct clones and each clone is maintained by the small proportion of self-renewing cells (CSCs). Metastatic dissemination is conducted by the selected CSC population and then the secondary tumor formation is completed through repopulation (generation of the progenies) by the CSCs. In the same time, the surrounding environment can influence the phenotype of the tumor cells. In this model, extracellular matrix (ECM), immune cells, fibroblast and vasculatures are depicted as components of tumor microenviroment.

Chapter 2

Molecularly targeted drug screening

by using metastatic and non-metastatic clones

of canine mammary gland tumor cell line

Introduction

Understanding of the cancer biology is essential for development of the effective therapy. As discussed in the previous chapter, the treatment focused on control of the metastatic cells will improve patient prognosis effectively since most of the cancer mortality is attributed to the systemic spread of the cancer cells including CMGT.

Previously, Murai et al. has cloned 23 clones in total from the single established cell line (CHMp) which had been derived from a dog with inflammatory mammary carcinoma (Fig. 2.1) (Murai et al., 2012). Three of these clonal lines, CHMp-5b, CHMp-11a and CHMp-13a, were transplanted into immune-deficient mice and they exhibited strikingly distinct behavior in the recipient animals; CHMp-5b formed huge primary tumors, CHMp-13a colonized as a slowly growing tumor which finally stopped to enlarge, and CHMp-11a behaved intermediately (Murai et al., 2012). Moreover, only CHMp-5b cells metastasized to the lung in an orthopedic injection model. These results were very similar to the previous results observed in mouse melanoma cells (Fidler, 1978) (Fig. 1.2A). Therefore, clonal diversity with phenotypic difference was strongly indicated in CMGT as well. Thus, it was suggested that metastatic clones in CMGT might be an effective therapeutic target and chemotherapy selective for these clones may improve treatment outcomes of CMGT.

Distinct metastatic potential between the CMGT clones was supposed to be derived from gain-of- or loss-of-function in some gene products as a consequence of the clonal evolution. Such genetic changes may cause not only enhanced malignant behaviors of the cells but also changes in other vital cellular signaling or functions. Therefore, it was speculated that CHMp-5b clone might have selective vulnerabilities in its complicated cellular signaling network which the other CMGT clones or normal cells did not carry. A possible approach to inquire the vulnerability was an unbiased molecularly targeted drug screening.

In 2009, Gupta et al. reported a chemical agent screening using the induced CSC model (Gupta et al., 2009). They searched more than ten thousands compounds to find out selective inhibitors against the induced CSC cells compared to the control cancer cells. As a result, salinomycin, a coccidiostat, was picked up due to its more than one hundred *in vitro* selectivity against CSCs. Salinomycin actually exhibited anti-cancer activity in a xenograft model. It was of great interest that the exact mechanism of anti-tumor activity of salinomycin had been unclear for years until the numerous following studies revealed involvement in apoptosis, interference with drug efflux transporters, inhibition of oxidative phosphorylation or inhibition of Wnt signaling (Naujokat and Steinhart, 2012). In other example, Kitambi et al. reported specific growth inhibitors

against human glioblastoma multiforme (GBM) cells (Kitambi et al., 2014). They screened approximately one thousand small molecule inhibitors comparing human GBM cell lines with human fibroblasts, mouse embryonic stem cells, mouse glial cells and mouse neurons. They found that GBM cells were specifically vulnerable to the one compound which they named as vaquinol. Vaquinol also showed anti-tumor effect against GBM cells *in vivo* without apparent toxicity. They further performed an unbiased short-hairpin RNA screening and concluded that anti-tumor effect of vaquinol was mediated by activation of MKK4, which belongs to the stress/GPCR agonists/cytokine/growth factor-activated pathway. Clear mechanism of vaquinol is still not fully understood since there has been only limited knowledge about the function of MKK4 molecule and its involvement in cancer. From these examples, an unbiased drug screening is considered to be one promising option to find out phenotypically distinct cell-specific vulnerability.

The hypothesis was that the metastatic CMGT clone had a distinct phenotype and unique cellular signaling when compared to the clone with lower malignancy, and this, in turn, might result in differential sensitivity to particular drugs. The aim of this study was to screen a novel class of agents using CMGT clones with different metastatic potentials to identify candidates for metastatic clone-specific chemotherapy. For that

purpose, I first performed expression analysis and phenotyping of two previously

established CMGT clonal cell lines. Next, an unbiased molecular targeting agent

screening system was adopted to select agents that differentially affected the growth of

the metastatic and non-metastatic clones. Finally, I explored the mechanism of action of

the candidate drugs to gain insight into the specific pathways responsible for the

observed differential sensitivity between the clones.

Materials and methods

Cell culture

The clonal cell lines (metastatic CHMp-5b and non-metastatic CHMp-13a) were previously established with a limiting dilution method from the canine mammary carcinoma cell line CHMp (Murai et al., 2012). The cells were maintained in RPMI 1640 medium (Wako Pure Chemical Industries) supplemented with 10% fetal bovine serum (Life Technologies) and 50 µg/mL gentamicin (Sigma-Aldrich) and incubated at 37°C in a humidified atmosphere of 5% CO_2.

cDNA microarray and real-time quantitative reverse-transcription (RT)-polymerase chain reaction (PCR)

Total RNA was extracted from both cell lines during exponential growth using an RNeasy Mini Kit (Qiagen) according to manufacturer instructions. Microarray analysis was performed as described (Tomiyasu et al., 2013). Briefly, RNA purity and integrity were assessed on an Agilent 2100 Bioanalyzer (Agilent Technologies). RNA integrity numbers were confirmed as being above 9.0. cDNA and Cy3-labeled cRNA were synthesized with a Quick Amp Labeling Kit and RNA Spike-In One-Color Kit (Agilent Technologies), respectively. The amplified cRNAs were isolated using the

RNeasy Mini Kit. The purified cRNAs were quantified and hybridized to a Canine ver.

2 (4 × 44K) array (Agilent Technologies) using a Gene Expression Hybridization Kit

(Agilent Technologies). The hybridized slide was washed with Gene Expression Wash

(Agilent Technologies) and scanned using a High-Resolution Microarray Scanner

(Agilent Technologies). Each cell line was analyzed in triplicate. Image analysis was

conducted using Feature Extraction software (Agilent Technologies) and the subsequent

data analysis was done using R software (Version 3.0.2) (R Development Core Team,

2005). Data incorporation, quantile normalization, and statistical analysis of

differentially expressed genes (DEGs) with the Empirical Bayes method were performed

using the *limma* R package (Smyth, 2005). The false discovery rate (FDR) threshold was

set at a *q* value < 0.001. A gene annotation file for this platform (GPL13605) was

retrieved from the NCBI Gene Expression Omnibus (Edgar et al., 2002) using the

GEOquery R package (Davis and Meltzer, 2007). The DEGs were sorted according to

the fold-change difference in expression between cell lines.

Selected DEGs were validated by quantitative RT-PCR (qPCR) according to

their reported association with tumor malignancy, prognosis, or cell differentiation in

epithelial cancers. The primers were designed using NCBI Primer-BLAST (Ye et al.,

2012) (Table 1). RNA was reverse-transcribed using RevaTra Ace qPCR RT Master Mix

(Toyobo) according to manufacturer instructions. qPCR was performed with

Thunderbird SYBR qPCR Mix (Toyobo). Amplification and fluorescence measurements

were performed using the Step One Plus Real-Time PCR system (Life Technologies).

The PCR condition was as follows: 1 cycle at 50°C for 2 min and 95°C for 10 min, and

40 cycles at 95°C for 15 s and 60°C for 1 min. Transcript expression was normalized to

the endogenous control glyceraldehyde-3-phosphate dehydrogenase (GAPDH).

Matrigel invasion assay

Culture inserts (24-well permeable support, 8.0 µm pore, Corning) were set on

a 24-well companion plate (Corning) and incubated with 200 µL Matrigel (500 µg/mL)

(Becton Dickinson) for 2 h at 37 °C. After removal of unsolidified residual liquid, a cell

suspension containing 25,000 cells in 500 µL serum-free RPMI medium was added to

each culture insert. RPMI medium supplemented with 10% fetal bovine serum was

added to the lower chamber of the companion plate as a chemoattractant. Uncoated wells

were used as a migration control. The plates were incubated for another 20 h at 37 °C in

a humidified 5% CO_2 atmosphere. Migrating and invading cells were fixed and stained

with phosphate-buffered saline (PBS) containing 6% glutaraldehyde and 0.5% crystal

violet. Cells were counted under a light microscope.

Measurement of aldehyde dehydrogenase (ALDH) activity

ALDH activity was measured using an Aldefluor assay kit (STEMCELL Technologies) as described previously (Michishita et al., 2012). Cells were suspended at a final density of 1×10^6 cells/mL in Aldefluor assay buffer containing 1 μM ALDH substrate (boron dipyrromethene aminoacetaldehyde) with or without the ALDH inhibitor diethylaminobenzaldehyde (DEAB), and incubated for 40 min at 37 °C. The frequency of high ALDH activity (ALDH[high]) was determined by flow cytometry using FACSAria and FACSDiva software (Becton Dickinson).

Inhibitor screening, cell viability assay, and colony forming assay

Inhibitor screening was performed using kits obtained from the Screening Committee of Anticancer Drugs (SCADS)[a] (kit 1, ver. 2.3; kit 2, ver. 1.3; kit 3, ver. 1.2; and kit 4, ver. 1.0). Two thousand cells were seeded in each well of a flat-bottom 96-well plate. After incubation for 24 h, 321 drugs were added at final concentrations of 0.1 and 1.0 μM (except for kit 4; 0.01 and 1.0 μM). After another 48 h of incubation, cell viability was analyzed using CCK-8 (Dojindo Laboratories).

---

[a] http://scads.jfcr.or.jp/kit/KIT_UI.html

Antimycin was obtained from LKT laboratories (St. Paul). Rotenone, oligomycin, doxorubicin hydrochloride, and paclitaxel were obtained from Wako Pure Chemical Industries. The cell viability results were fitted to a four-parameter logistic model and the 50% inhibitory concentration (IC50) values were calculated using R software and R package drc (Ritz and Streibig, 2005). Compound C (Merck Millipore MA) was added as an AMP-activated kinase (AMPK) inhibitor where indicated.

For the colony formation assay, 200 cells from a single suspension were seeded in a 6-well plate and incubated for 24 h. Rotenone, antimycin, or oligomycin were added and the plates were incubated for an additional 5 days. Colonies were fixed and stained as described for the Matrigel invasion assay. The number of colonies which consist of at least 50 cells were counted macroscopically.

Quantification of ATP from oxidative phosphorylation

Cells were suspended at 200,000 cells/mL in glucose-free RPMI (Sigma-Aldrich) supplemented with 2 g/L galactose (Sigma-Aldrich) to prevent ATP production from anaerobic glycolysis. A 100-µL aliquot of the cell suspension was added to a Nunc Luminunc 96-well plate (Thermo Fisher Scientific) and incubated for 24 h. Drugs were added and the amount of ATP in each well was quantified after 2 h by Mitochondrial

ToxGlo Assay (Promega Corporation).

Analysis of reactive oxygen species (ROS)

Twenty-thousand cells per well were seeded in a Nunc Fluoronunc 96-well plate (Thermo Fisher Scientific) and incubated for 24 h. After washing with PBS, cells were treated for 30 min with 0.001 to 1.0 μM antimycin. Subsequently, 2′,7′-dichlorofluorescein diacetate (10 μM; Wako Pure Chemical Industries) was added and fluorescence (Ex. 485 nm/Em. 535 nm) was measured immediately and 30 min later using an ARVO MX microplate reader.

Total ROS/Superoxide Detection Kit (Enzo Life Sciences) was used to assess ROS after longer drug exposures. Cells were treated with 0.1 μM of the indicated drugs for 6 h. Cells were then trypsinized, suspended in PBS, and labeled according to manufacturer instructions. Fluorescence was analyzed by FACS Calibur and BD Cellquest pro software (Becton Dickinson).

Western Blotting

Cells were lysed in RIPA buffer (50 mM Tris-HCl, 150 mM NaCl, 5 M EDTA, 1% Triton-X, and 0.1% sodium dodecyl sulfate [SDS]) with 10 mM NaF, 2 mM Na_3VO_4,

and Complete Mini proteinase inhibitor cocktail (Roche Diagnostics). Ten micrograms

of protein was resolved by SDS-polyacrylamide gel electrophoresis and blotted onto a

polyvinylidene difluoride membrane (Bio-Rad Laboratories). The membranes were

blocked for 1 h at room temperature in Tris-buffered saline with 0.1% Tween containing

5% non-fat dry milk. Antibody incubation conditions were as follows: polyclonal rabbit

anti-AMPK α1 antibody (Millipore, 1:1000, 4°C, overnight), polyclonal rabbit anti-

phospho-AMPKα antibody (Thr172) (Millipore, 1:500, 4°C, overnight), and

monoclonal mouse anti-actin antibody (Millipore, 1:10,000, 4°C, overnight). A

horseradish peroxidase-conjugated antibody against mouse IgG or rabbit IgG (GE

Healthcare) was used as the secondary antibody (1:10,000, room temperature, 1 h).

Membranes were developed using the ECL Prime Western Blotting Detection System

(GE Healthcare) and the ChemiDoc Image Lab system (Bio-Rad Laboratories).

Statistical analysis

All data are shown as means ± standard deviation (SD). Statistical methods and

software used were as follows: Two-sided Student's t test using Excel 2013 (Microsoft),

and Dunnett's test using R software and *multcomp* R package (Hothorn et al., 2008).

Choice of the statistical methods was described in each figure legend. Differences were

considered statistically significant when P value reached less than 0.05.

Results

Expression profiling and phenotype characterization

The two clonal cell lines used in this study had clearly distinct expression landscapes, with 2038 DEGs from 16206 differently annotated genes (Figs. 2.2A and B). The DEGs with the greatest fold change in CHMp-5b cells revealed higher expression of genes associated with tumor malignancy, such as *MMP1*, *PLS3*, *BMP2*, *MMP3, ABCC5,* and *ZEB1,* than in CHMp-13a cells. In contrast, CHMp-13a cells expressed significantly higher levels of several epithelium- and differentiation-related genes, including *KRT5*, *CLDN7, KRT19,* and *CDH1* (Figs. 2.2C and D). These expression profiles were validated by qPCR (Figs. 2.2E-N).

The Matrigel invasion assay showed a significantly higher percentage of CHMp-5b than CHMp-13a cells invaded the Matrigel layer (35.9 ± 13.8 vs. $5.9 \pm 0.7\%$) (Figs. 2.3A and B). CHMp-5b cells also contained a significantly larger proportion of ALDH^{high} cells ($9.6 \pm 5.1\%$) than CHMp-13a cells did ($0.2 \pm 0.1\%$) (Figs. 2.3C and D).

Drug screening using the SCADS inhibitor kits 1–4

The drug screening process and results are summarized in Figs 2.4A-C. Seven of the 321 tested drugs inhibited *in vitro* growth of CHMp-5b more strongly than CHMp-

29

13a under two different testing conditions (Fig. 2.4D). Three drugs in above candidate

seven drugs (antimycin, oligomycin, and rotenone) targeted the mitochondrial

respiratory chain complex (MRC), and thus, might inhibit mitochondrial oxidative

phosphorylation (OXPHOS). Because all the drugs targeting the MRC were listed up as

the selective inhibitors, this result indicated the importance or vulnerability of

mitochondrial OXPHOS in metastatic clone. We further focused on these drugs.

Sensitivity to mitochondrial respiratory complex inhibitors

MRC inhibitors (MRCIs) exerted a strong inhibitory effect on CHMp-5b cell

growth compared to CHMp-13a. The IC_{50} values of CHMp-5b and CHMp-13a cells for

rotenone, antimycin, and oligomycin, respectively, were 0.028, 0.0062, and 0.032 for

CHMp-5b and 0.12, not determined (> 1.0), and 10 µM for CHMp-13a (Figs. 2.5A-D).

Similarly, the three MRCIs inhibited the number of colonies formed by the CHMp-5b

line more strongly than that formed by the CHMp-13a line (Figs. 2.6A-C). The

sensitivities of CHMp-5b and CHMp-13a cells to doxorubicin were similar and

surprisingly, CHMp-5b was rather resistant to paclitaxel (Figs. 2.6D-E). The IC_{50} values

for doxorubicin and paclitaxel were 0.38 and 0.19 for CHMp-5b and 0.27 and 0.051 µM

for CHMp-13a, respectively.

Effect of MRCIs on ATP levels, AMPK activation, and ROS production

Treatment of CHMp-5b and CHMp-13a cells with MRCIs depleted mitochondrial ATP production almost completely (Fig. 2.7A). Subsequent activation of AMPK was observed in both cell lines, although the extent of activation was relatively stronger in CHMp-13a (Fig. 2.7B). The presence of an AMPK inhibitor limited the cytotoxic effect of MRCIs in CHMp-13a cells; treatment of CHMp-5b cells with MRCIs inhibited cell growth regardless of the presence or absence of an AMPK inhibitor (Figs. 2.8A-C).

ROS decreased in both cell lines after 30-min exposure to antimycin (Figs. 2.9A,B). However, by 6 h after treatment with each of the three MRCIs, cellular ROS levels were indistinguishable from the control except for oligomycin, which slightly increased ROS in both cell lines (Fig. 2.9C).

Discussion

The two clonal cell lines used in this study had quite distinct expression and phenotypic profiles even though they have been cloned simultaneously from one parental CMGT cell line. CHMp-5b cells exhibited higher expression of *MMP1, MMP3, PLS3, BMP2, ZEB1,* and *ABCC5.* MMP1 and MMP3 are enzymes which digest ECM molecules enabling cellular movement (Overall and Kleifeld, 2006). PLS3, BMP2, and ZEB1 are involved in the epithelial–mesenchymal transition (EMT) process of tumor cells which facilitate cell motility. ABCC5 belongs to a subfamily of ATP-binding cassette (ABC) transporters and associated with multidrug resistance in tumors and stem cell homeostasis in humans and dogs (Holohan et al., 2013; Oguri et al., 2006; Tomiyasu et al., 2010). With these mechanisms, most of these molecules have been associated with poor prognosis in human breast cancer and CMGT (Cheng et al., 2008; Remacle et al., 1998; Santos et al., 2012). As many publications about broad range of cancer have revealed so far (Hanahan and Weinberg, 2011), the phenotypically metastatic clone showed strong expression of EMT-related, CSC-related and invasion-related genes. These results were further validated by the matrigel invasion and ALDH assays. ALDH activity is a cancer stem cell phenotype marker in the CMGT cell line (Michishita et al., 2012).

In contrast, CHMp-13a cells showed high expression of *KRT5, CLDN7, KRT19,* and *CDH1*. These genes are indicators of epithelial differentiation in normal mammary glands and some are favorable prognostic markers in human breast cancer (Gusterson and Stein, 2012; Kashiwagi et al., 2011; Kominsky et al., 2003; Shao et al., 2012). Several studies have reported that maintenance of E-cadherin (*CDH1*) expression indicates a better prognosis in CMGT. (Gama et al., 2008; Restucci et al., 2007; Yoshida et al., 2014). These results of phenotyping supported the feasibility of adopting CHMp-5b cells as a representative of EMT-induced, undifferentiated, and metastatic clones, and CHMp-13a cells as a representative of epithelial, differentiated, and non-metastatic clones.

The MRCIs, rotenone, antimycin, and oligomycin, were relatively specific inhibitors for the proliferation of CHMp-5b cells compared with CHMp-13a cells. Rotenone, which binds to and inhibits mitochondrial complex 1 (NADH dehydrogenase), is a widespread agricultural insecticide and is used to induce a Parkinson's disease-like syndrome in animals (Coulom and Birman, 2004; Xiong et al., 2012). Antimycin is an inhibitor of mitochondrial complex 3 (ubiquinol-cytochrome-*c* reductase) and is used as a piscicide in industrial fish farming (Seipke and Hutchings, 2013). Oligomycin is a macrolide antibiotic generated by *Streptomyces spp.* that targets the final component of

the mitochondrial respiratory chain (mitochondrial complex 5, F_0F_1 ATP synthase complex). Oligomycin is commonly used to study mitochondrial ATP synthesis (Pagliarani et al., 2013).

Several studies have investigated MRCIs as anti-tumor agents. Their mechanism of action was suggested to be associated with the disruption of OXPHOS. Some studies have proposed that the anti-tumor effect of antimycin is cell cycle inhibition and apoptosis caused by elevated ROS production (Han and Park, 2009a, 2009b). In mitochondria, electrons derived from NADH and $FADH_2$ react with surrounding oxygen molecules to generate superoxide anion, which interacts with other molecules to yield additional ROS unless adequately scavenged. Disruption of OXPHOS can cause overproduction and leakage of ROS from mitochondria (Balaban et al., 2005; Ishikawa et al., 2008), which induces protein and DNA damage which lead to apoptosis and cell cycle arrest (Maryanovich and Gross, 2013). However, total ROS were diminished upon short-term exposure to antimycin, and there was no obvious difference in ROS levels between the two clones at any time. This result was different from that of previous studies (Han and Park, 2009a, 2009b), however data were not comparable because they used much higher concentrations (up to 100 µM) and longer exposure times (72 h). Antimycin, at the concentrations used in this study, may have

simply attenuated the OXPHOS activity, resulting in less ROS production.

Our experiments suggested that the toxic effect of MRCIs in CMGT cells was associated with the decrease in mitochondrial ATP production and activation of AMPK. This mechanism has been rarely addressed in studies of the anti-tumor effect of rotenone, antimycin, and oligomycin. However, a rigorous investigation has recently been performed using metformin, another mitochondrial complex 1 inhibitor and potent anti-tumor agent (Emami Riedmaier et al., 2013; Rizos and Elisaf, 2013). Metformin is used to treat type 2 diabetes and inhibits liver glucogenesis in an AMPK-dependent manner. AMPK resides in the cytoplasm and is activated when the cellular AMP/ATP ratio drops. Activated AMPK subsequently inhibits phosphorylation of mammalian target of rapamycin (mTOR) via interaction with the mTOR inhibitor TSC2. This inhibits cell proliferation. AMPK is thus thought to mediate cellular metabolic homeostasis under energetic stress and is considered to be a potent tumor suppressor due to its suppressive effect on mTOR, a well-known oncogene. The MRCIs in this study inhibited mitochondrial ATP production almost completely while activating AMPK in both CMGT clones. However, when the drugs were added with the AMPK inhibitor Compound C, their anti-proliferative effect was abolished in CHMp-13a, but not in CHMp-5b cells. Thus, the anti-proliferative effect of MRCIs in CHMp-13a cells was

dependent upon energy depletion and AMPK activation, but the effect on CHMp-5b

cells was considered to be largely AMPK-independent. This may contribute to the

differential sensitivity of the two CMGT clones.

An interesting correlation between the results of this study and those in previous

literature, including studies using metformin, is the finding that the MRCIs selectively

target a malignant subpopulation of cancer cells (Lonardo et al., 2013; Seipke and

Hutchings, 2013; Song et al., 2012). Lonardo et al. used a pancreatic cancer cell line and

showed that treatment with metformin decreased the expression of stem cell markers

and the clonal expansion capacity of the cancer stem cell population. Moreover, the

AMPK-independent and yet unspecified anti-tumor effect of MRCIs has also been

reported by others and has been recently focusing attention (Liu et al., 2014; Lonardo et

al., 2013).

The hypothesis of this chapter was that different phenotypes of the two clones

would be mediated by the different cellular signaling, and this difference may leave a

specific vulnerability in the signaling network of the metastatic clone. Thus, distinct

mechanism of response to the MRCIs is considered to indicate the existence of signaling

or functional difference related to OXPHOS which was the common biological process

disrupted by the drugs. On the other hand, two clones had similar sensitivity to the most

of the rest of the agents examined in the screening, including traditional chemotherapeutic agents such as doxorubicin and paclitaxel. This result would paradoxically support the hypothesis further because the both clones had come from the one cancer cell line, so should have similar sensitivity to most kind of disruption of the cellular function.

Conclusion

In this chapter, the potential of MRCIs as selective anti-tumor agents against a metastatic CMGT clone has been demonstrated. Different cellular responses to MRCIs exposure were observed between metastatic and non-metastatic clone, either AMPK dependent or independent. However, several important questions remain to be answered: the mechanism of action of the MRCIs in the metastatic clone, the relationship between the higher sensitivity of CHMp-5b cells and their malignancy, the effect of the MRCIs on cellular phenotype, and the potential to apply MRCIs as anti-tumor agents in veterinary medicine. Because the MRCIs used in this study are not approved for medical use, other drugs with a similar mechanism should be considered for further studies and potential clinical use.

Parental CHMp canine inflammatory mammary gland carcinoma

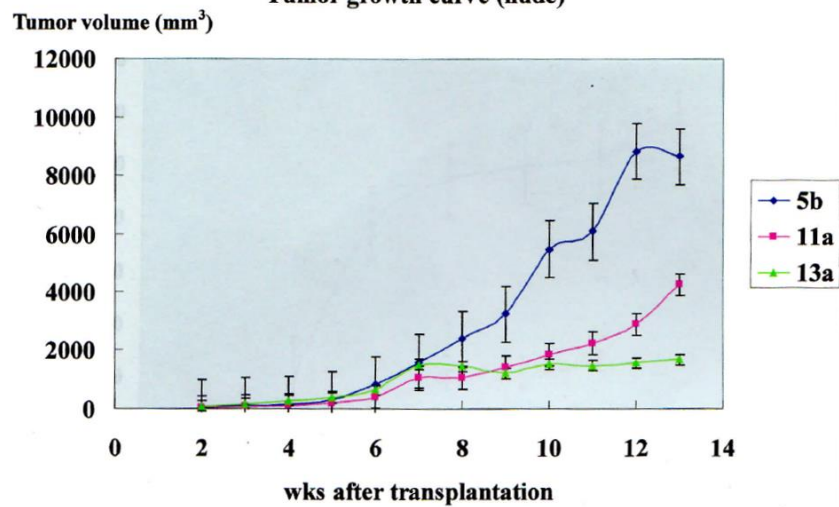Cloning of 23 different subclones
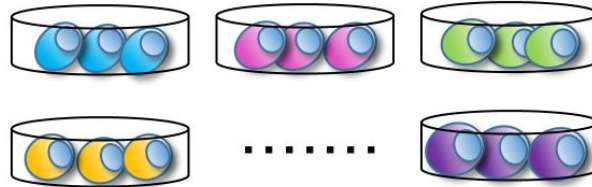
Orthotopic transplantation into nude mice

CHMp-5b

CHMp-11a

CHMp-13a

Tumor growth curve (nude)

Tumor volume (mm^3)

wks after transplantation

Clone name	Animals with lung nodules
CHMp-5b	4 / 6
CHMp-11a	0 / 6
CHMp-13a	0 / 6

Fig. 2.1. Clonal diversity of the canine mammary carcinoma cell line.

Cloning from the parental tumor cell line and evaluation of tumorigenic and metastatic potential of the selected clone were previously performed. Total of 23 clones were generated from the CHMp cell line, and three clones (CHMp-5b, CHMp-11a and CHMp-13a) were selected for further evaluation as the phenotypically representative clones. The results in xenograft experiment indicated that clonal diversity would exist in the CHMp cell line and metastatic potential would be restricted to the specific clone such as CHMp-5b. The results figure and table were reproduced from the previous study (Murai et al., 2012).
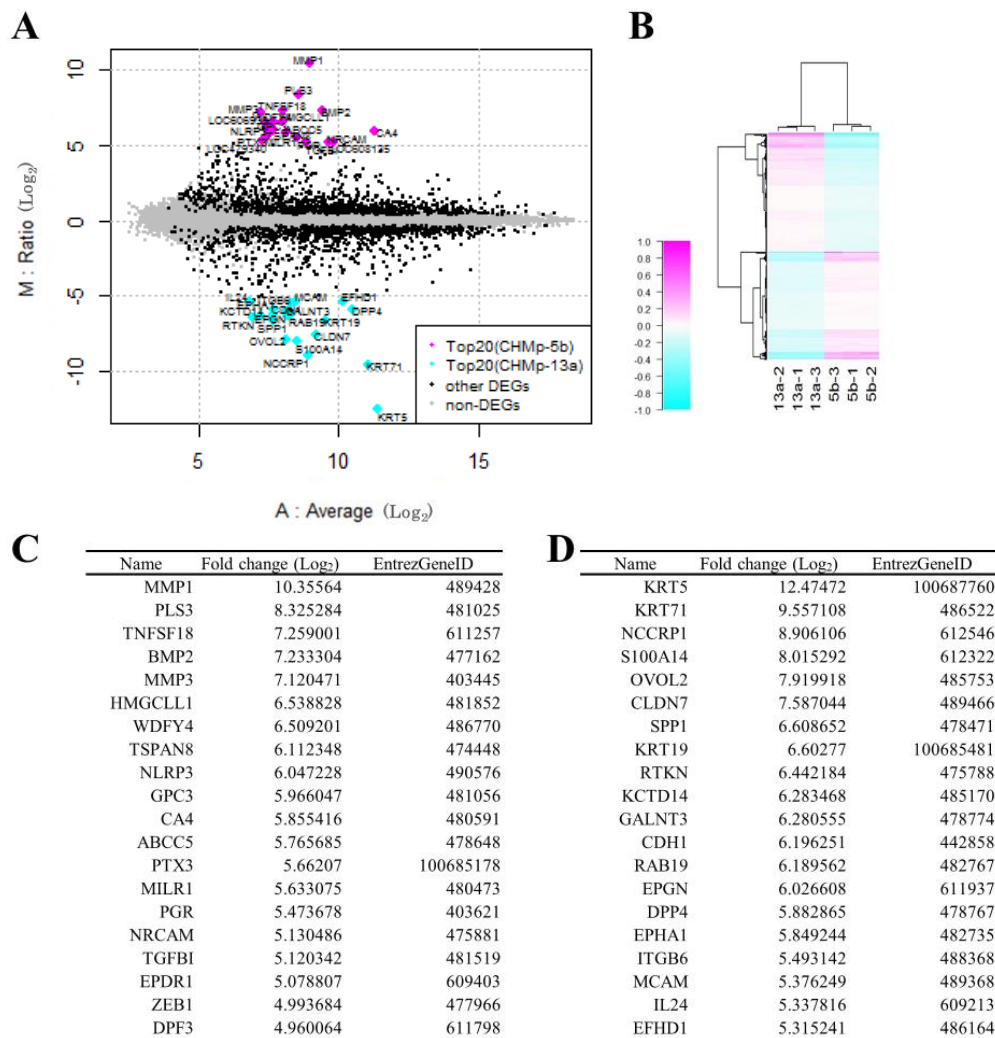
A

M : Ratio (Log$_2$)

A : Average (Log$_2$)

Legend:
- Top20(CHMp-5b)
- Top20(CHMp-13a)
- other DEGs
- non-DEGs

B

13a-2 13a-3 13a-1 5b-3 5b-1 5b-2

C

Name	Fold change (Log$_2$)	EntrezGeneID
MMP1	10.35564	489428
PLS3	8.325284	481025
TNFSF18	7.259001	611257
BMP2	7.233304	477162
MMP3	7.120471	403445
HMGCLL1	6.538828	481852
WDFY4	6.509201	486770
TSPAN8	6.112348	474448
NLRP3	6.047228	490576
GPC3	5.966047	481056
CA4	5.855416	480591
ABCC5	5.765685	478648
PTX3	5.66207	100685178
MILR1	5.633075	480473
PGR	5.473678	403621
NRCAM	5.130486	475881
TGFBI	5.120342	481519
EPDR1	5.078807	609403
ZEB1	4.993684	477966
DPF3	4.960064	611798

D

Name	Fold change (Log$_2$)	EntrezGeneID
KRT5	12.47472	100687760
KRT71	9.557108	486522
NCCRP1	8.906106	612546
S100A14	8.015292	612322
OVOL2	7.919918	485753
CLDN7	7.587044	489466
SPP1	6.608652	478471
KRT19	6.60277	100685481
RTKN	6.442184	475788
KCTD14	6.283468	485170
GALNT3	6.280555	478774
CDH1	6.196251	442858
RAB19	6.189562	482767
EPGN	6.026608	611937
DPP4	5.882865	478767
EPHA1	5.849244	482735
ITGB6	5.493142	488368
MCAM	5.376249	489368
IL24	5.337816	609213
EFHD1	5.315241	486164

Fig. 2.2. Gene expression profiles of the CMGT cell lines.

(A) M-A plot of the cDNA microarray analysis. The X-axis indicates the average expression of each gene. The Y-axis shows the fold change in expression between the two cell lines. (B) Gene expression heat map of DEGs and a hierarchical cluster analysis for the experimental replicates and the DEGs. (C, D) Listing of the most up-regulated genes in CHMp-5b (C) and CHMp-13a (D) cells. Hypothetical genes are omitted.. DEG: differentially expressed gene
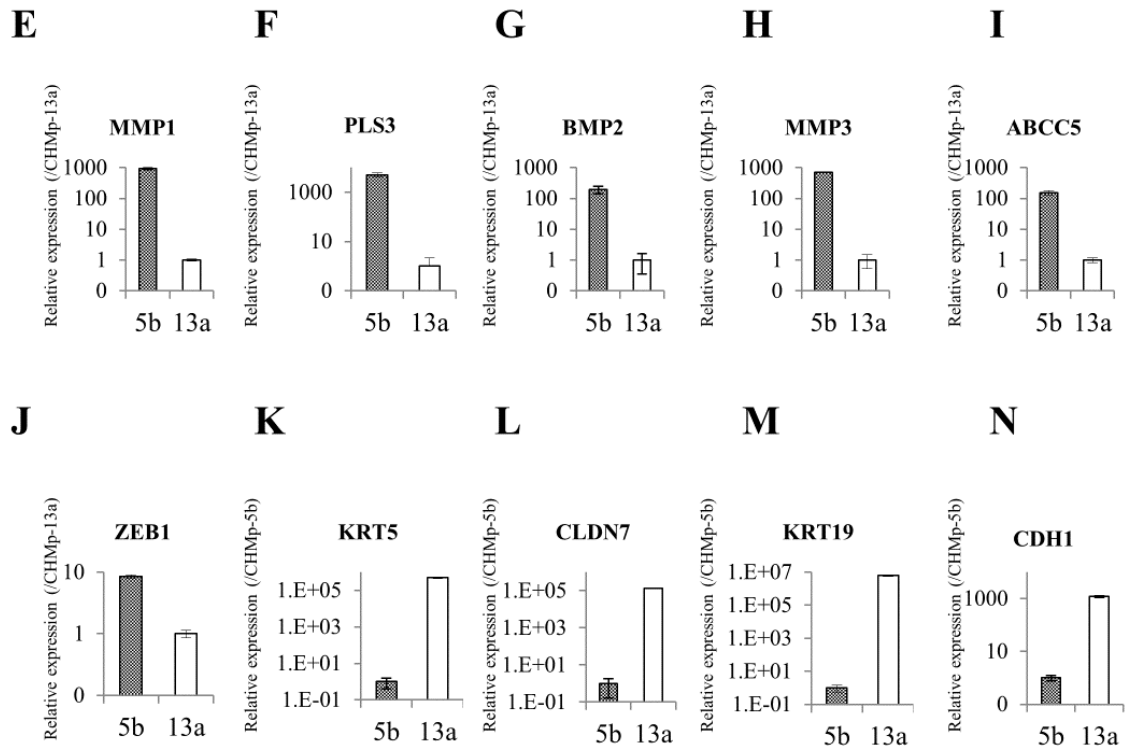
Fig. 2.2 Gene expression profiles of the CMGT cell lines (*continued*).

(E–N) RT-PCR validation of selected genes from the list of top DEGs. DEG: differentially expressed gene
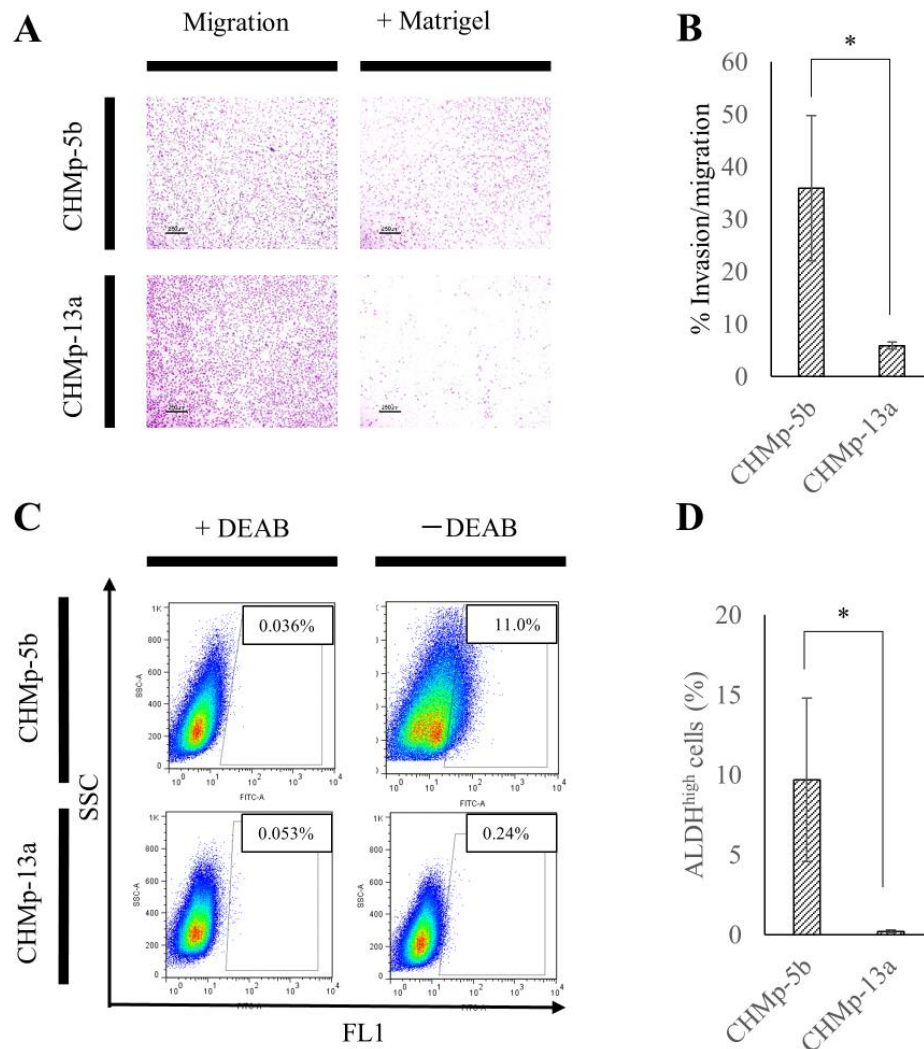
Fig. 2.3. Invasive capacity and ALDH activity in CHMp-5b and CHMp-13a.

(A, B) Matrigel invasion chamber assay; cells were incubated for 20 h on culture inserts with or without a Matrigel layer. (C, D) Aldefluor assay; cells were stained with the Aldefluor assay kit with or without 1.5 mM diethylaminobenzaldehyde (DEAB) (negative control, ALDH inhibitor). *P < 0.05 (t-test)
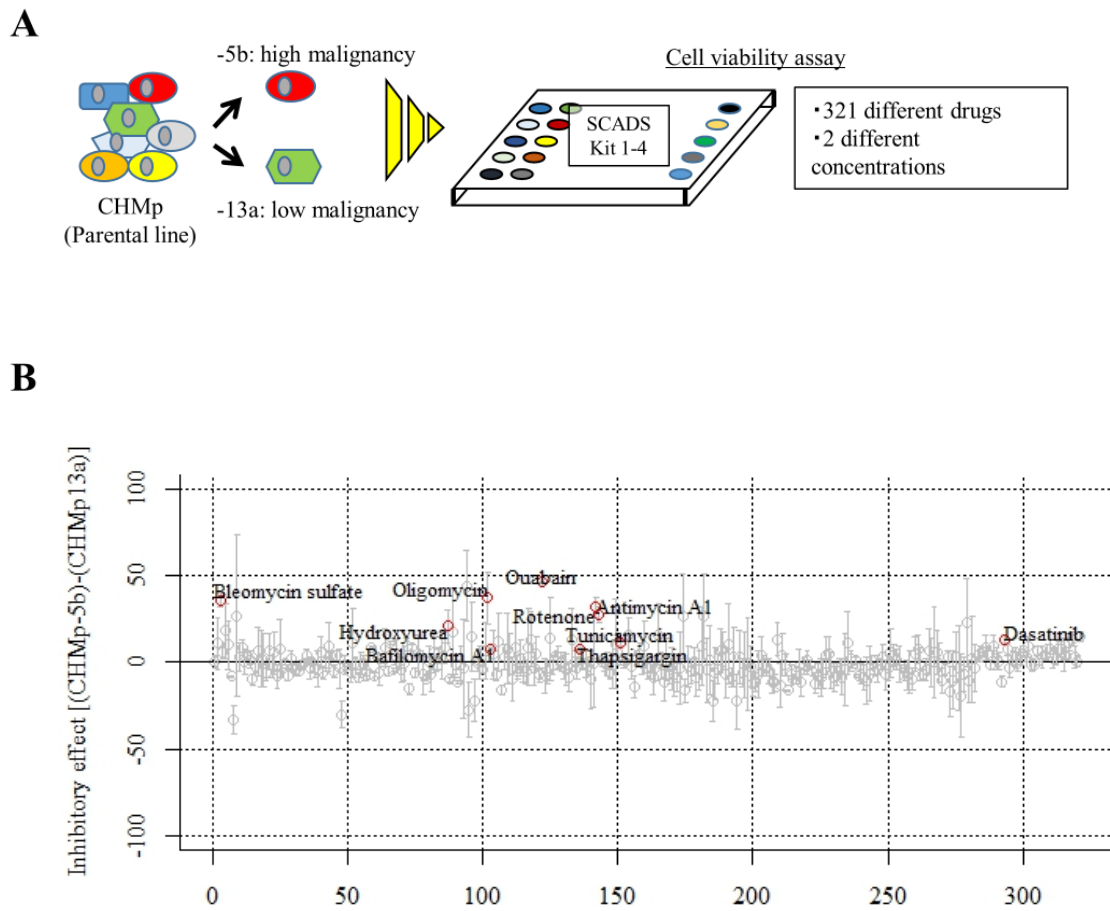
Fig. 2.4. Drug screening (SCADS inhibitor kits 1-4).

(A) Schematic of the procedure. The cell viability assay was performed at two different drug concentrations. (B) Drug screening at lower drug concentrations. The Y-axis shows the difference in inhibitory effect (% Control) between the two cell lines. Positive values indicate growth inhibition was greater in CHMp-5b. The X-axis represents drugs by number from 1 to 321. The drugs that significantly ($P < 0.05$) inhibited CHMp-5b growth are shown in red and labeled with the name of the drug.

C
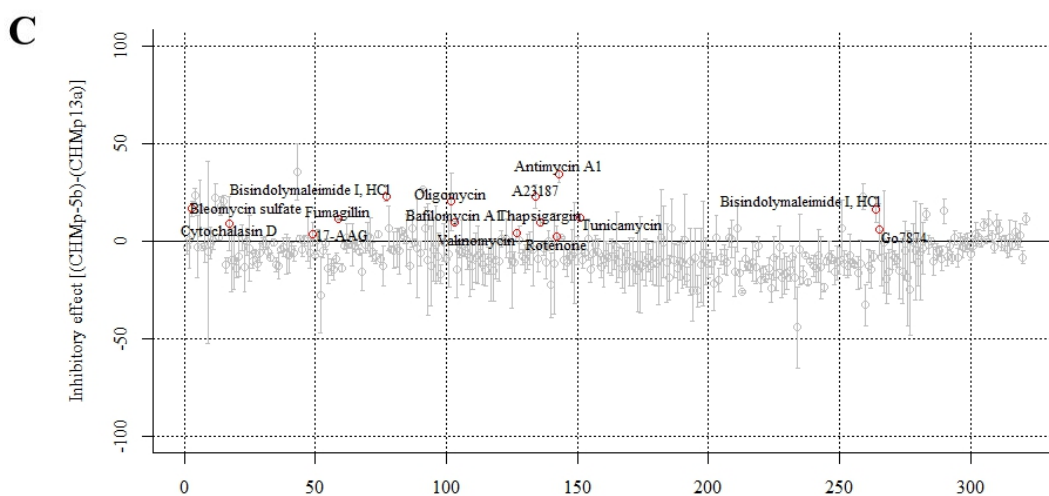
D

Drug	Molecular target	p value	
		0.1 μM	1.0 μM
Antimycin A1	mitochondrial complex III	0.0022	0.0024
Bafilomycin A1	V-ATPase	0.0030	0.0005
Bleomycin sulfate	DNA	0.0115	0.0486
Oligomycin	F1-ATPase (mitochondrial complex V)	0.0387	0.0045
Rotenone	mitochondrial complex I	0.0018	0.0279
Thapsigargin	Ca-ATPase	0.0162	0.0022
Tunicamycin	glycosylation	0.0056	0.0011

Fig. 2.4. Drug screening (SCADS inhibitor kits 1-4) (*continued*).

(C) Drug screening at higher drug concentration. The Y-axis shows the difference in inhibitory effect (% Control) between the two cell lines. Positive values indicate growth inhibition was greater in CHMp-5b. The X-axis represents drugs by number from 1 to 321. The drugs that significantly ($P < 0.05$) inhibited CHMp-5b growth are shown in red and labeled with the name of the drug. Bisindolymaleimide I, HCl was both on the kit 1 and 3. (D) Seven candidate drugs and their molecular targets.
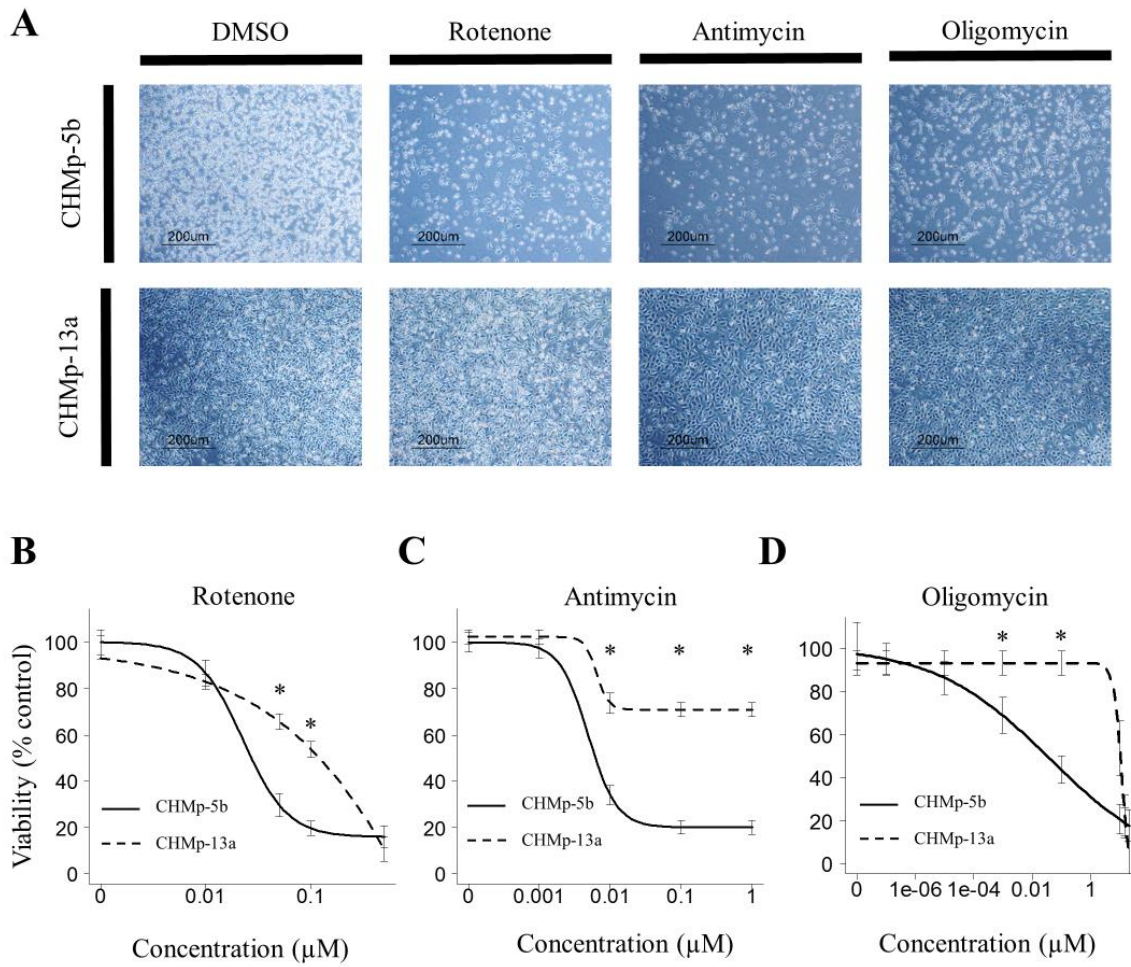
Fig. 2.5. The cytotoxic effect of rotenone, antimycin, and oligomycin in CHMp-5b and CHMp-13a. (A) Microscopic images after 48 h incubation with DMSO (control) and each MRCI at 0.1 µM. (B, C, D) Dose-response curves were generated based on the four-parameter logistic model. *$P < 0.05$ (t-test; CHMp-5b versus CHMp-13a)
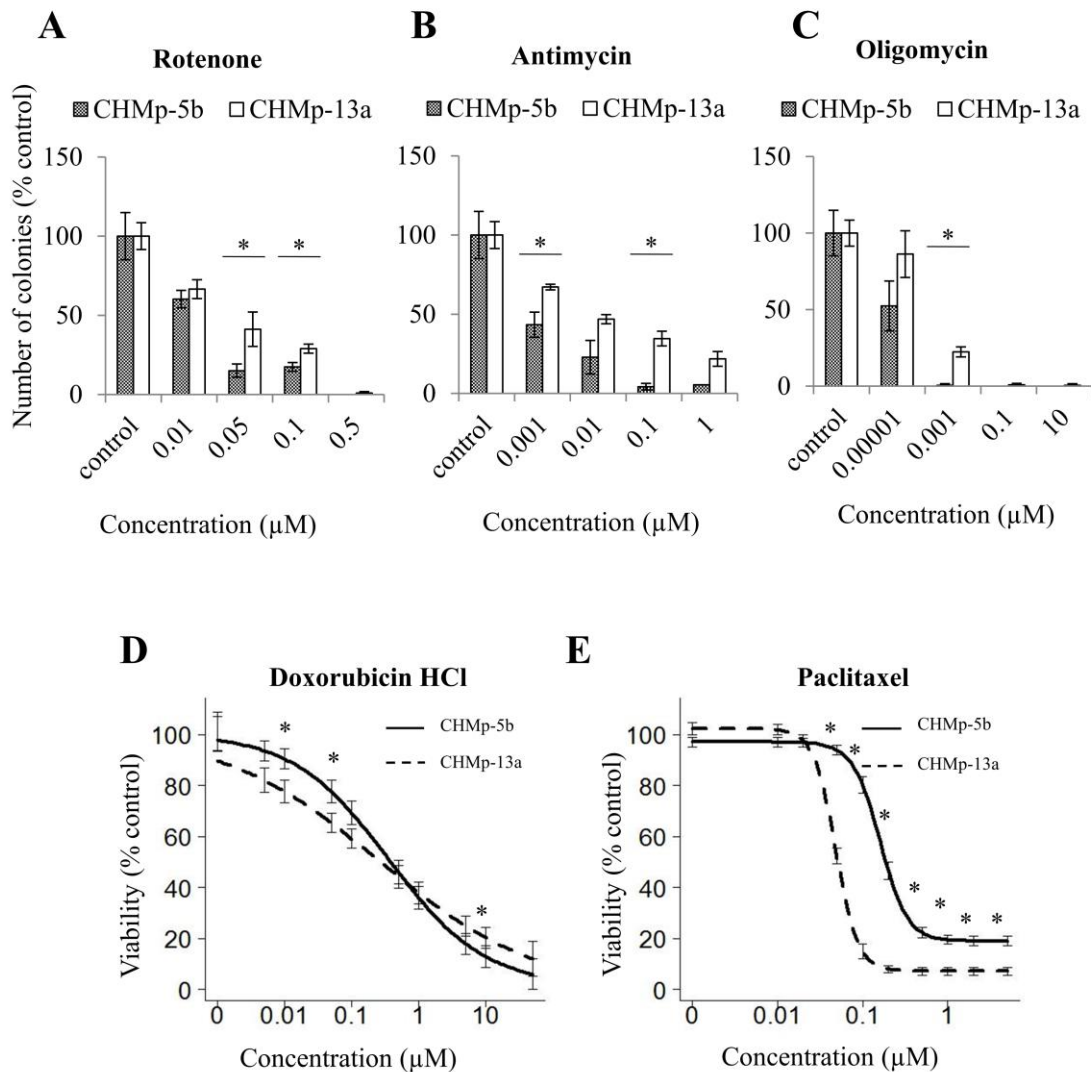
Fig. 2.6. Colony forming assay in the presence of the MRCIs and sensitivity to two typical chemotherapeutic agents.

(A, B, C) Colony forming assay of CHMp-5b and CHMp-13a cells with rotenone, antimycin, or oligomycin. (D, E) Viability of CHMp-5b and CHMp-13a cells after treatment with doxorubicin or paclitaxel. *$P < 0.05$ (t-test; CHMp-5b versus CHMp-13a)
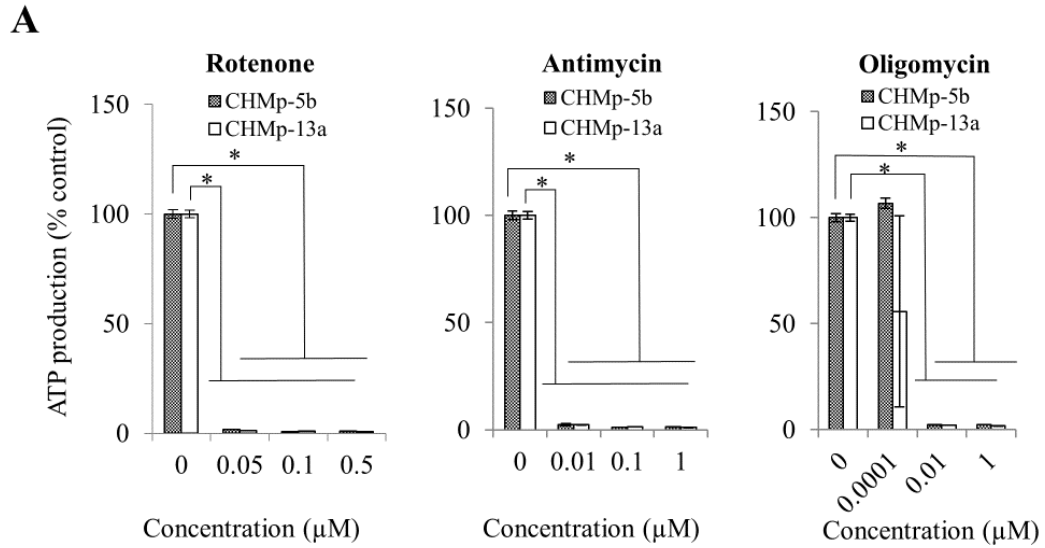
A

Fig. 2.7. The effect of MRCIs on cellular ATP production and AMPK activation in CHMp-5b and CHMp-13a cells.

(A) The change in ATP production in the absence of glucose was quantified using the Mitochondrial ToxGlo Assay after 90-m incubation with the MRCIs.. *$P < 0.05$ (Dunnett's test; Treatment versus control)
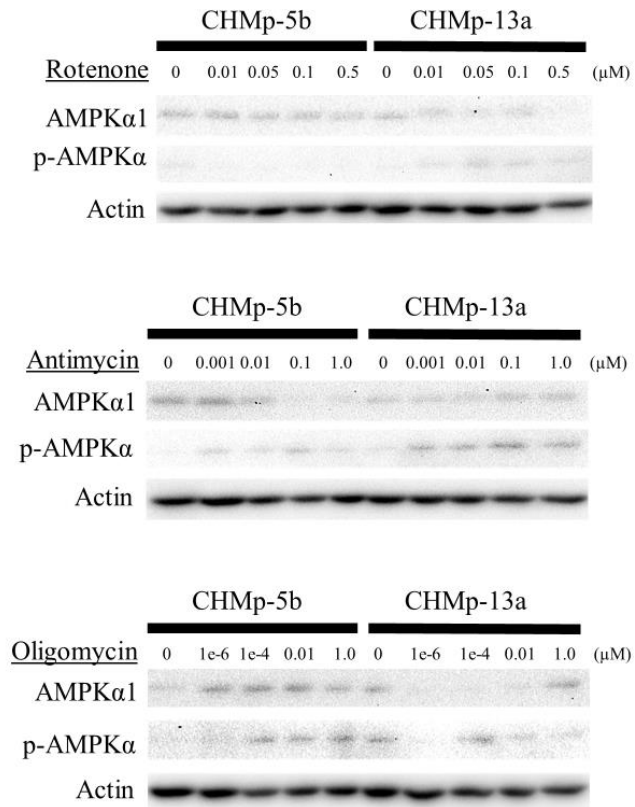
B

Fig. 2.7. The effect of MRCIs on cellular ATP production and AMPK activation in CHMp-5b and CHMp-13a cells (*continued*).

(B) Western blots of AMPKα1, phosphorylated AMPKα (activated), and actin (loading control) in CHMp-5b and CHMp-13a cells treated with the MRCIs.
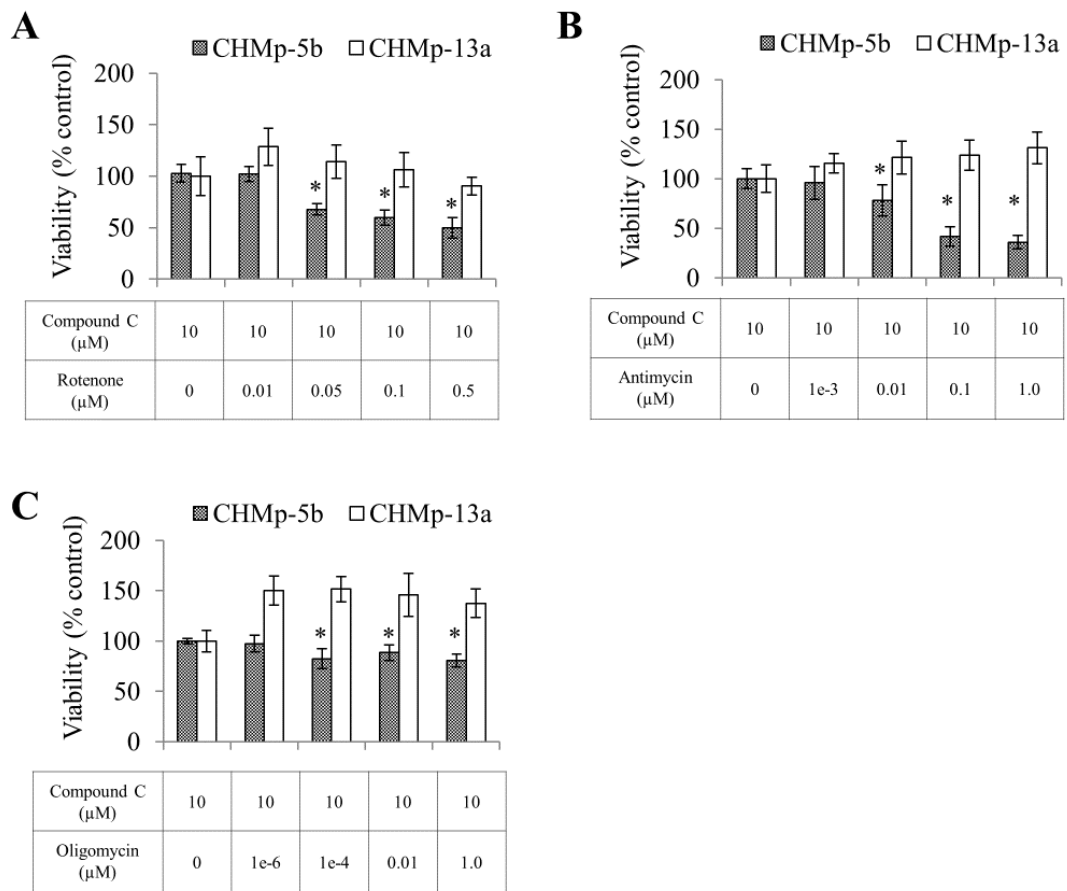
Fig. 2.8. Cytotoxic effect of the MRCIs in the presence of the AMPK inhibitor Compound C.

Cell viability after exposure to MRCIs in the presence of AMPK inhibitor Compound C

(A) Rotenone. (B) Antimycin. (C) Oligomycin. *$P < 0.05$ (t-test; CHMp-5b versus CHMp-13a)

Fig. 2.9. Change in cellular ROS content following exposure to the MRCIs.

(A, B) Change in ROS content in CHMp-5b and CHMp-13a cells after treatment with antimycin for 30- and 60-m. (C) Change in ROS content after a 6-h exposure to 0.1 μM MRCIs. *$P < 0.05$ (Dunnett's test; Control versus treatment).

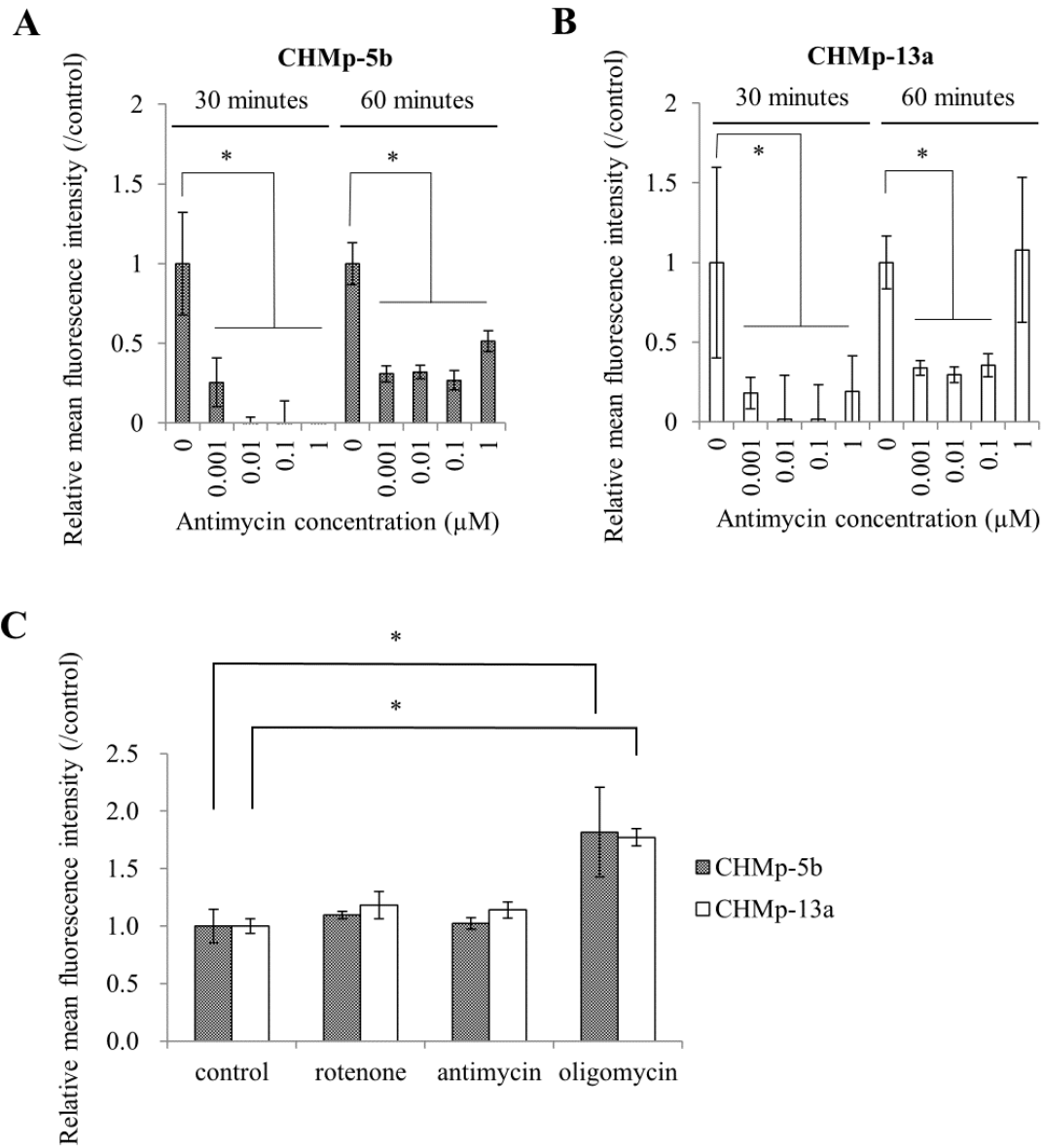| Gene	Accession number	Primer sequence	
		Forward (5′ to 3′)	Reverse (5′ to 3′)
MMP1	XM_546546.4	TTCGGGGAGAAGTGATGTTCC	AAGTCCGTTTGGCAGGTTTG
PLS3	XM_005641713.1	GCACCAAAAGGACAAAAGGAAGG	CATCAGCAGGGGTAACAAACTG
BMP2	XM_534351.4	CCTACATGCTGGACCTGTACC	ATCTCCGGGTTGTTTTCCCA
MMP3	NM_001002967.1*	ACGATGATGAACAATGGACAAGC	CAGCCGAGTGAAAGAGACCC
ABCC5	NM_001128100.1*	CCCATCGCCTACATACAGTCC	CTTGTTCTCCACAGCAGCAAAC
ZEB1	XM_003433703.2*	AATCAGGAGGAAAGGCAAGACA	CACACAAATCACAAGCATACATTCC
KRT5	XM_005636793.1*	TAGGCAGAGGACATGCTGTTTG	GAGATCGCCACCTACAGGAA
KRT19	NM_001253742.1	GCGACTACAGCCACTACTTCA	GCAGGACAATCTTGGAGTTCTCA
CDH1	NM_001287125.1	GGCAGGGTGAGTTTTGAAGGA	CACTTTGAATCGGGTGTCATCA
CLDN7	XM_005619967.1*	TGATGAGCTGCAAAATGTACGAC	ATGAAAATGATGCCTCCGGTCA
GAPDH	NM_001003142	TGACACCCACTCTTCCACCTTC	CGGTTGCTGTAGCCAAATTCA

*: Other transcript variants with the same amplicon size exist based on 100% sequence homology

Table 2.1. Primer information.

Chapter 3

Anti-tumor effect of metformin

in canine mammary gland tumor cells

Introduction

Metformin (1,1-dimethylbiguanide) is a biguanide derivative widely used for the treatment of type 2 diabetes. The primary molecular target of metformin is the mitochondrial respiratory complex 1, NADH dehydrogenase. Inhibition of mitochondrial oxidative phosphorylation (OXPHOS) reduces cellular synthesis of ATP, which in turn activates AMP-activated protein kinase (AMPK). Activated AMPK alters the cellular metabolism from anabolic to catabolic through multiple transcriptional regulatory elements, leading to inhibition of glucogenesis in the liver and enhanced uptake of glucose in muscle (Emami Riedmaier et al., 2013; Quinn et al., 2013). These mechanisms contribute to the decreased serum glucose levels observed in diabetic patients.

Epidemiology studies in diabetic patients have revealed a possible anti-tumor effect of metformin, as its use was associated with a 20–80% reduction in the incidence of various types of cancer, including hepatocellular, colorectal, pulmonary, and pancreatic carcinomas (Decensi et al., 2010; Franciosi et al., 2013; Noto et al., 2012). Other studies also reported a 35% reduction in tumor-related mortality with metformin (Franciosi et al., 2013; Noto et al., 2012).

Based on these observations, the anti-tumor effect of metformin has been

studied *in vitro* and *in vivo* using various human cancer cell lines and animal tumor models. Human cell lines have included glioblastoma and breast, pancreatic, liver, and prostate cancer cells (Ben Sahra et al., 2008; Dowling et al., 2007; Lonardo et al., 2013; Saito et al., 2013; Song et al., 2012; Würth et al., 2013; Zhu et al., 2014). The anti-tumor effect of metformin is thought to be mediated through AMPK activation, similar to the anti-diabetic effects (Dowling et al., 2007; Song et al., 2012). Activation of AMPK inhibits mammalian target of rapamycin (mTOR) complex 1, a signaling molecule involved in cellular survival and protein synthesis through its effector targets, such as S6 kinase (S6K) and 4E-BP (Mamane et al., 2006). Other possible anti-tumor mechanisms has been reported to involve inhibition of insulin-like growth factor signaling and induction of cell cycle arrest (Emami Riedmaier et al., 2013; Quinn et al., 2013).

Canine mammary gland tumors (CMGTs) are the most prevalent tumor in sexually intact female dogs as stated in the previous chapter (Withrow et al., 2012). Systematic chemotherapy is expected to improve prognosis of CMGT patients because the metastatic rate of malignant CMGT is high and metastasis is associated with poor prognosis (Clemente et al., 2010; Withrow et al., 2012). In the previous chapter, it was found that mitochondrial respiratory chain complex inhibitors (MRCIs) had a selective

anti-tumor effect on metastatic CMGT cells in vitro using unbiased molecular targeting

agent screening. However, the MRCIs studied in the previous chapter, namely rotenone,

antimycin, and oligomycin, were experimental drugs or pesticides, and not available for

medical use. Because long-term use of metformin is devoid of severe side effects

(Ekström et al., 2012), and metformin inhibits mitochondrial respiratory complex 1 in a

similar manner to rotenone, it was hypothesized that metformin has an anti-tumor effect

on CMGT cells, especially on the metastatic clone, and could be suggested for future

clinical use. The aim of this chapter was to evaluate the anti-tumor effects of metformin

on CMGT cells both *in vitro* and *in vivo*, and to investigate its mechanism of action.

Materials and methods

Cell culture

Two clonal CMGT cell lines with different phenotypes, CHMp-5b (metastatic) and CHMp-13a (non-metastatic) cells, were used (Murai et al., 2012). The cell lines were maintained in RPMI 1640 medium (Wako Pure Chemical Industries) supplemented with 10% fetal bovine serum (FBS; Life Technologies) and 50 µg/mL gentamicin (Sigma-Aldrich) at 37 °C in a humid atmosphere with 5% CO_2. All other cell incubation steps used these conditions unless otherwise stated.

Cell viability assay

CMGT cells were seeded at a density of 2000 cells/well in 96-well flat-bottom plates and allowed to attach and proliferate for 24 h. Metformin (1,1-dimethylbiguanide hydrochloride; Sigma-Aldrich; catalog number D150959) was diluted in the complete medium and added to each well at the indicated final concentrations. Plates were incubated for 6, 12, 24, or 48 h before cell viability was determined (Cell Counting Kit-8 [CCK8]; Dojindo Laboratories). The reaction mix (1:10 dilution of CCK-8 in medium) was incubated for another 2 h. The absorbance at 450 nm was measured using a plate reader (ARVO MX, PerkinElmer).

The effect of AMPK activation on cell viability was examined using the AMPK inhibitor, Compound C (InSolution Compound C, 10 mM in dimethyl sulfoxide, Merck Millipore). Compound C was diluted in medium and applied simultaneously with metformin at a final concentration of 10 μM.

The concentration response curves and half-maximal inhibitory concentration (IC_{50}) were estimated based on a four-parameter logistic model using R software (Version 3.0.2) (R Development Core Team, 2005) and R package *drc* (Ritz and Streibig, 2005).

Immunodeficient mouse xenograft model

The study protocol was approved by The University of Tokyo Animal Care and Use Committee (accession number 14-857). Four-week-old female balb/c nu/nu mice obtained from a domestic distributor (Japan SLC Inc.) were housed for one week prior to experimentation. The housing environment was kept at 25°C ± 2°C, 40–60% humidity, and 12-h light and dark cycle. The mice had free access to food and water throughout experiment. The mice received systemic irradiation (4 Gy) and were prepared for tumor cell inoculation 3 days later; they were anesthetized using isoflurane, after which subcutaneous injection of CHMp-5b cells suspended in phosphate-buffered saline (PBS;

5×10^6 cells in 100 μL per animal) was administered to their dorsal trunk. On day 5, when the tumors became palpable, the mice were randomly assigned to control (n = 5) and metformin (300 mg·kg-1·day-1 administered in drinking water; n = 5) groups. Treatment had continued for three weeks during which tumor radius, body weight, and water consumption were recorded every three days. On day 26, the mice were euthanized and the tumors were resected and weighed. The lungs were removed and processed by formalin fixation and paraffin embedding. The blocks were cut into 4-μm sections and stained using hematoxylin and eosin, and metastatic nodules were counted at ×200 magnification under a microscope (BX43, Olympus). The total number of nodules was recorded for each mouse using five random sections from five different lobes. Tumor volume was calculated using the following approximation formula:

$$(\textit{Tumor volume}) \approx \frac{1}{2} \times (\textit{major radius}) \times (\textit{minor radius})^2$$

Quantification of reactive oxygen species

Cellular reactive oxygen species (ROS) and superoxide anion were quantified using a detection kit (Total ROS/Superoxide Detection Kit, Enzo Life Sciences). Cells were seeded in normal culture flasks and allowed to settle for 24 h. Metformin (0, 1, 5, 10, and 20 mM) was added 6 h prior to analysis. After trypsinization, cells were labeled

according to the manufacturer's instructions. Dead cells were gated based on their forward scatter vs. side scatter area profiles. Fluorescence was measured and analyzed using a flow cytometer and software (BD FACSCalibur and BD CellQuest Pro software, Becton, Dickinson & Co.).

Quantification of ATP production from oxidative phosphorylation

Cells were suspended at a density of 200,000 cells/mL in glucose-free RPMI (Sigma-Aldrich) supplemented with 2 g/L galactose (Sigma-Aldrich), and 100 µL of the suspension was added to 96-well plates (Nunc LumiNunc, Thermo Fisher Scientific), followed by incubation for 24 h. Metformin was added and ATP production was quantified after a 2-h incubation period (Mitochondrial ToxGlo Assay, Promega Corporation). Luminescence was measured using a plate reader (ARVO MX).

Western blotting

Control and metformin-treated cells were lysed using RIPA buffer (50 mM Tris-HCl, 150 mM NaCl, 5 M EDTA, 1% Triton-X, and 0.1% sodium dodecyl sulfate [SDS]) supplemented with 10 mM NaF, 2 mM Na_3VO_4, and cOmplete Mini Protease Inhibitor Cocktail (Roche Diagnostics) after the indicated treatment. Protein content was

measured using the BCA Protein Assay Kit (Thermo Fisher Scientific), and a defined

amount of protein was mixed with the concentrated sample loading buffer with the final

composition of 100 mM Tris-HCl (pH 6.8), 2% SDS, 12% 2-mercaptoethanol, and 20%

glycerol. Proteins (10 μg) were resolved by SDS-polyacrylamide gel electrophoresis and

transferred onto polyvinylidene difluoride membranes (Biorad Laboratories). The

protein-transferred membranes were blocked in Tris-buffered saline with 0.1% Tween

(TBST) containing 5% non-fat dry milk for 1 h at room temperature. Subsequently, the

membranes were incubated with the following primary antibodies at the indicated

conditions in TBST containing 5% non-fat dry milk (TBST-milk) or 5% bovine serum

albumin (TBST-BSA): (1) polyclonal rabbit anti-AMPK α1 antibody (Millipore, 1:1000,

TBST-milk, 4°C, overnight); (2) polyclonal rabbit anti-phospho-AMPKα antibody

(Thr172, Millipore, 1:500, TBST-milk, 4°C, overnight); (3) polyclonal rabbit anti-

mTOR (Cell Signaling, 1:1000, TBST-BSA, 4°C, overnight); (4) monoclonal rabbit anti-

phospho-mTOR (Cell Signaling, 1:1000, TBST-BSA, 4°C, overnight); (5) monoclonal

rabbit anti-phospho p70 S6K (Cell Signaling, 1:1000, TBST-BSA, 4°C, overnight); (6)

polyclonal rabbit anti-phospho-4E-BP1 (Cell Signaling, 1:1000, TBST-BSA, 4°C,

overnight); (7) polyclonal rabbit anti-cyclin D1 antibody (Santa Cruz Biotechnology,

1:500, TBST-milk, 4°C, overnight); (8) monoclonal anti-phospho-retinoblastoma

protein (Rb, Cell Signaling, 1:1000, TBST-BSA, 4°C, overnight); and (9) monoclonal

mouse anti-actin antibody (Millipore, 1:10,000, TBST-milk, 4°C, overnight).

Horseradish peroxidase-conjugated anti-mouse or anti-rabbit IgG antibody (GE

Healthcare, 1:10,000, TBST-milk, room temperature) was then incubated with the

membranes for 1 h as the secondary antibody. The membranes were developed (ECL

Prime Western Blotting Detection System, GE Healthcare) and luminescence was

captured with an imaging system (ChemiDoc Image Lab, Biorad Laboratories).

cDNA microarray

Total RNA was extracted from CHMp-5b cells treated with 10 mM metformin

for 24 h using a purification kit (RNeasy Mini Kit, Qiagen) according to the

manufacturer's instructions. RNA purity and integrity were confirmed with an Agilent

2100 Bioanalyzer (Agilent Technologies); the RNA integrity numbers were above 9.0.

cDNA and Cy3-labeled cRNA were synthesized using amplification (Quick Amp

Labeling Kit, Agilent Technologies) and hybridization (RNA Spike-In One-Color Kit,

Agilent Technologies) kits. The amplified cRNAs were purified (RNeasy Mini Kit) and

then hybridized to a microarray (Canine V2 [4 × 44K], Agilent Technologies) using a

hybridization kit (Gene Expression Hybridization Kit, Agilent Technologies). The

hybridized slides were washed (Gene Expression Wash, Agilent Technologies) and

scanned (High-Resolution Microarray Scanner, Agilent Technologies). Experiments

were performed in triplicate. The scanned images were analyzed (Feature Extraction

software, Agilent Technologies), and the data were analyzed using R software. Control

expression data of CHMp-5b was incorporated from the previous chapter. Data

incorporation, quantile normalization, and statistical detection of differentially

expressed genes (DEGs) using the empirical Bayes method were performed using the

limma R package (Smyth, 2005). $q < 0.001$ was established as the threshold for false

discovery rate (FDR). The probes were annotated via the Database for Annotation,

Visualization, and Integrated Discovery (DAVID)[a] (Dennis et al., 2003). Gene ontology

(GO) term-based enrichment analysis (GTEA) was performed using Cytoscape v.3.1.1

software (Smoot et al., 2011) and the BiNGO Cytoscape plugin (Maere et al., 2005). The

canine gene association file (validated on 2014-06-15, v.2.0) and the ontology file

(released on 2014-06-14, v.1.2) were retrieved from the Gene Ontology Consortium[b]

(Ashburner et al., 2000). Gene lists in each GO term were obtained through QuickGO[c]

(Binns et al., 2009).

---

[a]See: http://david.abcc.ncifcrf.gov/

[b]See: http://www.geneontology.org/

[c]See: http://www.ebi.ac.uk/QuickGO/

Cell cycle analysis

Control and metformin-treated cells were trypsinized into single cell suspension and fixed with 70% ice-cold ethanol. After fixation, the cells were washed with PBS and stained with 50 µg/mL propidium iodide (Sigma-Aldrich), 0.1 mg/mL RNase A (Roche Diagnostics), and 0.05% Triton X-100 (Sigma-Aldrich) for 40 m at 37 °C. The stained cells were immediately analyzed (BD FACSCalibur, Becton, Dickinson & Co.) and the data were then processed (FlowJo software, TreeStar Inc.).

Statistical analysis

All data were shown as means ± standard deviation (SD). Statistical methods and software used were as follows: Two-sided Student's t test using Excel 2013 (Microsoft), and Dunnett's test using R software and *multcomp* R package (Hothorn et al., 2008). Choice of the statistical methods was described in each figure legend. Differences were considered statistically significant when *P* value reached less than 0.05.

Results

In vitro and in vivo anti-tumor effect of metformin on CMGT cells

Metformin decreased *in vitro* viability of the examined cell lines in a time- and concentration-dependent manners (Figs. 3.1A,B). CHMp-5b was significantly more sensitive to metformin than CHMp-13a, with IC_{50} values of 2.2 mM and >20 mM (not determined), respectively, for a 48-h exposure (Figs. 3.1C,D).

Oral metformin administration resulted in a significant reduction in primary tumor growth in the CHMp-5b xenograft mouse model without causing apparent side effects such as weight loss and anorexia (Figs. 3.1E,F), whereas no significant effect was observed on the metastasis of the tumor (Figs. 3.1G,H).

Evaluation of ROS generation and AMPK pathway activation with metformin exposure

A significant increase in total ROS and superoxide production in both cell lines following 6 h of exposure to metformin was observed (Figs. 3.2A,B). However, ROS levels were higher in CHMp-13a cell line. In CHMp-5b cells, the change in superoxide production was also similar to CHMp-13a cells at most concentrations, despite higher sensitivity to metformin.

Metformin caused a significant reduction in mitochondrial ATP production in

CMGT cells, and this effect was greater in CHMp-5b cells (Fig. 3.2C). However, AMPK activation was observed only in CHMp-13a cells (Fig. 3.2D), where mTOR and its downstream molecules p70S6K and 4E-BP were subsequently inactivated. This finding indicated that metformin exposure negatively affected cell proliferation in CHMp-13a cells through AMPK-mTOR axis, which was further confirmed by a cell viability assay using Compound C, an AMPK inhibitor (Figs. 3.2E,F). Compound C co-incubation diminished metformin-induced growth inhibition in CHMp-13a cells at most metformin concentrations, however this effect was not apparent in CHMp-5b cells.

Transcriptome analysis of the response pathway in CHMp-5b cells

I identified 1802 annotated DEGs after normalizing the data between control and metformin experiments (Figs. 3.3A,B). Among them, downregulated DEGs ($n =$ 971) proceeded to GTEA, and 30 GO terms were found to be significantly under-represented after metformin treatment with $P < 0.0001$ (Figs. 3.3C,D). The four nodes shown in Figs. 3.3E–H focused attention during a hierarchical exploration of the deepest nodes using BiNGO. Because two of these nodes (GO:280 nuclear division and GO:193047 mitotic cell cycle process) were related to cell cycle progression, the possibility of metformin-induced inhibition of the cell cycle process in CHMp-5b was

66

highly considered.

Effect of metformin on cell cycle in CMGT cells

In western blotting, an apparent decrease in cyclin D1 and phosphorylated Rb levels in CHMp-5b was observed in the absence of AMPK activation following 6-h exposure to metformin. This effect was not confirmed in CHMp-13a cells, where instead, low metformin concentrations led to greater Rb phosphorylation (Fig. 3.4A). A corresponding change was detected using flow cytometric analysis of the cell cycle. Metformin caused a greater increase in the G0/G1 phase proportion and a decrease in the S phase proportion in CHMp-5b cells compared with CHMp-13a cells (Figs. 3.4B–D).

Discussion

In this chapter, anti-tumor activity of metformin against CMGT cells was demonstrated both *in vitro* and *in vivo*. *In vitro*, metformin decreased tumor viability at a range of concentrations comparable with previous studies using human cancer cells (Lonardo et al., 2013; Song et al., 2012; Würth et al., 2013). Furthermore, metformin suppressed growth of metastatic CHMp-5b cells at lower concentrations.

In the previous chapter, the results obtained by an unbiased drug screening showed that MRCIs exerted selective inhibition on the proliferation of metastatic CMGT cells. Sensitive CHMp-5b cells and insensitive CHMp-13a cells responded to MRCIs through clearly distinct mechanisms, i.e., in either an AMPK-dependent or AMPK-independent manner. Phosphorylation of AMPK and inhibition of its downstream mTOR pathway by metformin indicated that it acted through an AMPK-dependent mechanism in CHMp-13a cells in a similar manner to other MRCIs. In contrast, metformin inhibited cell cycle progression at the G1/S checkpoint in an AMPK-independent manner in CHMp-5b cells. Cell cycle arrest was observed as early as 6 hours after exposure to metformin, whereas AMPK activation was not detected at 6, 12, or even 24 hour in CHMp-13a cells (data not shown). ROS production was not thought to be responsible for selective inhibition of cell growth. These findings suggested that

the effects of metformin were mediated through a different mechanism of action between the two clones tested.

Based on the results obtained in many studies using normal and tumor cells, an AMPK-dependent mechanism has been thought to be the canonical pathway for the effect of metformin (Quinn et al., 2013; Saito et al., 2013; Song et al., 2012). Studies using Martin-Derby canine kidney epithelial cell lines also suggested a metformin-induced AMPK-dependent effect on cells derived from dogs (Choi et al., 2010; Seo-Mayer et al., 2011). However, several AMPK-independent mechanisms have been also reported (Ben Sahra et al., 2008; Lonardo et al., 2013). In particular, Ben Sahra et al. (2008) showed AMPK-independent G0/G1 arrest using human prostate cancer cell lines. The cyclin D1 gene (CCND1) is a well-established oncogene and frequently dysregulated in human malignancies, including breast cancer (Musgrove et al., 2011). Rb is a main substrate of cyclin D-cyclin dependent kinase (CDK) 4/6 complex and a critical regulator of the G1–S transition. Rb is also a well-known tumor suppressor gene that is inactivated in the early phase of oncogenesis (Giacinti and Giordano, 2006). Because CCND1 and Rb both cooperatively control cell cycle progression from the G1 to the S phase and are involved in tumor cell proliferation, they have been intensely investigated as potential therapeutic targets. Therefore, metformin may be effective in

the treatment of tumors in which the cell cycle machinery is dysregulated. In CMGT, several studies suggested dysregulation of cell cycle progression. It was shown that the CDK inhibitor, p27, has been downregulated in lymph node metastases of CMGT compared to the normal mammary gland and primary tumors (Klopfleisch et al., 2010; Klopfleisch and Gruber, 2009). These studies indicated that dysregulation of cell cycle was also associated with malignant progression of CMGT as human malignancies. Although genetic and epigenetic changes in cell cycle-regulating molecules in the cell lines used in this study have not been fully evaluated, such changes may be associated with differing metformin sensitivity. The mechanism by which metformin controls expression of cyclin D1 is still unknown and requires further elucidation.

Recent evidence suggests that a small proportion of cells in cancer are cancer stem cells (CSC) that are responsible for chemoresistance, radioresistance, and tumor propagation (Kreso and Dick, 2014). Previous reports suggested that metformin had a selective anti-tumor effect on CSCs in breast carcinoma, glioblastoma, hepatocellular carcinoma, and pancreatic carcinoma (Lonardo et al., 2013; Saito et al., 2013; Song et al., 2012; Würth et al., 2013). In addition, metformin inhibited the epithelial-to-mesenchymal transition of tumor cells (EMT), which renders epithelial tumor cells motile and invasive (Chou et al., 2014; Qu et al., 2014; Vazquez-Martin et al., 2010).

EMT is also a hallmark of CSCs (Ansieau, 2013; Nieto, 2013). It was shown in the previous chapter that metastatic CHMp-5b cells present EMT- and stem cell-related phenotypes, such as decreased E-cadherin expression, increased invasive capacity, and high aldehyde dehydrogenase activity *in vitro,* in addition to tumorigenic and metastatic potential *in vivo* in the previous publication (Murai et al., 2012). Therefore, it is speculated that EMT and CSC phenotypes provide or require specific signaling changes in common, with which metformin could interfere. A recent study indicated that CSC-like cells generated by experimentally inducing EMT utilized mitochondrial energy production, which is the target of metformin, much more than the uninduced original cancer cells (Cuyàs et al., 2014). The association of cellular metabolic state, CSC-like phenotype, and metformin sensitivity requires further investigation.

The number of the studies reporting anti-tumor effects of metformin has rapidly increased. A major reason for this great interest in metformin is its safety profile, which has been confirmed through a long history of prescription for diabetic patients (Ekström et al., 2012). Although metformin is not widely used in veterinary medicine, it has been used experimentally in dogs, which indicated the feasibility of metformin use in this species (Nelson, 2000; Sasaki et al., 2009). Using an immunodeficient mouse xenograft model, it was possible to demonstrate an *in vivo* anti-tumor effect of metformin in this

chapter. Metformin suppressed CHMp-5b tumor growth by approximately 50%. There

was a tendency toward an inhibitory effect on metastasis formation ($P > 0.05$) as well.

These results may provide a basis for further clinical studies of metformin in dogs with

CMGTs. The less-sensitive cell line, CHMp-13a, was not applied to *in vivo* study

because it had failed to form a continuously growing tumor in the previous study (Murai

et al., 2012).

Human breast cancer clinical trials of metformin have utilized preoperative

administration of metformin as a single agent (Cazzaniga et al., 2013; Hadad et al., 2011).

In preclinical studies examining the *in vivo* anti-tumor potential of metformin, single-

agent metformin treatment led to a reduction in tumor growth, with the effect varying

from non-significant changes to a 60% reduction. It was suggested that metformin

should be combined with some chemotherapeutic agents because of its cytostatic anti-

tumor effect rather than cytotoxic (Takiguchi, 2012; Würth et al., 2013). Single use of

metformin did not completely eradicate tumors *in vivo*, including the result from this

chapter (Ben Sahra et al., 2008; Lonardo et al., 2013; Saito et al., 2013; Zhu et al., 2014).

The addition of systemic irradiation or adjunctive anti-angiogenic drugs appeared to

significantly improve the therapeutic potential of metformin (Saito et al., 2013; Song et

al., 2012). However, the combination of metformin and gemcitabine failed to produce

an additive effect (Lonardo et al., 2013). Therefore, future clinical applications of

metformin for CMGT treatment will require careful investigation of possible drug

combinations.

Conclusion

In this chapter, metformin showed anti-tumor effect on CMGT cells *in vitro* and *in vivo* through both AMPK-dependent and AMPK-independent mechanisms. Future work is necessary to reveal the mechanism by which metformin suppresses cell cycle progression and to investigate the association of cellular malignant phenotype with metformin sensitivity. Establishment of effective combination strategies with adjunctive therapy should also be investigated for clinical application.
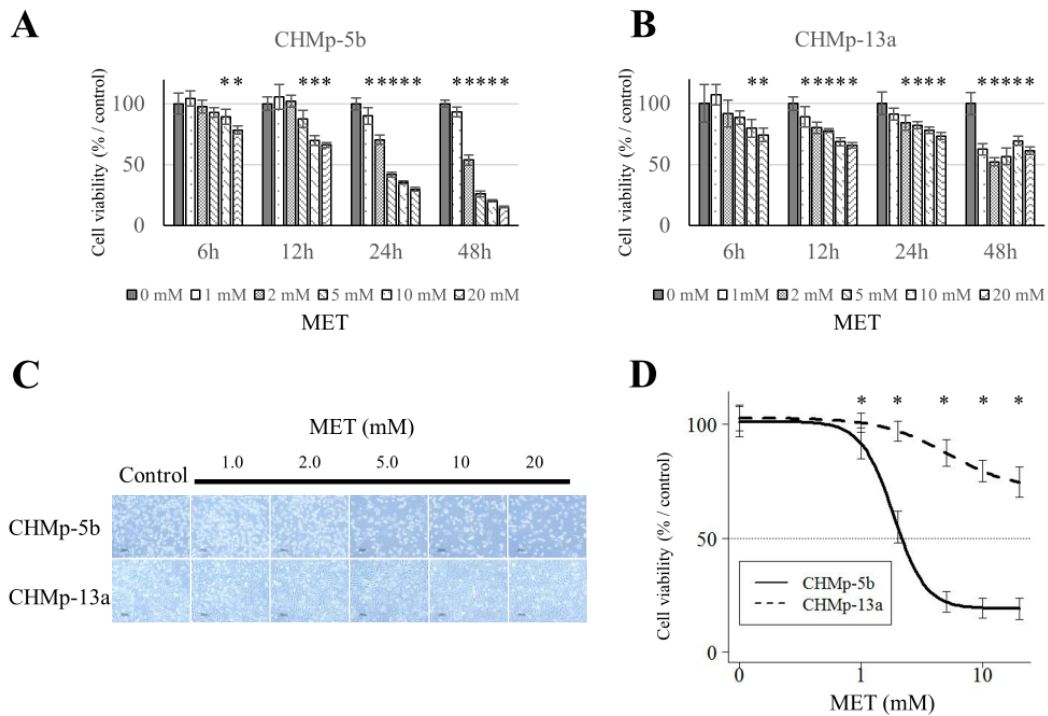
Fig. 3.1. *In vitro* **and** *in vivo* **effect of metformin on canine mammary gland tumor (CMGT) cells.**

(A–D): *In vitro* anti-proliferative effect on CMGT cells. Results of viability assays in CHMp-5b (A) and CHMp-13a (B) cell lines exposed to different concentrations of metformin for varying durations. (C) Representative microscopic images of CMGT cells after 24 h of metformin exposure. (D) Concentration response curves generated to estimate the half-maximal inhibitory concentration (IC_{50}) from the independent cell viability assay result (48 h) using the four parameters logistic model in *R* and *drc* (*R* package). *$P < 0.05$ (A,B; Dunnett's test, Control versus treatment, D; t-test, CHMp-5b versus CHMp-13a). MET, metformin.
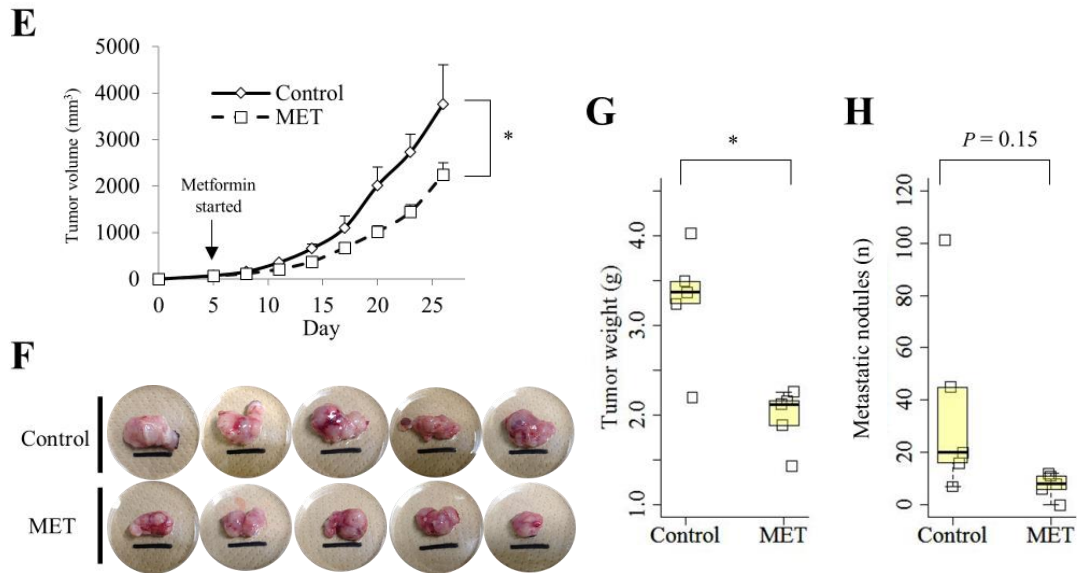
Fig. 3.1. *In vitro* and *in vivo* effect of metformin on canine mammary gland tumor (CMGT) cells (*continued*).

(E–H): Anti-tumor effect of metformin in a xenograft model. (E) Tumor growth curves for control and metformin (300 mg·kg^{-1}·day^{-1}) groups. (F) Macroscopic appearance of resected tumors on day 26. Scale bars, 1 cm. (G) Comparison of tumor weight after resection. (H) Comparison of the number of metastatic nodules in the lung. *$P < 0.05$ (t-test). MET, metformin.

Fig. 3.2. AMP-activated protein kinase (AMPK)-dependent and AMPK-independent effect of metformin on canine mammary gland tumor (CMGT) cells.

(A–C): Changes in cellular total reactive oxygen species (ROS; A), superoxide anion (B) and ATP (C) with exposure to metformin. [a, b, c]$P < 0.05$ between CHMp-5b treatment and control ([a]), CHMp-13a treatment and control ([b]), and CHMp-5b and CHMp-13a ([c]), respectively (a,b; Dunnett's test, c; t-test). MET, metformin.

D

E

F

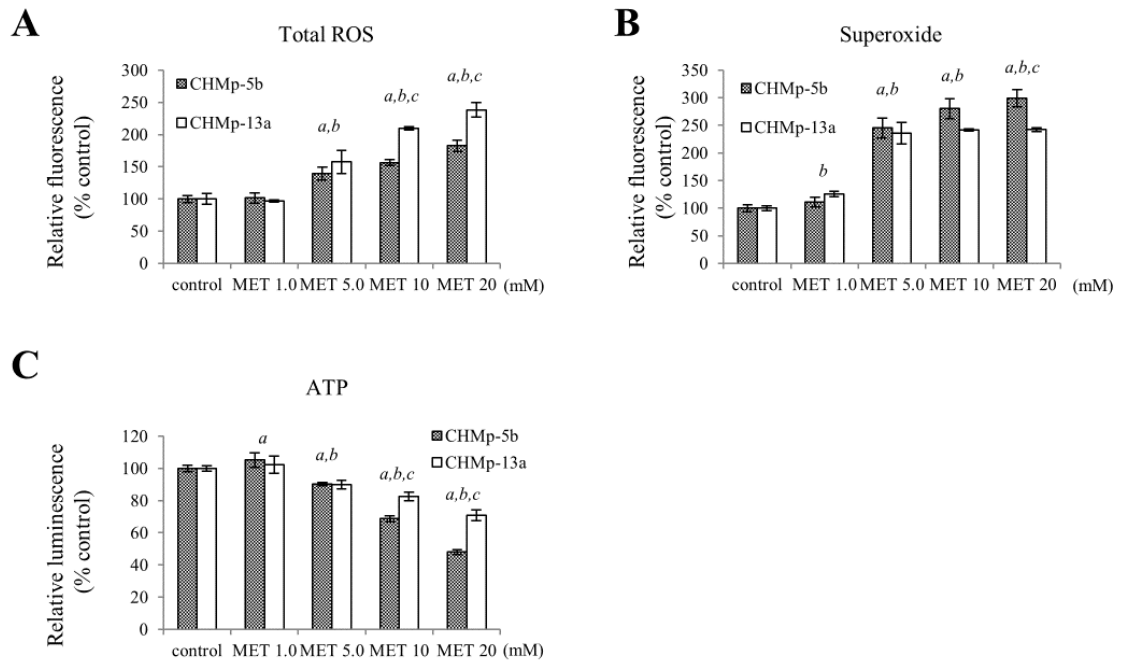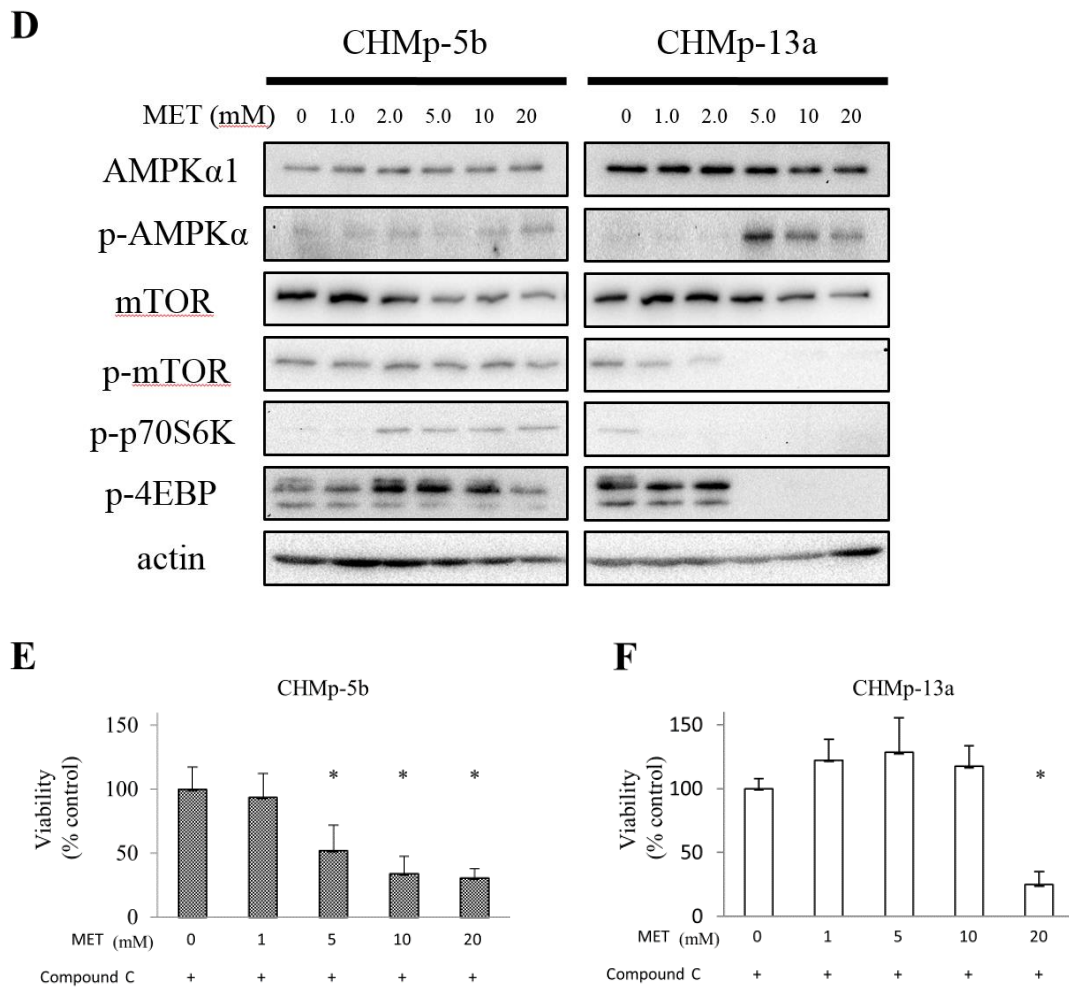**Fig. 3.2. AMP-activated protein kinase (AMPK)-dependent and AMPK-independent effect of metformin on canine mammary gland tumor (CMGT) cells (*continued*).**

(D) Western blotting analysis of AMPK activation and its downstream molecules. (E, F) Effect of co-incubation of metformin with the AMPK inhibitor, Compound C (10 μM), on CHMp-5b (E) and CHMp-13a (F) cells. $*P < 0.05$ (Dunnett's test; control versus treatment). MET, metformin; mTOR, mammalian target of rapamycin; p, phosphorylated.

A

Expression (log₂) / Sample: Cont-1, Cont-2, Cont-3, MET-1, MET-2, MET-3

B

M: Ratio / A: average
DEGs (n=1802)
non-DEGs (n=7347)

C

GO number	GO term	P value
44237	cellular metabolic process	2.04E-09
8152	metabolic process	2.04E-09
44710	single-organism metabolic process	8.17E-09
22402	cell cycle process	3.96E-08
71704	organic substance metabolic process	7.28E-08
7049	cell cycle	9.01E-08
6807	nitrogen compound metabolic process	1.81E-07
44238	primary metabolic process	1.13E-06
34641	cellular nitrogen compound metabolic process	1.80E-06
1901360	organic cyclic compound metabolic process	1.80E-06
6259	DNA metabolic process	2.24E-06
6139	nucleobase-containing compound metabolic process	4.02E-06
6725	cellular aromatic compound metabolic process	4.02E-06
6281	DNA repair	4.14E-06
46483	heterocycle metabolic process	4.46E-06
6082	organic acid metabolic process	6.87E-06
51301	cell division	7.19E-06
90304	nucleic acid metabolic process	7.19E-06
43436	oxoacid metabolic process	7.19E-06
19752	carboxylic acid metabolic process	8.77E-06
33554	cellular response to stress	1.14E-05
44281	small molecule metabolic process	1.20E-05
44260	cellular macromolecule metabolic process	1.43E-05
6974	cellular response to DNA damage stimulus	1.43E-05
1903047	mitotic cell cycle process	1.51E-05
278	mitotic cell cycle	2.08E-05
6950	response to stress	2.47E-05
43170	macromolecule metabolic process	2.69E-05
1901575	organic substance catabolic process	3.22E-05
280	nuclear division	8.70E-05

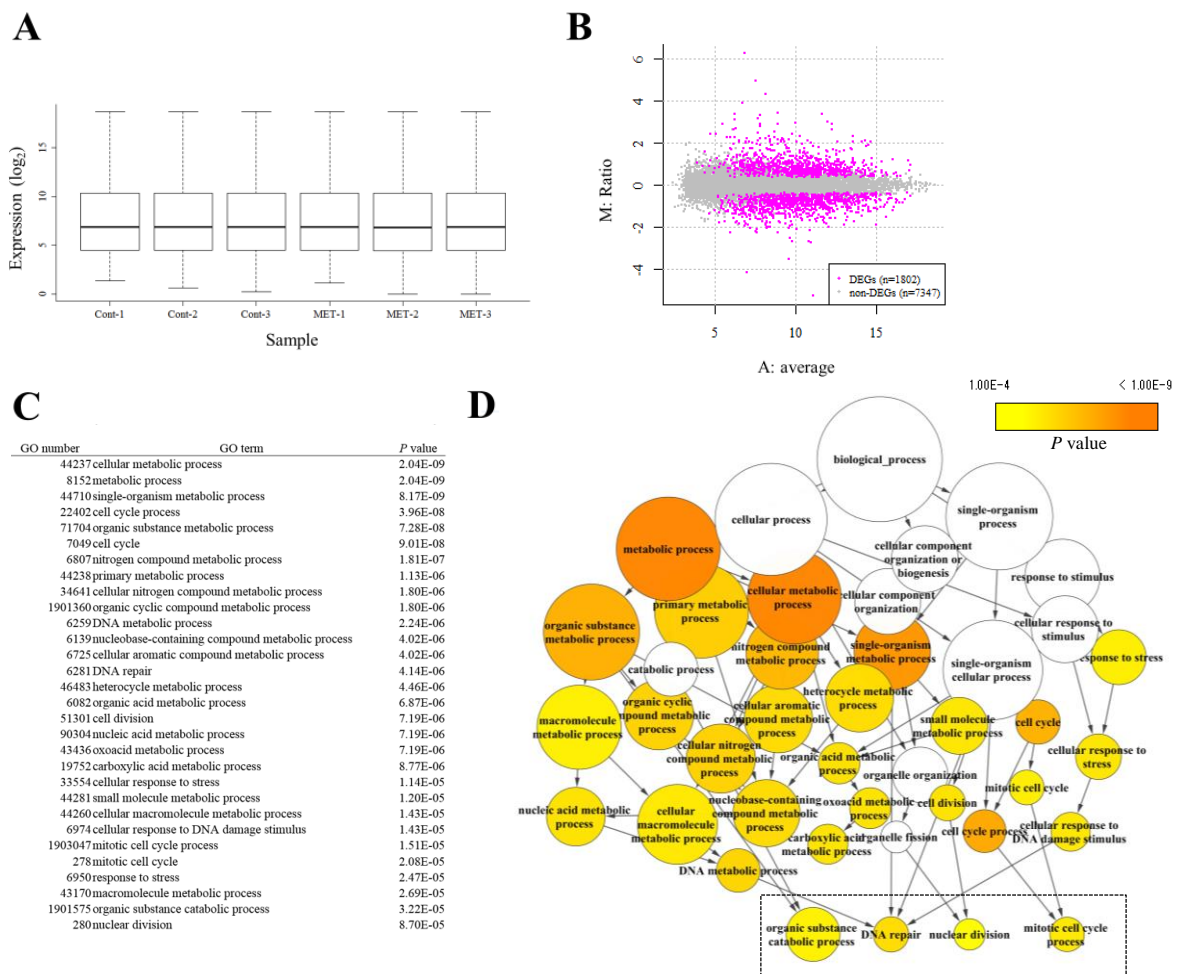**D**

P value: 1.00E-4 — < 1.00E-9

Fig. 3.3. Effect of 24-h metformin (10 mM) treatment on gene expression profile in CHMp-5b cells.

(A) Box-whisker plot of gene expression in each replicate after normalization. (B) M-A plot of cDNA microarray results. The X-axis indicates the average expression level of each gene in the experiment and the Y-axis indicates the fold change in gene expression between the two conditions. Magenta dots indicate differentially expressed genes (DEGs) determined by an empirical Bayes analysis (false discovery rate [FDR] < 0.001), and gray dots indicate non-DEGs. (C, D): Results of gene oncology term-based enrichment analysis (GTEA). (C) List of gene ontology (GO) terms significantly underrepresented upon metformin treatment (*P* < 0.0001). (D) Visualization of the GTEA results in the GO term network. Cont, control; MET, metformin.
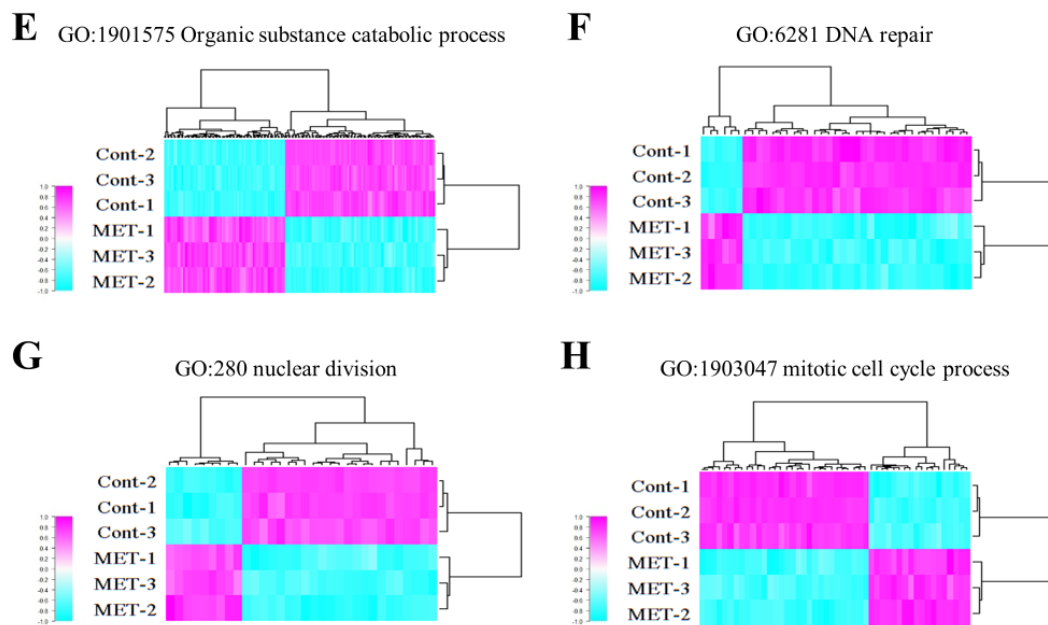
E GO:1901575 Organic substance catabolic process

F GO:6281 DNA repair

G GO:280 nuclear division

H GO:1903047 mitotic cell cycle process

Fig. 3.3. Effect of 24-h metformin (10 mM) treatment on gene expression profile in CHMp-5b cells (*continued*).

(E–H): Heat maps for DEGs mapped in the deepest nodes by GTEA analysis. (E) GO:1901575.

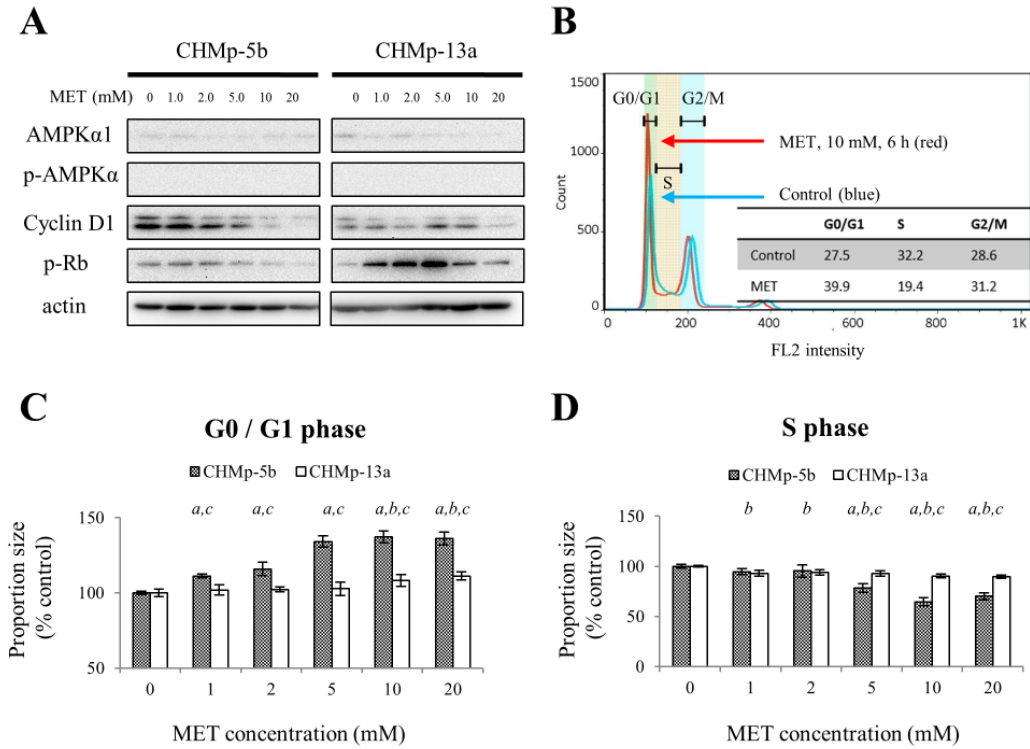(F) GO:6281. (G) GO:280. (H) GO:1903047. Cont, control; MET, metformin.

A

CHMp-5b   CHMp-13a

MET (mM)   0 1.0 2.0 5.0 10 20   0 1.0 2.0 5.0 10 20

AMPKα1

p-AMPKα

Cyclin D1

p-Rb

actin

B

G0/G1   G2/M

MET, 10 mM, 6 h (red)

S

Control (blue)

Count

FL2 intensity

	G0/G1	S	G2/M
Control	27.5	32.2	28.6
MET	39.9	19.4	31.2

C

G0 / G1 phase

■ CHMp-5b   □ CHMp-13a

a,c   a,c   a,c   a,b,c   a,b,c

Proportion size (% control)

0   1   2   5   10   20

MET concentration (mM)

D

S phase

■ CHMp-5b   □ CHMp-13a

b   b   a,b,c   a,b,c   a,b,c

Proportion size (% control)

0   1   2   5   10   20

MET concentration (mM)

Fig. 3.4. Effect of 6-h metformin exposure on cell cycle regulation.

(A) Western blot analysis of AMP-activated protein kinase (AMPK) and G1/S checkpoint proteins. (B) Representative result of flow cytometric cell cycle analysis using propidium iodide. X-axis indicates FL2 channel intensity (propidium iodide). The proportion of each cycle phase was determined by FlowJo software. (C, D) Summary of the effect of metformin treatment on the cell cycle. (C) G0/G1 population. (D) S population. [a, b, c]$P < 0.05$ between CHMp-5b treatment and control ([a]), CHMp-13a treatment and control ([b]), and CHMp-5b and CHMp-13a ([c]), respectively (a,b; Dunnett's test, c; t-test). MET, metformin; p, phosphorylated; Rb, retinoblastoma.

Chapter 4

Relationship of cellular nicotinamide adenine dinucleotide

amount to metformin-induced growth inhibition

in metastatic canine mammary gland tumor cell

Introduction

Metformin (1,1-dimethylbiguanide) is an oral hypoglycemic agent widely subscribed to type 2 diabetes patients. Of great interest, many studies in diabetic patients have suggested anti-tumor effect of metformin in various types of human epithelial malignancies, including hepatocellular, colorectal, pulmonary, and pancreatic carcinomas (Decensi et al., 2010; Franciosi et al., 2013; Noto et al., 2012). In the previous chapter, metformin also exhibited an anti-tumor effect in canine mammary gland tumor (CMGT).

The anti-tumor mechanism of metformin has been indicated to be mostly attributed to AMPK activation and subsequent inhibition of mammalian target of rapamycin (mTOR) pathway (Dowling et al., 2007; Mamane et al., 2006; Song et al., 2012). However, several other AMPK-independent mechanisms such as inhibition of insulin-like growth factor signaling and induction of cell cycle arrest have been also suggested (Emami Riedmaier et al., 2013; Quinn et al., 2013). The results in the previous chapter demonstrated that metformin exerted anti-proliferative effect through either AMPK-dependent or independent manner in two phenotypically contrasting CMGT cell lines. In particular, metformin caused AMPK-independent cell cycle arrest in the metformin-sensitive, metastatic CMGT cell line. However, exact AMPK-independent

mechanism of metformin was still unclear.

Rotenone is a natural compound extracted from several plant roots and widely used as an insecticide (Xiong et al., 2012). Rotenone has been also experimentally used to induce Parkinson's disease-like syndrome in several model animals with toxic effect on the cells in the neural system. Importantly, mechanism of action of rotenone is inhibition of mitochondrial respiratory chain complex (MRC) 1, which is similar to that of metformin (Xiong et al., 2012). Recent study revealed that rotenone decreased cellular content of nicotinamide adenine dinucleotide (NAD) as a result of inhibition of MRC1 (Hong et al., 2014). Moreover, rotenone-induced cytotoxicity was attenuated when external NAD was supplemented to the treated cells (Hong et al., 2014). NAD plays important biological roles not only in cellular metabolism but also in gene expression, axon maintenance and circadian rhythm (Di Stefano and Conforti, 2013; Verdin, 2014). In that study, major effect of inhibition of MRC1 was considered to be a decrease in conversion from NADH to NAD at the MRC1, rather than a decline in subsequent ATP production or a leakage of reactive oxygen species (ROS) (Hong et al., 2014).

Since metformin involves inhibition of the MRC1 as rotenone does, it is hypothesized that metformin exerts AMPK-independent anti-proliferative effect in the CMGT cell via decrease in cellular NAD amount. Understanding of the exact

mechanism of action is necessary for future patient selection in clinical application of

metformin. In this study, first, the effect of NAD depletion on the proliferation of the

CMGT cell line was evaluated using NAD depleting agent FK866. Next, effect of

external NAD supplementation on metformin- or FK866-induced growth inhibition and

cell cycle arrest was investigated. Finally, change in cellular ATP and NAD amount after

each treatment was quantified.

Materials and methods

Cell culture

A Clonal metastatic CMGT cell line, with high metformin sensitivity as demonstrated in the previous chapter, CHMp-5b was maintained in RPMI 1640 medium (Wako Pure Chemical Industries) supplemented with 10% fetal bovine serum (FBS; Life Technologies) and 50 µg/mL gentamicin (Sigma-Aldrich) at 37 °C in a humid atmosphere with 5% CO_2. All other cell incubation steps used these conditions unless otherwise stated.

Cell growth assay

CHMp-5b cells were seeded at a density of 2,000 cells/well in 96-well flat-bottom plates and incubated for 22 h. Then, NAD (beta-nicotinamide adenine dinucleotide hydrate; Sigma-Aldrich; catalog number N3014) or equal amount of vehicle saline were added at the final concentration of 0.1 mg/mL. Metformin (1,1-dimethylbiguanide hydrochloride; Sigma-Aldrich; catalog number D150959) or FK866 (Selective nicotinamide phosphoribosyltransferase (NAMPT) inhibitor; Sigma-Aldrich; catalog number F8557) were added after another 2-h incubation, at the final concentrations ranging from 1 mM to 50 mM or from 15 pM to 5 µM, respectively. Cell

viability was determined using Cell Counting Kit-8 (Dojindo Laboratories) at the indicated time point.

Real-time cell proliferation monitoring was performed using an iCELLigence system (ACEA Biosciences). CHMp-5b cells were seeded at a density of 4000 cells/well in E-Plates L8 (ACEA Biosciences) and allowed to grow for 22 h. NAD (0.1 mg/mL) or vehicle saline were added two hour prior to metformin (2 mM) addition at 24 h. Impedance of the bottom of the E-plates, that increases in accordance with the amount of area to which cells attach, were measured with at least 30-m interval throughout incubation period. Cell incubation had been continued until control cells got completely confluent and impedance started to decrease.

Cell cycle analysis

Control and metformin (2 mM)- or FK866 (2 nM)-treated cells with or without external NAD (0.1 mg/mL) supplementation were trypsinized and fixed with 70% ice-cold ethanol for 20 m on ice. The fixed cells were washed with PBS and stained with 50 µg/mL propidium iodide (Sigma-Aldrich), 0.1 mg/mL RNase A (Roche Diagnostics), and 0.05% Triton X-100 (Sigma-Aldrich) for 40 m at 37 °C. The stained cells were immediately analyzed (BD FACSCalibur, Becton, Dickinson & Co.) and the data were

processed (FlowJo software, TreeStar Inc.).

Quantification of ATP production from oxidative phosphorylation

CHMp-5b cells were suspended at a density of 200,000 cells/mL in glucose-free RPMI (Sigma-Aldrich) supplemented with 2 g/L glucose (Wako Pure Chemical Industries) or 2 g/L galactose (Sigma-Aldrich), and 100 µL of the suspension was added to white 96-well plates (Nunc LumiNunc, Thermo Fisher Scientific), followed by incubation for 24 h. NAD (0.1 mg/mL) or vehicle saline were added simultaneously with metformin (2 mM) or FK866 (2 nM) addition. ATP production was quantified after a 90-m incubation period using Mitochondrial ToxGlo Assay (Promega Corporation). Luminescence was measured using a plate reader (ARVO MX).

NAD/NADH quantification

Quantification of oxidized and reduced forms of nicotinamide adenine dinucleotide (NAD and NADH, respectively) were performed using a fluorometric NAD/NADH assay kit (abcam). Control and metformin (2 mM)- or FK866 (2 nM)-treated cells with or without external NAD (0.1 mg/mL) supplementation were lysed after 48-h incubation using a cell lysis buffer provided in the kit. The amount of NAD

and NADH was quantified according to manufacturer's instruction using black 96-well

plates (Nunc FluoroNunc plate, Thermo Fisher Scientific) and a plate reader (ARVO

MX).

Total protein amount of cell lysate was determined using Pierce BCA assay kit

(Pierce Biotechnology). Amount of NAD and NADH was normalized by total protein

amount.

Statistical analysis

Data were expressed as the mean value ± standard deviation (SD). Statistical

methods and software used were as follows: Two-sided Student's t test using Excel 2013

(Microsoft), Tukey-Kramer test using R software (ver. 3.0.2) (R Development Core

Team, 2005), and Dunnett's test using R software and *multcomp* R package (Hothorn et

al., 2008). Choice of the statistical methods was described in each figure legend.

Differences were considered statistically significant when *P* value reached less than 0.05,

unless otherwise indicated.

Results

Effect of FK866 or metformin on CMGT cell proliferation with or without external NAD

Metformin and FK866 decreased the *in vitro* viability of the CHMp-5b cells in a concentration-dependent manner (Figs. 4.1A,B). This decrease in cell viability was recovered at the wide range of the drug concentrations when 0.1 mg/mL NAD had been externally supplemented prior to drug exposure (Figs. 4.1A-D). The 50% growth inhibitory concentration (IC_{50}) for metformin alone and metformin with NAD were 2.45 $\pm$ 0.82 and 6.35 $\pm$ 1.54 mM, respectively ($P < 0.05$, Student's t test). IC_{50} values for FK866 alone and FK866 with NAD were 0.69 $\pm$ 0.23 and 78 $\pm$ 76 nM ($P = 0.22$, Student's t test). Real time monitoring of CHMp-5b cell proliferation also confirmed significant attenuation of metformin-induced growth inhibition by external NAD addition (Fig. 4.1E).

Effect of FK866 or metformin on CMGT cell cycle distribution with or without external NAD

It was revealed in the cell cycle analysis that metformin treatment led to significant decrease in the proportion of the dividing cells (S phase and G2/M phase) (Figs. 4.2A,B). This metformin-induced cell cycle arrest was diminished by co-

incubation with NAD to the level compatible with vehicle control. As for FK866

treatment, the similar tendency was observed although it was not statistically significant.

Effect of FK866 or metformin on cellular ATP content with or without external NAD

Single or combination treatment of NAD, metformin and FK866 did not affect

total cellular ATP production which was demonstrated under glucose-containing

condition (Fig. 4.3A). Quantification of mitochondrial ATP production was also

performed under a glucose-starved galactose-supplemented condition to reveal the effect

of metformin, FK866 and NAD treatment on mitochondrial oxidative phosphorylation

(OXPHOS). Except for antimycin, which was MRC3 inhibitor and used as a positive

control, neither of single agent nor combination treatment at the concentration used in

this study led to significant change in mitochondrial ATP production (Fig. 4.3B).

Effect of FK866 or metformin on cellular NAD content with or without external NAD

Cellular NAD content was significantly decreased by metformin (Fig. 4A).

Similarly, NAD/NADH ratio was disrupted by metformin treatment as well (Fig. 4C).

Most importantly, this change was almost completely recovered by external addition of

NAD, to the extent comparable to vehicle treated control (Figs. 4A,C). Single NAD

treatment alone led to the significant increase in both of NAD and NADH, with keeping

NAD/NADH ratio consistent with vehicle control (Figs. 4A-C).

On the other hand, exposure to FK866 caused CHMp-5b cells significant

decline in both of NAD and NADH (Figs. 4A,B). External NAD compensation to

FK866-treated cells resulted in recovery of both of NAD and NADH amount (Figs.

4A,B). However, amount of NAD and NADH, and NAD/NADH ratio in FK866- and

FK866 plus NAD-treated cells were still far less than vehicle control (Figs. 4A-C).

Discussion

In this chapter, selective NAMPT inhibitor FK866 showed anti-tumor effect in CMGT cells as well as metformin. It was also exhibited that both of FK866- and metformin-induced anti-proliferative effect were attenuated by external NAD supplementation. Metformin treatment led to significant reduction in cellular NAD content and NAD:NADH ratio, and inhibition of cell cycle progression without causing change in total cellular and mitochondrial ATP production. Furthermore, external compensation of NAD for metformin treatment almost completely restored cellular NAD content, NAD:NADH ratio and cell cycle distribution. NAD supplementation also recovered cell viability. From these results, it was suggested that anti-tumor effect of metformin in the metastatic CMGT cell line involved cellular NAD depletion and subsequent cell cycle arrest. At the same time, it was also inferred that NAD depleting treatment such as use of FK866 could be another choice of treatment for CMGT, although the exact mechanism of anti-tumor activity may differ between metformin and FK866.

Metformin, as a MRC1 inhibitor, was reported to exert its anti-tumor effect through inhibition of mitochondrial OXPHOS and following AMPK activation caused by cellular AMP:ATP imbalance (Liang and Mills, 2013; Rizos and Elisaf, 2013; Song

et al., 2012). Direct binding of AMP and ADP causes allosteric activation of kinase unit of AMPK protein, whereas ATP binding attenuates activity (Liang and Mills, 2013). Activated AMPK could inhibit tumor cell proliferation through inhibition of mTOR pathway (Dowling et al., 2007; Emami Riedmaier et al., 2013). On the other hand, several study indicated AMPK-independent anti-tumor effect of metformin (Dykens et al., 2008; Kisfalvi et al., 2009; Lonardo et al., 2013). It was reported that metformin caused AMPK-mTOR axis independent apoptosis in cancer stem-like cells in human pancreatic cancer cell line (Lonardo et al., 2013). In that study, metformin actually induced cellular ATP shortage, disruption of mitochondrial membrane potential and AMPK activation, however the cytotoxic effect was not mimicked by either of direct AMPK activator A769662 or mTOR inhibitor rapamycin. Previous chapters of this thesis also indicated that metformin caused AMPK-independent cell cycle arrest in metastatic CMGT cell line at the concentration lower than the range where metformin activated AMPK (> 5 mM). It may be oversimplification that metformin inhibits cancer cell growth solely through effect on AMPK-mTOR axis.

This chapter demonstrated that NAD can mediate anti-tumor effect of metformin. Interestingly, rotenone, which is known inhibitor of the MRC1 and selectively inhibited the growth of the metastatic CMGT cell line in the chapter 2, has

been reported to cause apoptosis and necrosis in the differentiated PC12 cells through

NAD-dependent mechanism (Hong et al., 2014). That cytotoxic effect of rotenone was

shown to be reversed by external NAD supplementation (Hong et al., 2014). Antimycin,

a MRC3 inhibitor used in the chapter 2 as well, also has been shown to decrease cellular

NAD content in the precious study (Ogita et al., 2009). In this chapter, metformin was

also demonstrated to induce cellular NAD deprivation at the concentration in which

mitochondrial ATP production was not inhibited. Since this decrease in NAD may be a

reflection of substantial disruption of MRC1, total activity of mitochondrial OXPHOS

was possibly maintained through the function of MRC2 where electrons were

incorporated into OXPHOS in the presence of succinate and flavin adenine dinucleotide,

independently of MRC1. On the other hand, results in this chapter showed that inhibition

of MRC3 by antimycin caused absolute reduction in mitochondrial ATP production. This

may be because MRC3 is a hub complex where electrons coming from both MRC1 and

MRC2 pass through.

NAD has been reported to play a determinant role in several important

biological signaling. Its central function is as a mediator of redox reaction with hydrogen

transfer which is essential for mitochondrial OXPHOS, Krebs cycle, β oxidation of fatty

acids and glycolysis (Berger et al., 2004; Di Stefano and Conforti, 2013). Recently, more

diverse participation of NAD in other important cellular processes also has been described, that is post-transcriptional modifications of proteins such as deacetylation by sirtuins and poly ADP-ribosylation by poly ADP-ribosyl polymerases (PARPs) (Di Stefano and Conforti, 2013). This chapter showed that cellular NAD was diminished by metformin, but mitochondrial and whole ATP production in the presence of glucose was maintained. These results indicated that deprivation of NAD less likely influenced Krebs cycle, fatty acid metabolism or glycolysis, which may result in decrease in net ATP production.

NAD-dependent enzymes such as PARPs and sirtuins require NAD as an exclusive substrate (Michels et al., 2014). PARPs are the molecules involved in DNA repair, genomic stability and programmed death of cells. Since DNA repair function of PARP enzymes renders cancer cells protective profile against DNA damage including radiotherapy and chemotherapy, PARP inhibitors have been studied as anti-tumor agents (Michels et al., 2014; Reinbolt and Hays, 2013; Rouleau et al., 2010). Physiological roles of the proteins which belong to a sirtuin family are mainly involved in metabolism regulation and DNA repair pathways (Choi and Mostoslavsky, 2014). In the oncological settings, sirtuins have been indicated as both tumor promoting and suppressing molecules (Choi and Mostoslavsky, 2014; Roth and Chen, 2014). Sirtuins have been

reported to function as a tumor suppressor against critical genomic mutations during

oncogenesis, whereas, in the fully developed tumor cells, sirtuins sometimes seem to

work to overcome the catastrophic genomic rearrangement otherwise lethal to the cells,

and promote tumor survival and progression (Herranz et al., 2013; Roth and Chen, 2014).

Especially, SIRT1, a well-studied member of sirtuin family, has been reported to be

overexpressed in several human cancers and related to tumor progression through

numerous mechanisms such as genomic repair, epigenetic modulation by histone

deacetylation, inhibition of cellular apoptotic pathways and epithelial-to-mesenchymal

transition (Eades et al., 2011; Huffman et al., 2007; Luo et al., 2001; Roth and Chen,

2014; Vaziri et al., 2001). Recent studies indicated that activity of some members of

PARPs and SIRTs family are dominantly regulated by cellular level of NAD (Sahar and

Sassone-Corsi, 2009; Verdin, 2014). Moreover, of great interest, cDNA microarray and

following Gene Ontology analysis in the previous chapter 3 exhibited that metformin

treatment could disrupt DNA repair pathway by down-regulating multiple related

molecules in metastatic CMGT cell line (Fig. 3.3F). Since both of PARPs and SIRTs

families are involved in DNA repair pathway, it is possible that metformin inhibited

activity of these NAD-dependent enzymes by diminishing cellular NAD concentration.

Inhibition of such NAD-dependent enzymes may have led to the anti-tumor effect of

metformin.

FK866, used in this study as a representative NAD-depleting agent, inhibited
the growth of metastatic CMGT cell at the concentration less than one nanomolar, which
was equivalent or lower concentration compared to the previous reports using human
cancer cell lines (Gehrke et al., 2014; Hasmann and Schemainda, 2003). Although this
cytotoxic effect of FK866 was mostly masked by external NAD similar to the result of
metformin and the previously published study (Gehrke et al., 2014), the exact
mechanism of action seemed to be not completely equal to that of metformin. FK866 at
the higher concentration than the IC_{50} value did not cause significant effect on cell cycle
progression. Furthermore, NAD depletion by FK866 was more radical than that by
metformin; FK866 also almost eradicated cellular NADH pool; and external NAD
supplementation did not fully recover cellular NAD content although cell cycle
distribution and cell viability were recovered. These results were different from that of
metformin. FK866 inhibits NAMPT which is a rate-limiting enzyme in NAD salvage
pathway where nicotinamide is catalyzed into nicotinamide mononucleotide, the vital
precursor of NAD (Michels et al., 2014). Since NAD does not path through the
mitochondrial membrane of the mammalian cells and mitochondrial isoform of NAMPT
has not been reported so far, the initial result of NAD depletion by FK866 and metformin,

especially change in NAD content of each cellular compartment, is thought to differ incomparably (Di Stefano and Conforti, 2013; Michels et al., 2014). Further study is needed to clarify this point by quantifying NAD content of each cell compartment. As NAD was quantified only using the whole cell lysate in this chapter, effect of supplementation of external NAD on NAD pool of each cellular compartment needs more sophisticated evaluation as well. Nevertheless, anti-tumor effect of FK866 on canine malignancies and its clinical applicability was worthwhile to be addressed and should be further evaluated in another context.

Conclusion

From the result of this chapter, anti-tumor effect of metformin in metastatic CHMp-5b cell line was supposed to be mediated by cellular decrease in NAD, independently of cellular ATP content. This novel finding could contribute to exact understanding of mechanism of action of metformin and could be exploited for future clinical application. Since some NAD-dependent enzymes such as PARP1 and SIRT1 have been reported to be dominantly regulated by cellular NAD amount, it was suggested that anti-tumor effect of metformin could involve inhibition of these enzymes. Therefore, cellular expression or function of such NAD-dependent enzymes may have relationship with metformin sensitivity of the tumor cells.

A

FK866+NAD(CHMp-5b)

IC50(FK866)=4.66e-10
IC50(FK866+NAD)=1.67102e-07

B

Metformin+NAD(CHMp-5b)

IC50(MET)=1.83
IC50(MET+NAD)=8.12
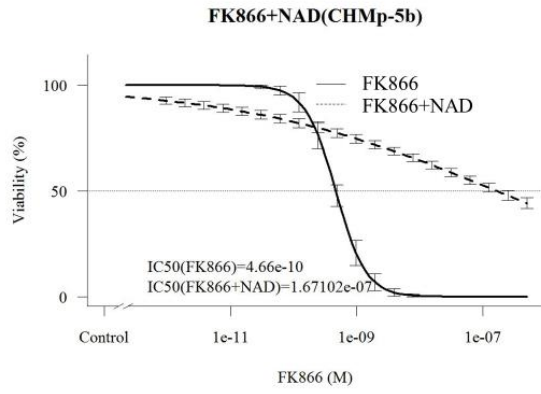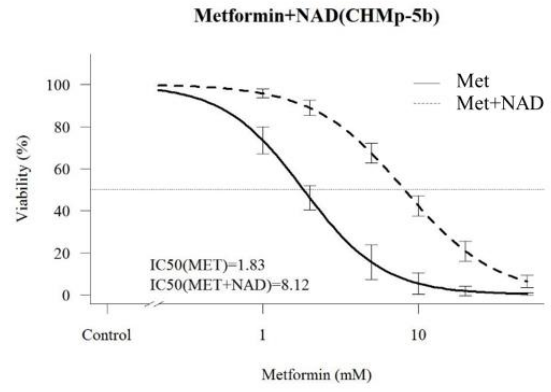
C
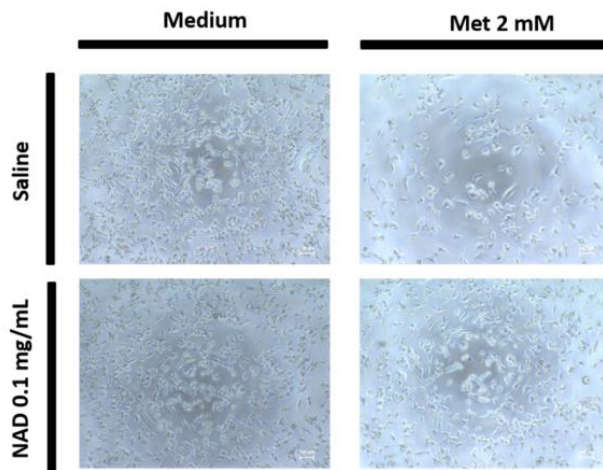
D

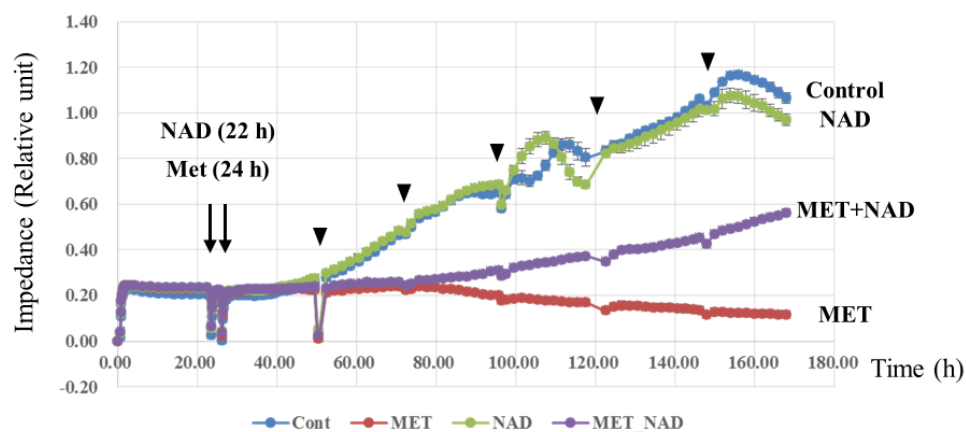**Fig. 4.1. *In vitro* effect of metformin or FK866 on cell growth of CHMp-5b with or without external NAD supplementation.**

(A, B): Concentration response curves of CHMp-5b viability for FK866 (A) and metformin (B) with or without external NAD (0.1 mg/mL) supplementation. Concentration response curves were generated to estimate the half-maximal inhibitory concentration (IC_{50}) using the four parameters logistic model in *R* and *drc* (*R* package). (C) Representative microscopic images of CHMp-5b after 48 h treatment of metformin (2 mM) with or without the presence of external NAD (0.1 mg/mL). (D) Summary of protective effect of NAD (0.1 mg/mL) on metformin- (2 mM) induced anti-proliferative effect in CHMp-5b cells. Data were pooled from three independent experiments. *$P < 0.05$ (t-test). Met, metformin.

Fig. 4.1. *In vitro* **effect of metformin or FK866 on cell growth of CHMp-5b with or without external NAD supplementation (***continued***).**

(E) Real-time evaluation of the protective effect of NAD (0.1 mg/mL) against metformin (2 mM)-induced growth inhibition using an iCELLigence system. Arrowheads indicate pulse artifact of the impedance by dairy microscopic examinations. MET, metformin.
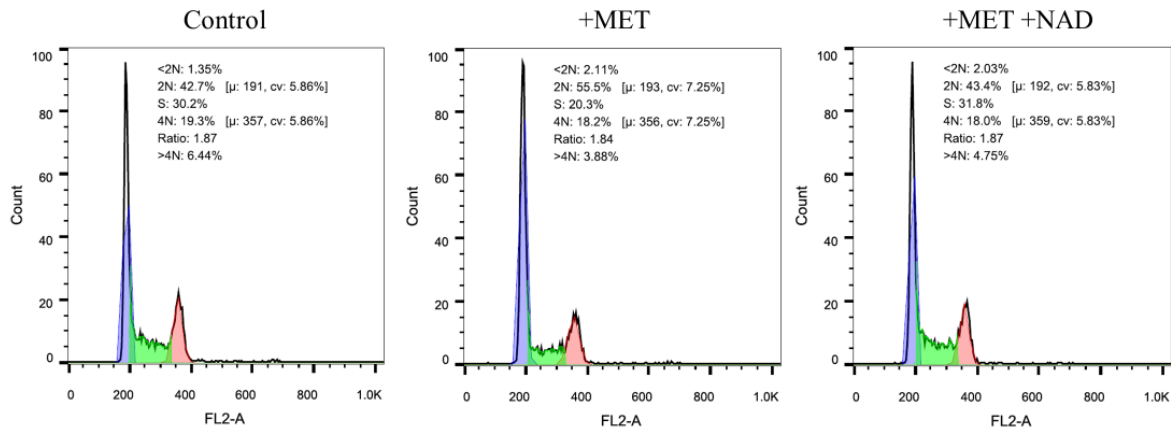
A

Fig. 4.2. Effect of metformin or FK866 treatment on cell cycle distribution of CHMp-5b with or without external NAD supplementation.

(A) Representative results of cell cycle analysis after 48 h treatment of metformin (2 mM) in the presence or absence of external NAD (0.1 mg/mL). Propidium iodide was used to stain nucleus. Cell cycle distribution was determined by FlowJo software. MET, metformin; <2N, sub-G1 phase; 2N, G0 and G1 phase; S, S phase; 4N, G2 and M phase; >4N, multinucleated cells; μ, population mean of fluorescence intensity; CV, coefficient of variation; Ratio, ratio of mean fluorescence intensity of G2/M phase and G0/G1 phase.
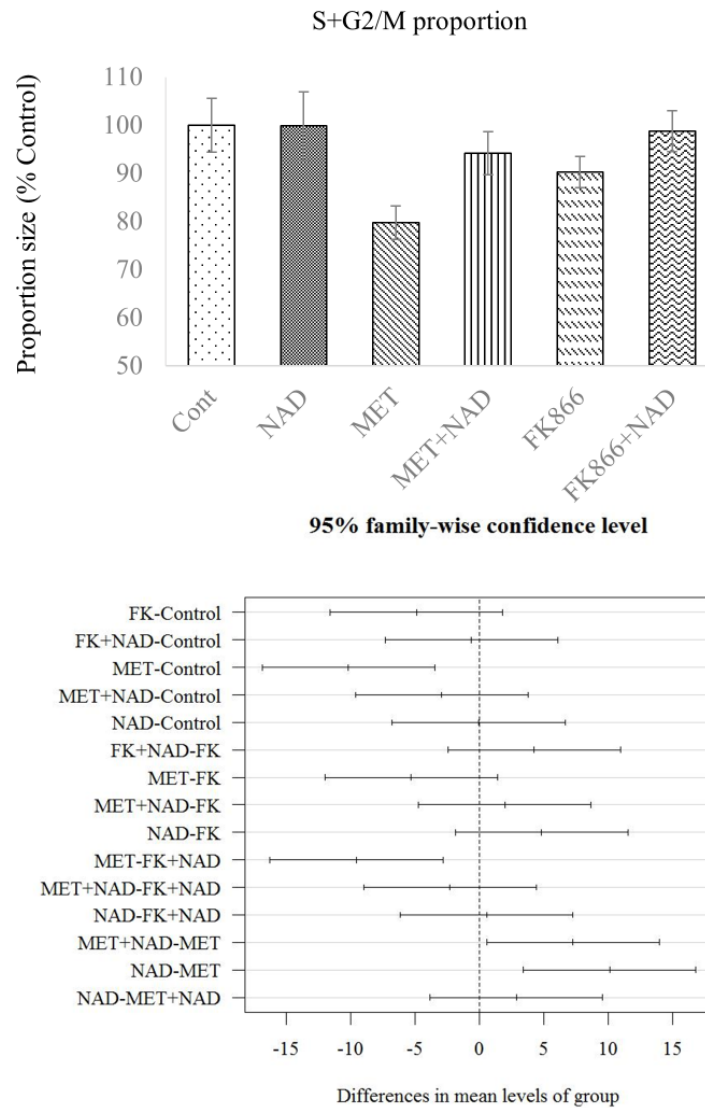
B

Fig. 4.2. Effect of metformin or FK866 on cell cycle distribution of CHMp-5b with or without external NAD supplementation (*continued*).

(B) Summary of change in dividing cell population by the indicated treatment for 48 h. Dividing cell population includes S, G2 and M phase. NAD, metformin and FK866 were used at following concentrations; 0.1 mg/mL, 2 mM and 2 nM, respectively. Results of Tukey-Kramer test was shown as well. MET, metformin.
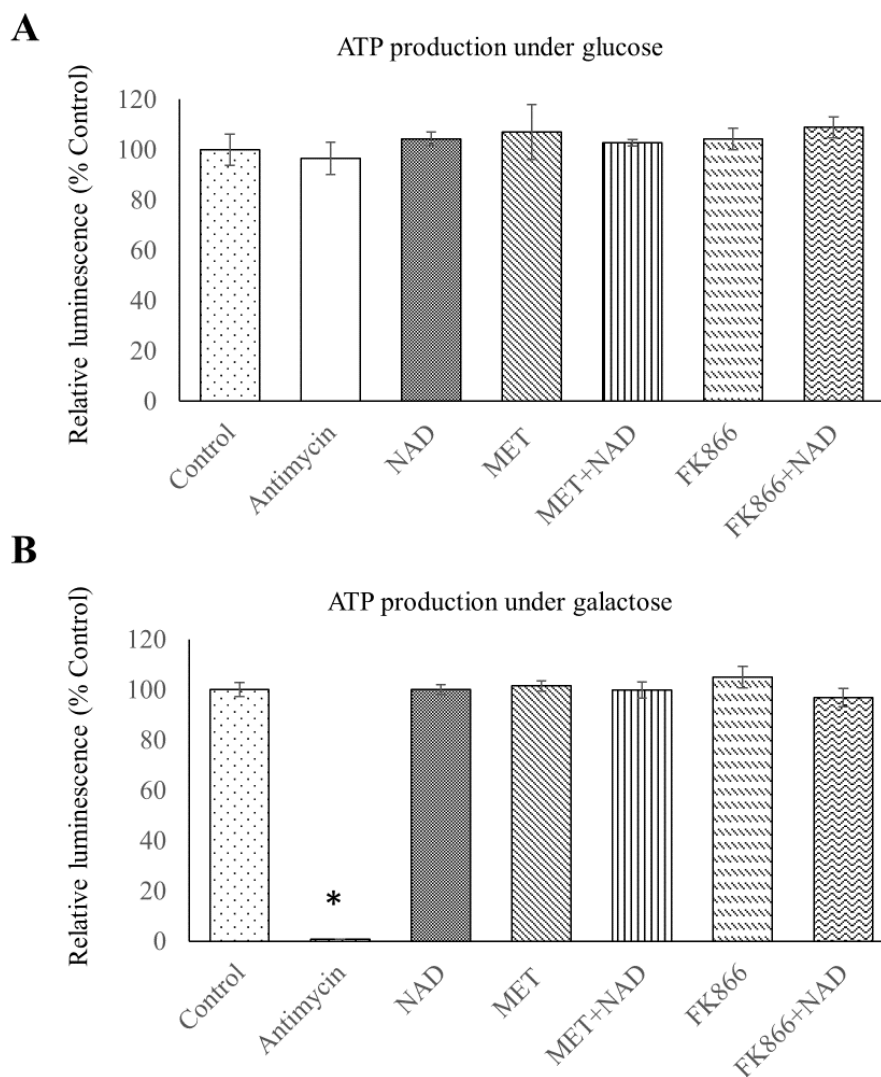
Fig. 4.3. Change in mitochondrial ATP production by the treatment of NAD, metformin, FK866 or their combination.

(A,B) ATP production was quantified under the glucose-containing condition (A) or completely glucose-starving condition (B) after 90 m exposure to the agents of interest. NAD (0.1 mg/mL), metformin (2 mM) or FK866 (2 nM) were used as a single agent or the indicated combinations. Antimycin, a known mitochondrial toxin, was also used as a positive control. Dunnett's test was performed to evaluate statistical significance when compared to control sample. *$P < 0.05$ (Dunnett's test). MET, metformin.
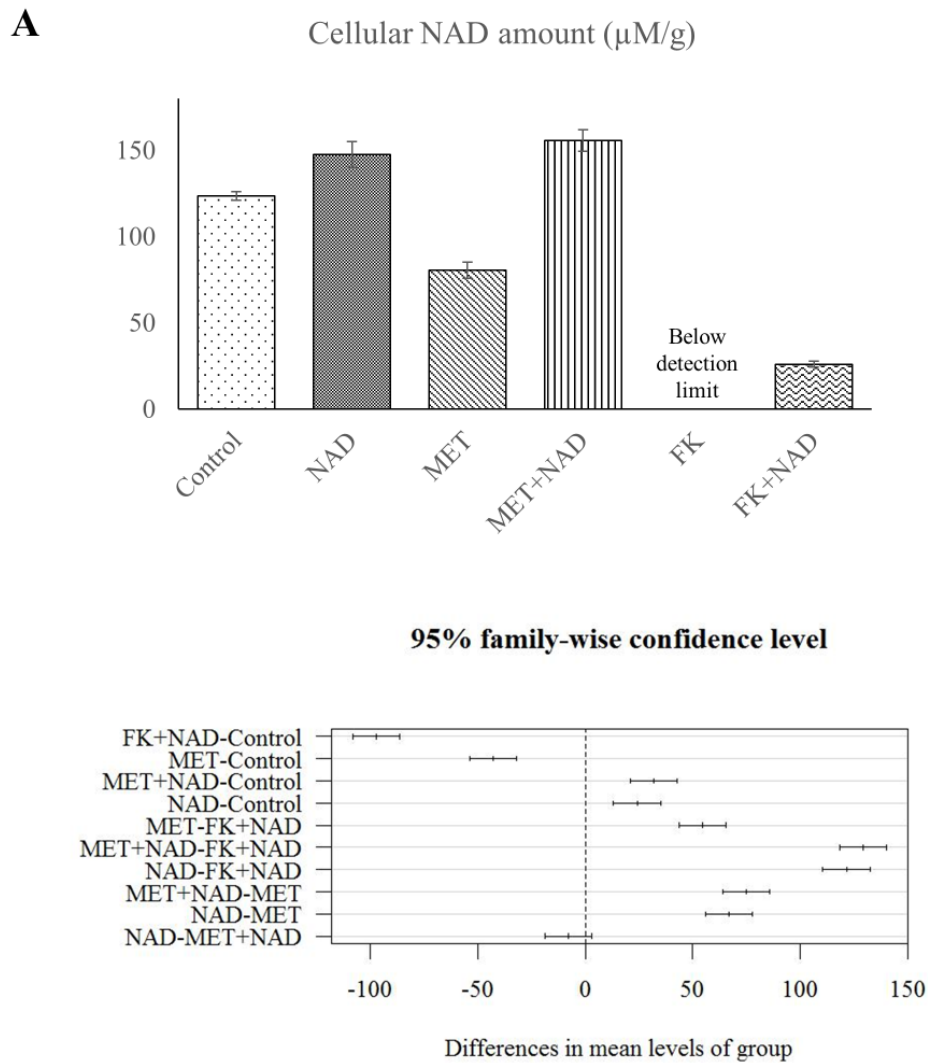
A Cellular NAD amount (μM/g)

95% family-wise confidence level

Differences in mean levels of group

Fig. 4.4. Change in cellular NAD and NADH content by the treatment of NAD, metformin, FK866 or their combination.

NAD (0.1 mg/mL), metformin (2 mM), FK866 (2 nM) were added to cultured cells as a single agent or the indicated combinations and incubated for 48 h. (A) NAD content of the treated cells. Values were normalized using total protein concentration determined by BCA assay. Results of Tukey-Kramer test was displayed as well. MET, metformin.
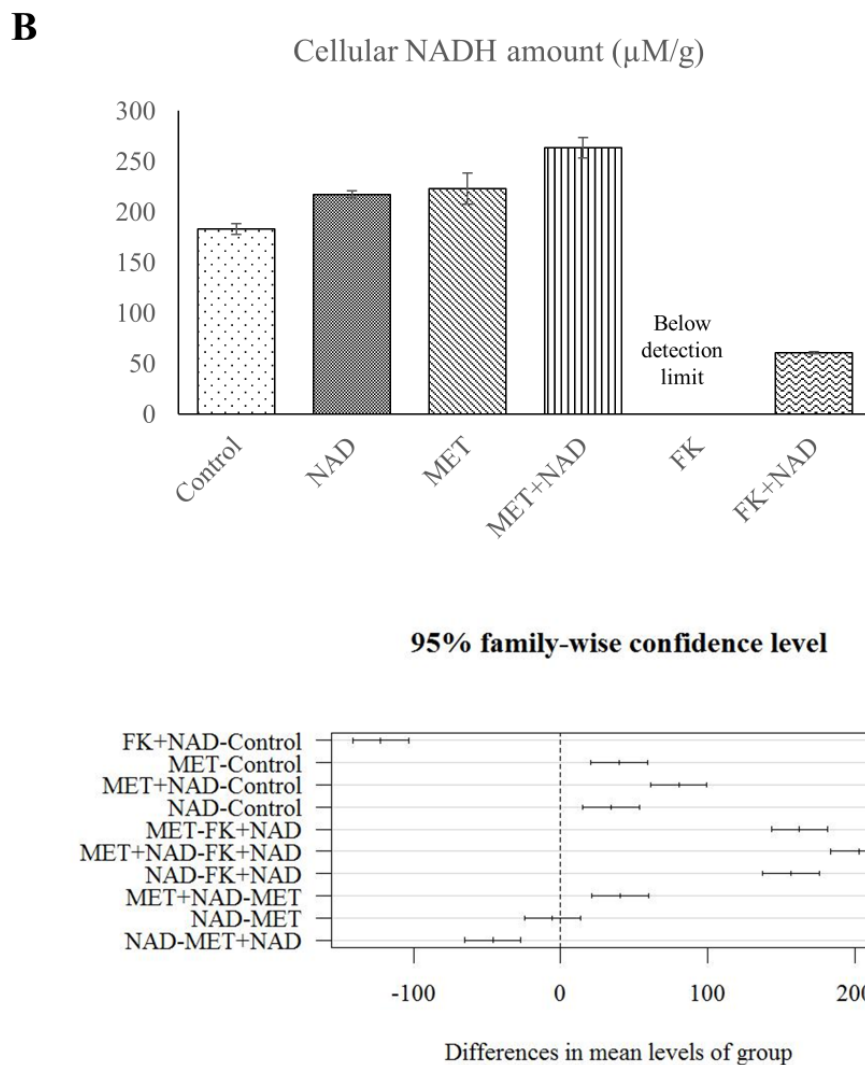
B

Cellular NADH amount (µM/g)

95% family-wise confidence level

Differences in mean levels of group

Fig. 4.4. Change in cellular NAD and NADH content by the treatment of NAD, metformin, FK866 or their combination (*continued*).

(B) NADH content of the treated cells. Values were normalized using total protein concentration determined by BCA assay. Results of Tukey-Kramer test was displayed as well. MET, metformin.
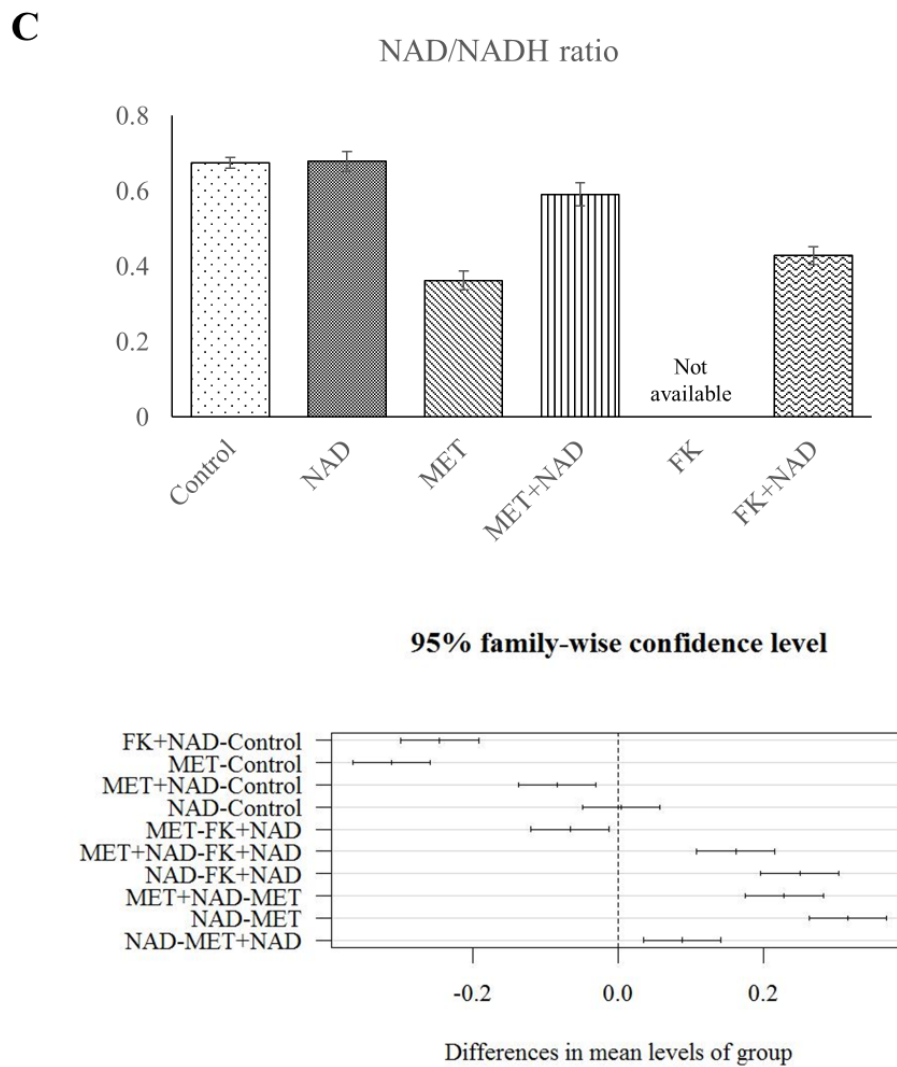
C

NAD/NADH ratio

95% family-wise confidence level

Fig. 4.4. Change in cellular NAD and NADH content by the treatment of NAD, metformin, FK866 or their combination (*continued*).

(C) NAD:NADH ratio was calculated from the result of NAD and NADH content. Results of Tukey-Kramer test was displayed as well. MET, metformin.

Chapter 5

General discussion and conclusion

AMPK is the molecule regarded as an energy sensor which has an important

evolutionary role to tackle low nutrient supply, turning cellular metabolism into

energy-sparing state (Foretz et al., 2014). Therefore, mTOR pathway inhibition and

associated attenuation of cell proliferation in CHMp-13a and other previous reports

would be one consequence of cellular response to restriction of energy consumption.

However, with its protective role against energy shortage, AMPK is also known to

improve cell survival under energy stress. The clear example has come from the liver

kinase B1 (LKB1)-deficient mouse transgenic model (Shackelford et al., 2013). LKB1

molecule locates upstream of AMPK, and controls phosphorylation and activation of

AMPK under energetic stress. In that study, combining LKB1 deficiency with KRAS-

induced murine lung carcinoma model, the authors reported that LKB1 deficient tumor

was more likely to respond to phenformin treatment, which was the other biguanide

derivative with similar function to metformin. Thus, it was concluded that cancer cells

functionally deficient in AMPK activation may be not able to handle and suppress their

energy consumption under energy-restricting circumstance, such as a biguanide

treatment, eventually resulting in fatal energy crisis.

Other enhanced sensitivity to the biguanides has been recently reported in the

mitochondrial respiratory complex 1-mutated or glucose incorporation-impaired cancer

cells (Birsoy et al., 2014). These cancer cells were also strikingly sensitive to low

glucose condition. The authors concluded that the cancer cells with such deficiency

were sensitive to the biguanide because their ATP production in mitochondria might be

easily disrupted due to low reserve capacity of mitochondria (complex 1 deficiency) or

substrate shortage (impaired glucose incorporation).

However, high sensitivity to metformin and AMPK-independent cell cycle

arrest observed in the metastatic CHMp-5b was not likely to be explained by

functional AMPK deficiency, impaired glucose incorporation or intrinsic mitochondrial

dysfunction, at least under 2 mM metformin treatment. In the serial experiments in this

thesis, it was noticed that metformin could exert anti-proliferative effect at the

concentration where mitochondrial ATP production was not yet disrupted. The

suggested mechanisms for elevated sensitivity to the biguanides in the previous studies

expect cellular ATP shortage and fatal energy crisis at the low drug concentration

exposure, at which normal cells could keep ATP production with enhanced glucose

utilization or reserve mitochondria function. Or sometimes, functionally normal cells

such as CHMp-13a also could reduce cellular ATP consumption by activating AMPK

molecule to meet the restricted energy supply. Therefore, it was speculated that

decrease in mitochondrial ATP production should have become apparent under 2 mM-

metformin treatment in the metastatic CHMp-5b if such explanation could be applied to. Our results in the subsequent experiment suggested cellular NAD deprivation as a novel key phenomenon on the exposure to metformin.

It was of great interest that the identified selective anti-metastatic agents were inhibitors of the mitochondrial oxidative (OXPHOS) because well-known hallmark of the cancer cell was enhanced glycolytic activity regardless of the oxygen availability (Hanahan and Weinberg, 2011). This aerobic glycolysis or "Warburg effect" was discovered approximately one century ago by Otto Warburg (Weinhouse et al., 1956). This glycolytic character of the cancer cell even under the normoxia condition has been exploited successfully for the diagnostic imaging of cancer (such as [18]Fluoro-deoxyglucose positron emission tomography). In addition, several therapeutic approach targeting cancer glycolysis, such as glucose analogs, are currently under investigation (Ganapathy-Kanniappan and Geschwind, 2013; Granchi et al., 2014). Enhanced glycolysis is considered be beneficial for cancer cells because it could support cancer cell survival under hypoxic condition and supply more building blocks of the cellular component as intermediates from the enhanced pentose phosphate pathway.

On the other hand, the recent studies also indicated the importance of OXPHOS

in cancer cells, especially in CSC populations (Birsoy et al., 2014; Pastò et al., 2014), indicating the significance of the mitochondria-targeting strategy for cancer management. These studies focused on ATP production from mitochondria and showed resistance of CSC populations to glucose-deprivation. The findings in this thesis may also indicate importance of the OXPHOS in the malignant population in the cancer from the view of proper recycling of NAD. Complicated cancer cell metabolism should be further evaluated taking tumor heterogeneity into account.

In conclusion, in this thesis, it was suggested that MRCIs may serve as a metastatic clone specific agents. Clinical applicability of one such MRCI, metformin was also demonstrated. In addition, distinct cellular signaling or function at the OXPHOS was indicated between the metastatic and the non-metastatic clones. There still exists a gap between anti-tumor mechanism of metformin (and other MRCIs) and selective vulnerability of the metastatic clone, however, these novel findings, especially the involvement of NAD, would contribute to the understanding and future clinical application of metformin. In human medicine, metformin has been attracting great attention due to the plenty of the reports which have demonstrated selective anti-tumor effect of the drug on CSC population, the other side of cancer heterogeneity. Future study

should be performed to identify the functional molecules which must connect fluctuation

of NAD with the cell cycle machinery and may have relationship with cancer malignancy.

The findings in this thesis also should be translated into future clinical application.

Acknowledgements

First of all, I wish to express my sincere gratitude to my mentor, Professor Ryohei Nishimura[a] for his supervision, support, suggestion and guidance during this period as well as his warm advisement about whole my life as a graduate student, researcher, veterinarian and one human. I deeply appreciate every single word in our conversation and discussion.

Additionally, I would like to present great appreciation to my previous mentor Professor Emeritus Nobuo Sasaki, The University of Tokyo who encouraged me to study abroad and proceed to a graduate study with great support. I also would like to show my great thanks to Assistant Professor Takayuki Nakagawa[a], who have taken care of the team and my study from all aspects. His support and advisement always encouraged me, and kept me activated. His introduction of numerous researchers gave me much stimuli and opportunity to open my eyes to the novel fields.

I also deeply appreciate my key collaborators; Professor Sumio Sugano[b], Associate professor Manabu Watanabe[b] and Research Assistant Professor Masaya Tsuboi[c] who supported me a lot and worked together to perform cDNA microarray analysis; Lecturer Masaki Michishita[d] who helped ALDEFLUOR assay and educated me about CSC theory.

I would like to express my thanks to the people who substantially contributed to the thesis as well; Research Assistant Professor Naoki Fujita[a] who gave me a lot of advisement and technical support in doing experiments as well as building up, maintaining and controlling daily laboratory activities; Drs. Yumiko Ishii[e] who technically supported me performing flowcytometric analysis; Mr.

---

[a] Laboratory of Veterinary Surgery, Graduate School of Agricultural and Life Sciences, The University of Tokyo

[b] Department of Medical Genome Science, Graduate School of Frontier Sciences, The University of Tokyo

[c] Laboratory of Veterinary Pathology, Graduate school of Agricultural and Life Sciences, The University of Tokyo

[d] Laboratory of Veterinary Pathology, School of Veterinary Medicine, Nippon Veterinary and Life Science University

[e] FACS core laboratory, The Institute of Medical Sciences, The University of Tokyo

Ryohei Yoshitake[a] who devoted much time to work together and helped me. I also would like to show my great appreciation to Professor Hiroyuki Nakayama and Professor Keiichiro Maeda, as representatives of Laboratory of Veterinary Pathology and Laboratory of Theriogenology, The University of Tokyo, respectively, for providing and sharing experimental instruments otherwise most of the thesis could not be accomplished.

Furthermore, I deeply appreciate Professor Moriaki Kusakabe[f] and Lecturer Yoshifumi Endo[g] for their continuous care and useful, fair advisement. I also would like to show my gratitude to all the members in our laboratory and in Veterinary Medical Center, The University of Tokyo for their encouragement, support, advisement and friendship.

Finally, I cannot help expressing my best gratitude to my wife Yukari Saeki, my parents and my wife's parents who allowed me to pursue a career in the graduate school. They also understood, supported and encouraged me all the time with big patience and tender love. This thesis would not be completed without help and understanding by the people listed above. I would like to thank you all very much.

---

[f] Research Center for Food Safety, Graduate School of Agricultural and Life Sciences, The University of Tokyo

[g] Laboratory of Veterinary Clinical Oncology, Graduate School of Veterinary Medicine, Rakuno Gakuen University

References

Al-Hajj, M., Wicha, M.S., Benito-Hernandez, A., Morrison, S.J., Clarke, M.F., 2003. Prospective identification of tumorigenic breast cancer cells. Proc. Natl. Acad. Sci. U. S. A. 100, 3983–3988.

Ansieau, S., 2013. EMT in breast cancer stem cell generation. Cancer Lett., Cancer Stem Cells 338, 63–68.

Ashburner, M., Ball, C.A., Blake, J.A., Botstein, D., Butler, H., Cherry, J.M., Davis, A.P., Dolinski, K., Dwight, S.S., Eppig, J.T., Harris, M.A., Hill, D.P., Issel-Tarver, L., Kasarskis, A., Lewis, S., Matese, J.C., Richardson, J.E., Ringwald, M., Rubin, G.M., Sherlock, G., 2000. Gene ontology: tool for the unification of biology. The Gene Ontology Consortium. Nat. Genet. 25, 25–29.

Balaban, R.S., Nemoto, S., Finkel, T., 2005. Mitochondria, Oxidants, and Aging. Cell 120, 483–495.

Barker, N., 2014. Adult intestinal stem cells: critical drivers of epithelial homeostasis and regeneration. Nat. Rev. Mol. Cell Biol. 15, 19–33.

Ben Sahra, I., Laurent, K., Loubat, A., Giorgetti-Peraldi, S., Colosetti, P., Auberger, P., Tanti, J.F., Le Marchand-Brustel, Y., Bost, F., 2008. The antidiabetic drug metformin exerts an antitumoral effect in vitro and in vivo through a decrease of cyclin D1 level. Oncogene 27, 3576–3586.

Berger, F., Ramírez-Hernández, M.H., Ziegler, M., 2004. The new life of a centenarian: signalling functions of NAD(P). Trends Biochem. Sci. 29, 111–118.

Bhatia, M., Wang, J.C.Y., Kapp, U., Bonnet, D., Dick, J.E., 1997. Purification of primitive human hematopoietic cells capable of repopulating immune-deficient mice. Proc. Natl. Acad. Sci. 94, 5320–5325.

Binns, D., Dimmer, E., Huntley, R., Barrell, D., O'Donovan, C., Apweiler, R., 2009. QuickGO: a web-based tool for Gene Ontology searching. Bioinforma. Oxf. Engl. 25, 3045–3046.

Birsoy, K., Possemato, R., Lorbeer, F.K., Bayraktar, E.C., Thiru, P., Yucel, B., Wang, T., Chen, W.W., Clish, C.B., Sabatini, D.M., 2014. Metabolic determinants of cancer cell sensitivity to glucose limitation and biguanides. Nature 508, 108–112.

Burrell, R.A., McGranahan, N., Bartek, J., Swanton, C., 2013. The causes and consequences of genetic heterogeneity in cancer evolution. Nature 501, 338–345.

Burrell, R.A., Swanton, C., 2014. The evolution of the unstable cancer genome. Curr.

Opin. Genet. Dev., Cancer genomics 24, 61–67.

Cazzaniga, M., DeCensi, A., Pruneri, G., Puntoni, M., Bottiglieri, L., Varricchio, C., Guerrieri-Gonzaga, A., Gentilini, O.D., Pagani, G., Dell'Orto, P., Lazzeroni, M., Serrano, D., Viale, G., Bonanni, B., 2013. The effect of metformin on apoptosis in a breast cancer presurgical trial. Br. J. Cancer 109, 2792–2797.

Chang, S.-C., Chang, C.-C., Chang, T.-J., Wong, M.-L., 2005. Prognostic factors associated with survival two years after surgery in dogs with malignant mammary tumors: 79 cases (1998-2002). J. Am. Vet. Med. Assoc. 227, 1625–1629.

Cheng, S., Tada, M., Hida, Y., Asano, T., Kuramae, T., Takemoto, N., Hamada, J.-I., Miyamoto, M., Hirano, S., Kondo, S., Moriuchi, T., 2008. High MMP-1 mRNA expression is a risk factor for disease-free and overall survivals in patients with invasive breast carcinoma. J. Surg. Res. 146, 104–109.

Choi, J.-E., Mostoslavsky, R., 2014. Sirtuins, metabolism, and DNA repair. Curr. Opin. Genet. Dev. 26, 24–32.

Choi, M.-K., Jin, Q.-R., Ahn, S.-H., Bae, M.-A., Song, I.-S., 2010. Sitagliptin attenuates metformin-mediated AMPK phosphorylation through inhibition of organic cation transporters. Xenobiotica Fate Foreign Compd. Biol. Syst. 40, 817–825.

Chou, C.-C., Lee, K.-H., Lai, I.-L., Wang, D., Mo, X., Kulp, S.K., Shapiro, C.L., Chen, C.-S., 2014. AMPK Reverses the Mesenchymal Phenotype of Cancer Cells by Targeting the Akt-MDM2-Foxo3a Signaling Axis. Cancer Res 74, 4783-95.

Clemente, M., Pérez-Alenza, M.D., Peña, L., 2010. Metastasis of Canine Inflammatory versus Non-Inflammatory Mammary Tumours. J. Comp. Pathol. 143, 157–163.

Coulom, H., Birman, S., 2004. Chronic Exposure to Rotenone Models Sporadic Parkinson's Disease in Drosophila melanogaster. J. Neurosci. 24, 10993–10998.

Cuyàs, E., Corominas-Faja, B., Menendez, J.A., 2014. The nutritional phenome of EMT-induced cancer stem-like cells. Oncotarget 5, 3970–3982.

Davis, S., Meltzer, P.S., 2007. GEOquery: a bridge between the Gene Expression Omnibus (GEO) and BioConductor. Bioinformatics 23, 1846–1847.

Decensi, A., Puntoni, M., Goodwin, P., Cazzaniga, M., Gennari, A., Bonanni, B., Gandini, S., 2010. Metformin and cancer risk in diabetic patients: a systematic review and meta-analysis. Cancer Prev. Res. 3, 1451–1461.

Dennis, G., Sherman, B.T., Hosack, D.A., Yang, J., Gao, W., Lane, H.C., Lempicki,

R.A., 2003. DAVID: Database for Annotation, Visualization, and Integrated Discovery. Genome Biol. 4, P3.

Dieter, S.M., Ball, C.R., Hoffmann, C.M., Nowrouzi, A., Herbst, F., Zavidij, O., Abel, U., Arens, A., Weichert, W., Brand, K., Koch, M., Weitz, J., Schmidt, M., von Kalle, C., Glimm, H., 2011. Distinct Types of Tumor-Initiating Cells Form Human Colon Cancer Tumors and Metastases. Cell Stem Cell 9, 357–365.

Ding, L., Ley, T.J., Larson, D.E., Miller, C.A., Koboldt, D.C., Welch, J.S., Ritchey, J.K., Young, M.A., Lamprecht, T., McLellan, M.D., McMichael, J.F., Wallis, J.W., Lu, C., Shen, D., Harris, C.C., Dooling, D.J., Fulton, R.S., Fulton, L.L., Chen, K., Schmidt, H., Kalicki-Veizer, J., Magrini, V.J., Cook, L., McGrath, S.D., Vickery, T.L., Wendl, M.C., Heath, S., Watson, M.A., Link, D.C., Tomasson, M.H., Shannon, W.D., Payton, J.E., Kulkarni, S., Westervelt, P., Walter, M.J., Graubert, T.A., Mardis, E.R., Wilson, R.K., DiPersio, J.F., 2012. Clonal evolution in relapsed acute myeloid leukaemia revealed by whole-genome sequencing. Nature 481, 506–510.

Di Stefano, M., Conforti, L., 2013. Diversification of NAD biological role：the importance of location. FEBS J. 280, 4711–4728.

Dorn, C.R., Taylor, D.O., Schneider, R., Hibbard, H.H., Klauber, M.R., 1968. Survey of animal neoplasms in Alameda and Contra Costa Counties, California. II. Cancer morbidity in dogs and cats from Alameda County. J. Natl. Cancer Inst. 40, 307–318.

Dowling, R.J.O., Zakikhani, M., Fantus, I.G., Pollak, M., Sonenberg, N., 2007. Metformin Inhibits Mammalian Target of Rapamycin–Dependent Translation Initiation in Breast Cancer Cells. Cancer Res. 67, 10804–10812.

Dykens, J.A., Jamieson, J., Marroquin, L., Nadanaciva, S., Billis, P.A., Will, Y., 2008. Biguanide-induced mitochondrial dysfunction yields increased lactate production and cytotoxicity of aerobically-poised HepG2 cells and human hepatocytes in vitro. Toxicol. Appl. Pharmacol. 233, 203–210.

Eades, G., Yao, Y., Yang, M., Zhang, Y., Chumsri, S., Zhou, Q., 2011. miR-200a Regulates SIRT1 Expression and Epithelial to Mesenchymal Transition (EMT)-like Transformation in Mammary Epithelial Cells. J. Biol. Chem. 286, 25992–26002.

Edgar, R., Domrachev, M., Lash, A.E., 2002. Gene Expression Omnibus: NCBI gene expression and hybridization array data repository. Nucleic Acids Res. 30, 207–210.

Ekström, N., Schiöler, L., Svensson, A.-M., Eeg-Olofsson, K., Jonasson, J.M.,

Zethelius, B., Cederholm, J., Eliasson, B., Gudbjörnsdottir, S., 2012. Effectiveness and safety of metformin in 51 675 patients with type 2 diabetes and different levels of renal function: a cohort study from the Swedish National Diabetes Register. BMJ Open 2, e001076.

Emami Riedmaier, A., Fisel, P., Nies, A.T., Schaeffeler, E., Schwab, M., 2013. Metformin and cancer: from the old medicine cabinet to pharmacological pitfalls and prospects. Trends Pharmacol. Sci. 34, 126–135.

Fidler, I.J., 1978. Tumor Heterogeneity and the Biology of Cancer Invasion and Metastasis. Cancer Res. 38, 2651–2660.

Fidler, I.J., Kripke, M.L., 1977. Metastasis results from preexisting variant cells within a malignant tumor. Science 197, 893–895.

Foretz, M., Guigas, B., Bertrand, L., Pollak, M., Viollet, B., 2014. Metformin: From Mechanisms of Action to Therapies. Cell Metab. 20, 953–966.

Franciosi, M., Lucisano, G., Lapice, E., Strippoli, G.F.M., Pellegrini, F., Nicolucci, A., 2013. Metformin Therapy and Risk of Cancer in Patients with Type 2 Diabetes: Systematic Review. PLoS ONE 8, e71583.

Gama, A., Paredes, J., Gärtner, F., Alves, A., Schmitt, F., 2008. Expression of E-cadherin, P-cadherin and beta-catenin in canine malignant mammary tumours in relation to clinicopathological parameters, proliferation and survival. Vet. J. 1997 177, 45–53.

Ganapathy-Kanniappan, S., Geschwind, J.-F.H., 2013. Tumor glycolysis as a target for cancer therapy: progress and prospects. Mol. Cancer 12, 152.

Gehrke, I., Bouchard, E.D.J., Beiggi, S., Poeppl, A.G., Johnston, J.B., Gibson, S.B., Banerji, V., 2014. On-Target Effect of FK866, a Nicotinamide Phosphoribosyl Transferase Inhibitor, by Apoptosis-Mediated Death in Chronic Lymphocytic Leukemia Cells. Clin. Cancer Res. 20, 4861–4872.

Gerlinger, M., Rowan, A.J., Horswell, S., Larkin, J., Endesfelder, D., Gronroos, E., Martinez, P., Matthews, N., Stewart, A., Tarpey, P., Varela, I., Phillimore, B., Begum, S., McDonald, N.Q., Butler, A., Jones, D., Raine, K., Latimer, C., Santos, C.R., Nohadani, M., Eklund, A.C., Spencer-Dene, B., Clark, G., Pickering, L., Stamp, G., Gore, M., Szallasi, Z., Downward, J., Futreal, P.A., Swanton, C., 2012. Intratumor Heterogeneity and Branched Evolution Revealed by Multiregion Sequencing. N. Engl. J. Med. 366, 883–892.

Giacinti, C., Giordano, A., 2006. RB and cell cycle progression. Oncogene 25, 5220–5227.

Granchi, C., Fancelli, D., Minutolo, F., 2014. An update on therapeutic

opportunities offered by cancer glycolytic metabolism. Bioorg. Med. Chem. Lett. 24, 4915–4925.

Gupta, P.B., Onder, T.T., Jiang, G., Tao, K., Kuperwasser, C., Weinberg, R.A., Lander, E.S., 2009. Identification of Selective Inhibitors of Cancer Stem Cells by High-Throughput Screening. Cell 138, 645–659.

Gusterson, B.A., Stein, T., 2012. Human breast development. Semin. Cell Dev. Biol., Cell Regulation by Selective Protein Degradation & Biology of Mammary Gland Development 23, 567–573.

Hadad, S., Iwamoto, T., Jordan, L., Purdie, C., Bray, S., Baker, L., Jellema, G., Deharo, S., Hardie, D.G., Pusztai, L., Moulder-Thompson, S., Dewar, J.A., Thompson, A.M., 2011. Evidence for biological effects of metformin in operable breast cancer: a pre-operative, window-of-opportunity, randomized trial. Breast Cancer Res. Treat. 128, 783–794.

Hanahan, D., Weinberg, R.A., 2011. Hallmarks of Cancer: The Next Generation. Cell 144, 646–674.

Han, Y.H., Park, W.H., 2009a. Growth inhibition in antimycin A treated-lung cancer Calu-6 cells via inducing a G1 phase arrest and apoptosis. Lung Cancer Amst. Neth. 65, 150–160.

Han, Y.H., Park, W.H., 2009b. Tiron, a ROS scavenger, protects human lung cancer Calu-6 cells against antimycin A-induced cell death. Oncol. Rep. 21, 253–261.

Hasmann, M., Schemainda, I., 2003. FK866, a Highly Specific Noncompetitive Inhibitor of Nicotinamide Phosphoribosyltransferase, Represents a Novel Mechanism for Induction of Tumor Cell Apoptosis. Cancer Res. 63, 7436–7442.

Herranz, D., Maraver, A., Cañamero, M., Gómez-López, G., Inglada-Pérez, L., Robledo, M., Castelblanco, E., Matias-Guiu, X., Serrano, M., 2013. SIRT1 promotes thyroid carcinogenesis driven by PTEN deficiency. Oncogene 32, 4052–4056.

Holohan, C., Van Schaeybroeck, S., Longley, D.B., Johnston, P.G., 2013. Cancer drug resistance: an evolving paradigm. Nat. Rev. Cancer 13, 714–726. 9

Hong, Y., Nie, H., Wu, D., Wei, X., Ding, X., Ying, W., 2014. NAD(+) treatment prevents rotenone-induced apoptosis and necrosis of differentiated PC12 cells. Neurosci. Lett. 560, 46–50.

Hothorn, T., Bretz, F., Westfall, P., 2008. Simultaneous inference in general parametric models. Biom. J. Biom. Z. 50, 346–363.

Huffman, D.M., Grizzle, W.E., Bamman, M.M., Kim, J., Eltoum, I.A., Elgavish, A., Nagy, T.R., 2007. SIRT1 Is Significantly Elevated in Mouse and Human Prostate Cancer. Cancer Res. 67, 6612–6618.

Ishikawa, K., Takenaga, K., Akimoto, M., Koshikawa, N., Yamaguchi, A., Imanishi, H., Nakada, K., Honma, Y., Hayashi, J.-I., 2008. ROS-Generating Mitochondrial DNA Mutations Can Regulate Tumor Cell Metastasis. Science 320, 661–664.

Junttila, M.R., de Sauvage, F.J., 2013. Influence of tumour micro-environment heterogeneity on therapeutic response. Nature 501, 346–354.

Kashiwagi, S., Yashiro, M., Takashima, T., Aomatsu, N., Ikeda, K., Ogawa, Y., Ishikawa, T., Hirakawa, K., 2011. Advantages of adjuvant chemotherapy for patients with triple-negative breast cancer at Stage II: usefulness of prognostic markers E-cadherin and Ki67. Breast Cancer Res. 13, R122.

Kienast, Y., von Baumgarten, L., Fuhrmann, M., Klinkert, W.E.F., Goldbrunner, R., Herms, J., Winkler, F., 2010. Real-time imaging reveals the single steps of brain metastasis formation. Nat. Med. 16, 116–122.

Kisfalvi, K., Eibl, G., Sinnett-Smith, J., Rozengurt, E., 2009. Metformin Disrupts Crosstalk between G Protein–Coupled Receptor and Insulin Receptor Signaling Systems and Inhibits Pancreatic Cancer Growth. Cancer Res. 69, 6539–6545.

Kitambi, S.S., Toledo, E.M., Usoskin, D., Wee, S., Harisankar, A., Svensson, R., Sigmundsson, K., Kalderén, C., Niklasson, M., Kundu, S., Aranda, S., Westermark, B., Uhrbom, L., Andäng, M., Damberg, P., Nelander, S., Arenas, E., Artursson, P., Walfridsson, J., Forsberg Nilsson, K., Hammarström, L.G.J., Ernfors, P., 2014. Vulnerability of Glioblastoma Cells to Catastrophic Vacuolization and Death Induced by a Small Molecule. Cell 157, 313-328.

Klopfleisch, R., Gruber, A.D., 2009. Differential expression of cell cycle regulators p21, p27 and p53 in metastasizing canine mammary adenocarcinomas versus normal mammary glands. Res. Vet. Sci. 87, 91–96.

Klopfleisch, R., Schütze, M., Gruber, A.D., 2010. Loss of p27 expression in canine mammary tumors and their metastases. Res. Vet. Sci. 88, 300–303.

Kominsky, S.L., Argani, P., Korz, D., Evron, E., Raman, V., Garrett, E., Rein, A., Sauter, G., Kallioniemi, O.-P., Sukumar, S., 2003. Loss of the tight junction protein claudin-7 correlates with histological grade in both ductal carcinoma in situ and invasive ductal carcinoma of the breast. Oncogene 22, 2021–2033.

Kreso, A., Dick, J.E., 2014. Evolution of the Cancer Stem Cell Model. Cell Stem Cell

14, 275–291.

Liang, J., Mills, G.B., 2013. AMPK: A Contextual Oncogene or Tumor Suppressor? Cancer Res. 73, 2929–2935.

Liu, X., Chhipa, R.R., Pooya, S., Wortman, M., Yachyshin, S., Chow, L.M.L., Kumar, A., Zhou, X., Sun, Y., Quinn, B., McPherson, C., Warnick, R.E., Kendler, A., Giri, S., Poels, J., Norga, K., Viollet, B., Grabowski, G.A., Dasgupta, B., 2014. Discrete mechanisms of mTOR and cell cycle regulation by AMPK agonists independent of AMPK. Proc. Natl. Acad. Sci. 111, E435–E444.

Lonardo, E., Cioffi, M., Sancho, P., Sanchez-Ripoll, Y., Trabulo, S.M., Dorado, J., Balic, A., Hidalgo, M., Heeschen, C., 2013. Metformin Targets the Metabolic Achilles Heel of Human Pancreatic Cancer Stem Cells. PLoS ONE 8, e76518.

Luo, J., Nikolaev, A.Y., Imai, S., Chen, D., Su, F., Shiloh, A., Guarente, L., Gu, W., 2001. Negative Control of p53 by Sir2α Promotes Cell Survival under Stress. Cell 107, 137–148.

Luzzi, K.J., MacDonald, I.C., Schmidt, E.E., Kerkvliet, N., Morris, V.L., Chambers, A.F., Groom, A.C., 1998. Multistep Nature of Metastatic Inefficiency: Dormancy of Solitary Cells after Successful Extravasation and Limited Survival of Early Micrometastases. Am. J. Pathol. 153, 865–873.

Maere, S., Heymans, K., Kuiper, M., 2005. BiNGO: a Cytoscape plugin to assess overrepresentation of gene ontology categories in biological networks. Bioinforma. 21, 3448–3449.

Mamane, Y., Petroulakis, E., LeBacquer, O., Sonenberg, N., 2006. mTOR, translation initiation and cancer. Oncogene 25, 6416–6422.

Marte, B., 2013. Tumour heterogeneity. Nature 501, 327–327.

Maryanovich, M., Gross, A., 2013. A ROS rheostat for cell fate regulation. Trends Cell Biol. 23, 129–134.

Meacham, C.E., Morrison, S.J., 2013. Tumour heterogeneity and cancer cell plasticity. Nature 501, 328–337.

Michels, J., Obrist, F., Castedo, M., Vitale, I., Kroemer, G., 2014. PARP and other prospective targets for poisoning cancer cell metabolism. Biochem. Pharmacol. 92, 164–171.

Michishita, M., Akiyoshi, R., Suemizu, H., Nakagawa, T., Sasaki, N., Takemitsu, H., Arai, T., Takahashi, K., 2012. Aldehyde dehydrogenase activity in cancer stem cells from canine mammary carcinoma cell lines. Vet. J. 193, 508–513.

Murai, K., Nakagawa, T., Endo, Y., Kamida, A., Yoshida, K., Mochizuki, M., Nishimura, R., Sasaki, N., 2012. Establishment of a pair of novel cloned

tumour cell lines with or without metastatic potential from canine mammary adenocarcinoma. Res. Vet. Sci. 93, 468–472.

Musgrove, E.A., Caldon, C.E., Barraclough, J., Stone, A., Sutherland, R.L., 2011. Cyclin D as a therapeutic target in cancer. Nat. Rev. Cancer 11, 558–572.

Naujokat, C., Steinhart, R., 2012. Salinomycin as a Drug for Targeting Human Cancer Stem Cells. BioMed Res. Int. 2012, e950658.

Nelson, R.W., 2000. Oral medications for treating diabetes mellitus in dogs and cats. J. Small Anim. Pract. 41, 486–490.

Nieto, M.A., 2013. Epithelial Plasticity: A Common Theme in Embryonic and Cancer Cells. Science 342, 1234850–1234850.

Noto, H., Goto, A., Tsujimoto, T., Noda, M., 2012. Cancer Risk in Diabetic Patients Treated with Metformin: A Systematic Review and Meta-analysis. PLoS ONE 7, e33411.

Ogita, M., Ogita, A., Usuki, Y., Fujita, K., Tanaka, T., 2009. Antimycin A-induced cell death depends on AIF translocation through NO production and PARP activation and is not involved in ROS generation, cytochrome c release and caspase-3 activation in HL-60 cells. J. Antibiot. (Tokyo) 62, 145–152.

Oguri, T., Achiwa, H., Sato, S., Bessho, Y., Takano, Y., Miyazaki, M., Muramatsu, H., Maeda, H., Niimi, T., Ueda, R., 2006. The determinants of sensitivity and acquired resistance to gemcitabine differ in non–small cell lung cancer: a role of ABCC5 in gemcitabine sensitivity. Mol. Cancer Ther. 5, 1800–1806.

Overall, C.M., Kleifeld, O., 2006. Validating matrix metalloproteinases as drug targets and anti-targets for cancer therapy. Nat. Rev. Cancer 6, 227–239.

Pagliarani, A., Nesci, S., Ventrella, V., 2013. Modifiers of the oligomycin sensitivity of the mitochondrial F1F0-ATPase. Mitochondrion 13, 312–319.

Pastò, A., Bellio, C., Pilotto, G., Ciminale, V., Silic-Benussi, M., Guzzo, G., Rasola, A., Frasson, C., Nardo, G., Zulato, E., Nicoletto, M.O., Manicone, M., Indraccolo, S., Amadori, A., 2014. Cancer stem cells from epithelial ovarian cancer patients privilege oxidative phosphorylation, and resist glucose deprivation. Oncotarget 5, 4305–4319.

Qu, C., Zhang, W., Zheng, G., Zhang, Z., Yin, J., He, Z., 2014. Metformin reverses multidrug resistance and epithelial-mesenchymal transition (EMT) via activating AMP-activated protein kinase (AMPK) in human breast cancer cells. Mol. Cell. Biochem. 386, 63–71.

Quinn, B.J., Kitagawa, H., Memmott, R.M., Gills, J.J., Dennis, P.A., 2013. Repositioning metformin for cancer prevention and treatment. Trends

Endocrinol. Metab. 24, 469–480.

R Development Core Team, 2005. R: A language and environment for statistical computing. R Foundation for Statistical Computing, Vienna, Austria. ISBN 3-900051-07-0, URL http://www.R-project.org

Reinbolt, R.E., Hays, J.L., 2013. The role of PARP inhibitors in the treatment of gynecologic malignancies. Cancer Mol. Targets Ther. 3, 237.

Remacle, A.G., Noël, A., Duggan, C., McDermott, E., O'Higgins, N., Foidart, J.M., Duffy, M.J., 1998. Assay of matrix metalloproteinases types 1, 2, 3 and 9 in breast cancer. Br. J. Cancer 77, 926–931.

Restucci, B., Maiolino, P., Martano, M., Esposito, G., Filippis, D.D., Borzacchiello, G., Muzio, L.L., 2007. Expression of β-Catenin, E-cadherin and APC in Canine Mammary Tumors. Anticancer Res. 27, 3083–3089.

Ritz, C., Streibig, J.C., 2005. Bioassay analysis using R. J. Stat. Softw. 12, 1–22.

Rizos, C.V., Elisaf, M.S., 2013. Metformin and cancer. Eur. J. Pharmacol. 705, 96–108.

Rostami, M., Tateyama, S., Uchida, K., Naitou, H., Yamaguchi, R., Otsuka, H., 1994. Tumors in domestic animals examined during a ten-year period (1980 to 1989) at Miyazaki University. J. Vet. Med. Sci. Jpn. Soc. Vet. Sci. 56, 403–405.

Roth, M., Chen, W.Y., 2014. Sorting out functions of sirtuins in cancer. Oncogene 33, 1609–1620.

Rouleau, M., Patel, A., Hendzel, M.J., Kaufmann, S.H., Poirier, G.G., 2010. PARP inhibition: PARP1 and beyond. Nat. Rev. Cancer 10, 293–301.

Saeki, K., Endo, Y., Uchida, K., Nishimura, R., Sasaki, N., Nakagawa, T., 2012. Significance of Tumor-Infiltrating Immune Cells in Spontaneous Canine Mammary Gland Tumor: 140 Cases. J. Vet. Med. Sci. 74, 227–230.

Sahar, S., Sassone-Corsi, P., 2009. Metabolism and cancer: the circadian clock connection. Nat. Rev. Cancer 9, 886–896.

Saito, T., Chiba, T., Yuki, K., Zen, Y., Oshima, M., Koide, S., Motoyama, T., Ogasawara, S., Suzuki, E., Ooka, Y., Tawada, A., Tada, M., Kanai, F., Takiguchi, Y., Iwama, A., Yokosuka, O., 2013. Metformin, a diabetes drug, eliminates tumor-initiating hepatocellular carcinoma cells. PloS One 8, e70010.

Santos, A.A., Lopes, C.C., Marques, R.M., Amorim, I.F., Gärtner, M.F., de Matos, A.J.F., 2012. Matrix metalloproteinase-9 expression in mammary gland tumors in dogs and its relationship with prognostic factors and patient

outcome. Am. J. Vet. Res. 73, 689–697.

Sasaki, H., Asanuma, H., Fujita, M., Takahama, H., Wakeno, M., Ito, S., Ogai, A., Asakura, M., Kim, J., Minamino, T., Takashima, S., Sanada, S., Sugimachi, M., Komamura, K., Mochizuki, N., Kitakaze, M., 2009. Metformin prevents progression of heart failure in dogs: role of AMP-activated protein kinase. Circulation 119, 2568–2577.

Seipke, R.F., Hutchings, M.I., 2013. The regulation and biosynthesis of antimycins. Beilstein J. Org. Chem. 9, 2556–2563.

Seo-Mayer, P.W., Thulin, G., Zhang, L., Alves, D.S., Ardito, T., Kashgarian, M., Caplan, M.J., 2011. Preactivation of AMPK by metformin may ameliorate the epithelial cell damage caused by renal ischemia. Am. J. Physiol. Renal Physiol. 301, F1346–1357.

Shackelford, D.B., Abt, E., Gerken, L., Vasquez, D.S., Seki, A., Leblanc, M., Wei, L., Fishbein, M.C., Czernin, J., Mischel, P.S., Shaw, R.J., 2013. LKB1 Inactivation Dictates Therapeutic Response of Non-Small Cell Lung Cancer to the Metabolism Drug Phenformin. Cancer Cell 23, 143–158.

Shao, M.-M., Chan, S.K., Yu, A.M.C., Lam, C.C.F., Tsang, J.Y.S., Lui, P.C.W., Law, B.K.B., Tan, P.-H., Tse, G.M., 2012. Keratin expression in breast cancers. Virchows Arch. 461, 313–322.

Smoot, M.E., Ono, K., Ruscheinski, J., Wang, P.-L., Ideker, T., 2011. Cytoscape 2.8: new features for data integration and network visualization. Bioinforma. 27, 431–432.

Smyth, G.K., 2005. Limma: linear models for microarray data, in: Bioinformatics and Computational Biology Solutions Using R and Bioconductor. Springer, pp. 397–420.

Song, C.W., Lee, H., Dings, R.P.M., Williams, B., Powers, J., Santos, T.D., Choi, B.-H., Park, H.J., 2012. Metformin kills and radiosensitizes cancer cells and preferentially kills cancer stem cells. Sci. Rep. 2, 362.

Szczubiał, M., Łopuszynski, W., 2011. Prognostic value of regional lymph node status in canine mammary carcinomas. Vet. Comp. Oncol. 9, 296–303.

Takiguchi, Y., 2012. Antiproliferative action of metformin in human lung cancer cell lines. Oncol. Rep. 28, 8-14.

Tomiyasu, H., Goto-Koshino, Y., Takahashi, M., Fujino, Y., Ohno, K., Tsujimoto, H., 2010. Quantitative Analysis of mRNA for 10 Different Drug Resistance Factors in Dogs with Lymphoma. J. Vet. Med. Sci. 72, 1165–1172.

Tomiyasu, H., Watanabe, M., Goto-Koshino, Y., Fujino, Y., Ohno, K., Sugano, S.,

Tsujimoto, H., 2013. Regulation of expression of *ABCB1* and *LRP* genes by mitogen-activated protein kinase/extracellular signal-regulated kinase pathway and its role in generation of side population cells in canine lymphoma cell lines. Leuk. Lymphoma 54, 1309–1315.

Vascellari, M., Baioni, E., Ru, G., Carminato, A., Mutinelli, F., 2009. Animal tumour registry of two provinces in northern Italy: incidence of spontaneous tumours in dogs and cats. BMC Vet. Res. 5, 39.

Vaziri, H., Dessain, S.K., Eaton, E.N., Imai, S.-I., Frye, R.A., Pandita, T.K., Guarente, L., Weinberg, R.A., 2001. hSIR2SIRT1 Functions as an NAD-Dependent p53 Deacetylase. Cell 107, 149–159.

Vazquez-Martin, A., Oliveras-Ferraros, C., Cufí, S., Del Barco, S., Martin-Castillo, B., Menendez, J.A., 2010. Metformin regulates breast cancer stem cell ontogeny by transcriptional regulation of the epithelial-mesenchymal transition (EMT) status. Cell Cycle 9, 3807–3814.

Verdin, E., 2014. The Many Faces of Sirtuins: Coupling of NAD metabolism, sirtuins and lifespan. Nat. Med. 20, 25–27.

Vogelstein, B., Kinzler, K.W., 1993. The multistep nature of cancer. Trends Genet. 9, 138–141.

Vogelstein, B., Papadopoulos, N., Velculescu, V.E., Zhou, S., Diaz, L.A., Kinzler, K.W., 2013. Cancer Genome Landscapes. Science 339, 1546–1558.

Walter, M.J., Shen, D., Ding, L., Shao, J., Koboldt, D.C., Chen, K., Larson, D.E., McLellan, M.D., Dooling, D., Abbott, R., Fulton, R., Magrini, V., Schmidt, H., Kalicki-Veizer, J., O'Laughlin, M., Fan, X., Grillot, M., Witowski, S., Heath, S., Frater, J.L., Eades, W., Tomasson, M., Westervelt, P., DiPersio, J.F., Link, D.C., Mardis, E.R., Ley, T.J., Wilson, R.K., Graubert, T.A., 2012. Clonal Architecture of Secondary Acute Myeloid Leukemia. N. Engl. J. Med. 366, 1090–1098.

Weinhouse, S., Warburg, O., Burk, D., Schade, A.L., 1956. On Respiratory Impairment in Cancer Cells. Science 124, 267–272.

Withrow, S.J., Vail, D.M., Page, R., 2012. Tumors of the Mammary Gland. In: Withrow and MacEwen's Small Animal Clinical Oncology, Fifth Ed. Saunders Elsevier, St. Louis, MO, USA, pp. 538–556

Würth, R., Pattarozzi, A., Gatti, M., Bajetto, A., Corsaro, A., Parodi, A., Sirito, R., Massollo, M., Marini, C., Zona, G., Fenoglio, D., Sambuceti, G., Filaci, G., Daga, A., Barbieri, F., Florio, T., 2013. Metformin selectively affects human glioblastoma tumor-initiating cell viability: A role for metformin-induced

inhibition of Akt. Cell Cycle 12, 145–156.

Xiong, N., Long, X., Xiong, J., Jia, M., Chen, C., Huang, J., Ghoorah, D., Kong, X., Lin, Z., Wang, T., 2012. Mitochondrial complex I inhibitor rotenone-induced toxicity and its potential mechanisms in Parkinson's disease models. Crit. Rev. Toxicol. 42, 613–632.

Ye, J., Coulouris, G., Zaretskaya, I., Cutcutache, I., Rozen, S., Madden, T.L., 2012. Primer-BLAST: A tool to design target-specific primers for polymerase chain reaction. BMC Bioinformatics 13, 134.

Yoshida, K., Yoshida, S., Choisunirachon, N., Saito, T., Matsumoto, K., Saeki, K., Mochizuki, M., Nishimura, R., Sasaki, N., Nakagawa, T., 2014. The Relationship between Clinicopathological Features and Expression of Epithelial and Mesenchymal Markers in Spontaneous Canine Mammary Gland Tumors. J. Vet. Med. Sci. E-pub ahead of print.

Zhu, P., Davis, M., Blackwelder, A.J., Bachman, N., Liu, B., Edgerton, S., Williams, L.L., Thor, A.D., Yang, X., 2014. Metformin Selectively Targets Tumor-Initiating Cells in ErbB2-Overexpressing Breast Cancer Models. Cancer Prev. Res. 7, 199–210.